TENMAK BOREN BOR ARAŞTIRMA ENSTİTÜSÜ
TENMAK BOREN BORON RESEARCH INSTITUTE

ISSN: 2149-9020
e-ISSN: 2667-8438

BOR DERGİSİ
JOURNAL OF BORON

CİLT/VOL 08 | SAYI/ISSUE 02 | YIL/YEAR 2023

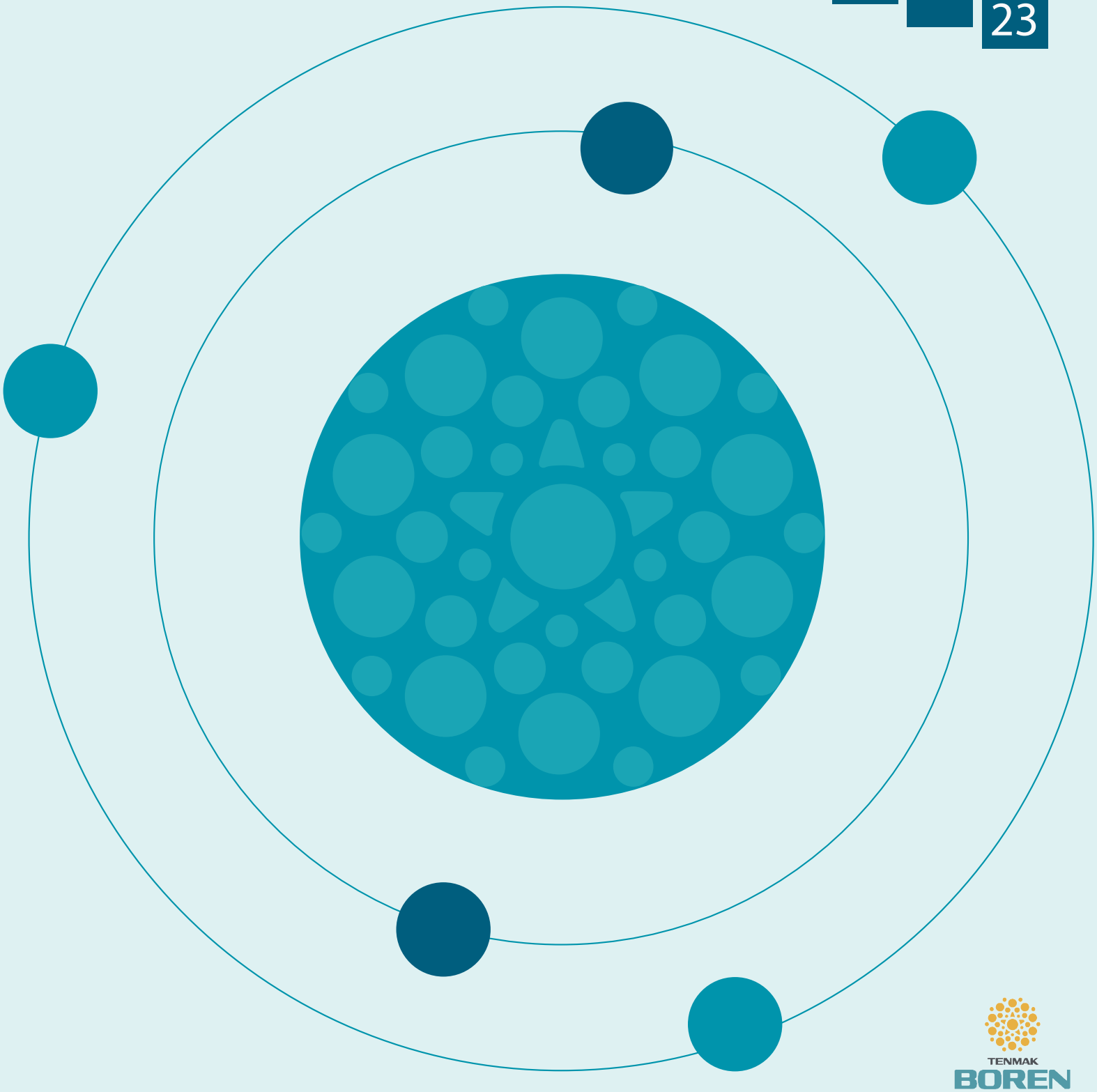

TENMAK BOREN

ISSN: 2149-9020
e-ISSN: 2667-8438

BOR DERGİSİ

JOURNAL OF BORON

CİLT VOL **08** **SAYI** ISSUE **02** **YIL** YEAR **2023**

Sorumlu Yazı İşleri Müdürü
Manager of Publication
Dr. Serap Topsoy Kolukısa
Serap.Kolukisa@tenmak.gov.tr

Yayıncı/Publisher
TENMAK BOREN Bor Araştırma Enstitüsü

Yayın İdare Adresi/Adress of Publication Manager
Dumlupınar Bulvarı (Eskişehir Yolu 7. km), No:166, D Blok,
Ankara, 06530, Türkiye
Tel: (0312) 201 36 00
Fax: (0312) 219 80 55
E-posta: boren.journal@tenmak.gov.tr
Web: https://dergipark.org.tr/boron

Editoryal Teknik Personel
Editorial Technical Staff
Dr. Abdulkadir Solak
Ayça Karamustafaoğlu
Sema Akbaba
Sinem Erdemir Guran

Yayın Türü/Type of Publication: Yaygın süreli yayın
Yayın Aralığı/Range of Publication: 3 Aylık
Yayın Tarihi/Publication Date: 31/06/2023

ANKARA
HAZİRAN 2023 / JUNE 2023

TENMAK BOREN
BOR ARAŞTIRMA ENSTİTÜSÜ

BOR DERGİSİ
JOURNAL OF BORON
https://dergipark.org.tr/boron

İÇİNDEKİLER/CONTENTS

BOR DERGİSİ
JOURNAL OF BORON
https://dergipark.org.tr/boron

Antimicrobial chitosan-sodium tetrafluoroborate ($NaBF_4$) hydrogels for topical applications

Zeynep İyigündoğdu [1,*]

[1]*Adana Alparslan Turkes Science and Technology University, Department of Bioengineering, Adana, 01250, Turkiye*

ARTICLE INFO

Article history:
Received January 9, 2023
Accepted April 18, 2023
Available online June 30, 2023

Research Article

DOI: 10.30728/boron.1231447

Keywords:
Antimicrobial hydrogel
Chitosan
Cytotoxicity
Sodium tetrafluoroborate

ABSTRACT

Infection of a wound is one of the most important reasons delaying the recovery of an injured tissue. In this study, chitosan-based hydrogels were loaded with different concentrations of sodium tetrafluoroborate ($NaBF_4$) to fabricate an antimicrobial wound care system. Antimicrobial activity, and cytotoxicity of $NaBF_4$, and surface morphology, chemical bond structures and antimicrobial activity of Chitosan:$NaBF_4$ hydrogels against a broad spectrum of microorganisms including an antibiotic resistant specie were investigated. $NaBF_4$ showed higher antibacterial activity for gram-positive bacteria than gram-negative bacteria. MIC values of $NaBF_4$ were 3.906, 1.953, and 7.813 µg/µL for every gram-negative, gram-positive, and fungal species, respectively. Direct cytotoxicity of $NaBF_4$ on the L929 cell line was investigated by the 3-(4,5-Dimethylthiazol-2-yl)-2,5-Diphenyltetrazolium Bromide (MTT) assay. IC_{50} value after 24 h incubation was calculated as 3.2 µg/µL which is within the range of concentration with antimicrobial activity. The antimicrobial activities of chitosan hydrogels were investigated by disc diffusion method. Antimicrobial activity of hydrogel increased with increasing $NaBF_4$ concentration while high molecular weight chitosan-based hydrogel did not show antimicrobial activity. According to the results, group 1:3 (546.5mM $NaBF_4$ containing hydrogel) was enough to achieve broad spectrum antimicrobial activity and hydrogels prepared with this formulation can be used as a potential antimicrobial wound care product.

1. Introduction

Microbial contamination is a great concern, especially in terms of wound healing and biomedical implant fouling [1,2]. Presence of harmful microorganisms in the injured areas can cause various infections and these infections can prolong the healing process and may lead to tissue morbidity or sepsis depending on the severity of the infection. Moreover, the rapid development of antibiotic-resistant microorganisms complicates the situation [3,4]. For this reason, many researchers are interested in designing wound care systems that do not allow microbial contamination while accelerating the wound healing process. Designing a wound care system begins with the selection of the material. There are various polymeric materials used as wound dressing such as cellulose, gelatin, alginate, chitosan etc. [5-8]. Among these biopolymers, chitosan is one of the most widely used one due to its favorable properties such as hemostasis, biocompatibility, biodegradability, bacteriostasis and controlled drug release ability [9-11].

Chitosan is a linear natural polysaccharide obtained by partial deacetylation (>40%) of chitin, the major constituent of the exoskeleton of crustaceans, and comprised of glucosamine and N-acetyl-glucosamine monomers linked through β(1-4) bonds. Chitosan, which has many uses in its pure form, offers easy functionalization or modification by chemical and enzymatic processing due to the existence of hydroxyl (-OH) and amine ($-NH_2$) functional groups in its structure, and can be made suitable for use in many different areas by improving its physical and biological properties [12,13]. Chitosan, the second most abundant natural polysaccharide after cellulose, finds a wide range of applications in different medical and pharmaceutical devices due to its non-toxic, biocompatible, biodegradable and antimicrobial and antifungal properties [14,15].

Aside of its numerous advantages, chitosan is sensitive to water and has relatively low hardness and low durability that limits its use. In this context, crosslinkers are used to protect the biological properties of chitosan-containing biomaterials, to increase their mechanical strength and chemical stability, and to control their water permeability, solubility and swelling properties

*Corresponding author: ziyigundogdu@atu.edu.tr

[16]. Crosslinking can be achieved either by formation of chemical bonds or physical crosslinking. So far, chemicals such as glutaraldehyde, tripolyphosphate, ethylene glycol, diglycidyl ether, diisocyanate and genipin have been used as chemical crosslinkers for chitosan. However, most of the synthetic cross-linkers are cytotoxic and may reduce the biocompatibility of the developed biomaterial. Among the chemicals, genipin stands out with its biocompatibility and high stability. Chitosan and genipin-containing biomaterials are used in many important areas such as preparation of elastic cartilage tissue material, production of carrier materials for controlled drug release, encapsulation of biological products and living cells, bio fabrication of muscle and vascular wall tissues, and production of wound dressing materials for humans and animals [17].

Chitosan is a water insoluble polymer. In order to induce the solubility of chitosan in water, an acidic media is required. The amino groups of chitosan are protonated by the acidic environment and the protonation of the amino groups present in the chitosan adversely affects the bonding forces between the polysaccharide chains. By increasing chitosan concentration or by adjusting the solution pH, gels can be formed by precipitation of chitosan chains. Glycerol phosphate is a basic salt that can be used as physical crosslinker. When a basic salt is added to a chitosan solution, pH of the solution increases by neutralizing phosphate groups, therefore solution remains liquid in these conditions. When temperature is increased to 37°C, due to hydrogen bonding, hydrophobic, and electrostatic interactions, original solution begins to be transformed into the gel matrix. This solution remains liquid below room temperature at pH values between 6.8 to 7.2 and turns into a gel when heated to body temperature which can be defined as heat-induced gelation which is very important for injectable gel applications [18-22].

In this study, glycerol phosphate and genipin have been used to obtain co-crosslinked chitosan hydrogels. These two physical and chemical crosslinkers have been used in a previous study and some advantages have been listed as reduced gelation time, improved mechanical properties and storage modulus due to physical and covalent crosslinking. Even co-crosslinked hydrogels display small pore size, and swelling properties were similar to those physically crosslinked ones [22].

Although chitosan is known as an antimicrobial biopolymer the antimicrobial efficiency changes with various factors such as type of microorganism, molecular weight, concentration, pH, temperature, ionic strength, reactive time etc. [23]. Therefore, researchers have been working on enhancing the antimicrobial property of chitosan by adding different antimicrobial agents [24-27]. Sodium tetrafluoroborate ($NaBF_4$), is a water-soluble molecule and releases high electronegative anion (BF_4^-) when dissociated into ions. Microbial cell walls have ionic charges and negatively signed ions may interact with microbial cell walls and alter membrane integrity which could be resulted by antimicrobial activity. To the best of the author's knowledge, there is no scientific study in the literature about broad spectrum antimicrobial activity and cytotoxicity properties of $NaBF_4$. In this study, the antimicrobial properties of high molecular weight chitosan hydrogels were crosslinked by using genipin and glycerol phosphate, and different concentrations of $NaBF_4$ addition were investigated for a potential wound care product.

2. Materials and Methods

2.1. Materials

High molecular weight chitosan was purchased from Sigma-Aldrich (USA). The degree of deacetylation (DD) and the molecular weight of the chitosan were >75% and between 310-375 kDa, respectively. Isomeric mixture of glycerol phosphate disodium salt hydrate and acetic acid glacial, puriss. 99.8-100.5% were purchased from Sigma-Aldrich (USA). Genipin was purchased from Challenge Bioproducts Co., Ltd. (Taiwan). $NaBF_4$ was purchased from Acros Organics (Belgium). Nutrient agar (NA), nutrient broth (NB), potato dextrose agar (PDA), and potato dextrose broth (PDB) were purchased from Sigma Aldrich. Ofloxacin, nystatin, and blank discs were purchased from Oxoid (UK). Cell culture chemicals were purchased from Biowest (France) unless it was stated. Microbial species used in antimicrobial activity tests, given in Table 1, were obtained from American Type Culture Collection (ATCC, USA). *Penicillium* sp. was kindly provided by the culture collection of Yeditepe University, Department of Genetics and Bioengineering. L929 mouse fibroblast cell line was also obtained from ATCC.

Table 1. Microbial species used for $NaBF_4$ and $NaBF_4$ incorporated chitosan hydrogels antimicrobial activity tests.

	Species	ATCC Code
Bacteria	*Eschericia coli*	25922
	Pseudomonas aeruginosa	27853
	Acinetobacter baumannii	9606
	Salmonella typhi	19430
	Klebsiella pneumoniae	13883
	Staphylococcus aureus	29213
	Methicillin-resistant *Staphylococcus aureus* (MRSA)	33592
Fungi	*Candida albicans*	10231
	Aspergillus niger	16404
	Penicillium sp.	-

2.2. Disk Diffusion Tests of $NaBF_4$

The antimicrobial property of $NaBF_4$ was determined by using the disk diffusion method described previously

[28]. $NaBF_4$ solution was prepared in 500 mg/mL concentration by using ultrapure water. On the other hand, 100 µL of 0.5 McFarland bacterial suspension were inoculated on the agar plate, for yeast and fungus 1 McFarland suspensions was used. NA and PDA were used for bacterial and fungal isolates, respectively. Blank discs were impregnated with 20 µL of $NaBF_4$ solution and placed on the inoculated plates. Ofloxacin and nystatin discs were used as positive control (PC) for bacteria and fungus, respectively. The plates were kept in incubators for 24 h at 36±1 °C for bacterial strains, 48 h at 36±1 °C for yeast and 72 h for fungus isolates at 27±1 °C to promote microbial growth. Inhibition zone diameters around $NaBF_4$ doped discs were measured to determine the antimicrobial activity.

2.3. Minimum Inhibitory Concentration of $NaBF_4$

The MIC values were determined according to the broth microdilution method described previously in a previous study [29]. Microbial species given in Table 1 were inoculated on NA for bacterial strains and for PDA of yeast and fungal species. Inoculated plates were incubated 24 h at 36±1 °C for bacterial strains, 48 h at 36±1 °C for yeast and 72 h for fungus isolates at 27±1 °C. Fresh grown cultures were used to prepare 0.5 McFarland microbial suspensions. Bacterial and yeast suspensions were prepared in sterile phosphate-buffered saline (PBS) and fungal suspensions were prepared in 0.5% (v/v) Tween 80 + PBS solution. On the other hand, $NaBF_4$ was dissolved in sterile ultrapure water with a concentration of 500 µg/µL in sterile test tubes. The 96-well plates were used for MIC tests, 200 µL from the stock solutions of $NaBF_4$ prepared at the concentration of 500 µg/µL was added into the first well. One hundred µL sterile ultrapure water was added to the sequential nine wells. Then, 100 µL from their serial dilutions was transferred into nine sequential wells. Then, 95 µL broth and 5 µL of each inoculum were added into each well. NB were used for bacterial species and PDB were used for fungal isolates. Two hundred µL pure broth was added into the 11^{th} wells as positive control and 12^{th} wells containing 195 µL broth and 5 µL of the inoculum was used as a negative control. Plates were incubated in a shaker incubator at 180 rpm at appropriate time and temperature. The lowest concentration of $NaBF_4$ inhibits the growth of microorganisms (MIC values), was determined using a microplate reader with absorbance (Abs) at 600 nm for bacteria and 530 nm for fungal isolates.

2.4. Minimum Bactericidal (MBC) and Fungicidal (MFC) Concentration of $NaBF_4$

MBC/MFC values were determined in accordance with the lowest concentrations of $NaBF_4$ which showed no microbial growth. Starting from the MIC values to higher concentrations 100 µL suspensions were spread on NA for bacteria, and PDA for yeast and fungi. Inoculated plates were incubated for appropriate time and temperature and the lowest concentrations of $NaBF_4$ that showed no microbial growth were recorded as MBC/MFC value [29].

2.5. Cytotoxicity of $NaBF_4$ by MTT Analysis

Cytotoxicity of $NaBF_4$ was directly determined in cell culture medium. L929, mouse fibroblast cell line, was used in cell culture studies. Cells were cultured in Dulbecco's Modified Eagle Medium (DMEM) High Glucose containing 10% (v/v) fetal bovine serum (FBS), 1% (v/v) L-glutamine and 10 units/mL penicillin, 10 µg/mL streptomycin solution. L929 cells were seeded as 10^4 cells/well on 96 well plate and cultured at 37°C in 5% CO_2 atmosphere. The cells were cultured for one day to cover the surface. The day after, the stock solution of $NaBF_4$ was prepared in complete cell culture medium and diluted in cell culture medium between 100-0.098 mM. $NaBF_4$ containing cell culture media was applied to L929 cells (n=6). Cellular viabilities after 24 h $NaBF_4$ exposure were analyzed by 3-(4,5-Dimethylthiazol-2-yl)-2,5-Diphenyltetrazolium Bromide (MTT) analysis. Used cell culture medium was aspirated and MTT containing culture media without FBS was added onto the cells. The cells were cultured in MTT containing media for 4 h at 37°C in 5% CO_2 atmosphere. At the end of the incubation period, used media was removed and formazan crystals were dissolved in dimethyl sulfoxide (DMSO). Absorbance values were recorded at 570 nm reference to 690 nm with BMG Labtech, Spectrostar Nano, Germany. Cell viability is given as % viability of control cells cultured without $NaBF_4$.

2.6. Hydrogel Synthesis

High molecular weight chitosan was dissolved in 100 mL 1% (v/v) aqueous acetic acid solution in ultrapure water as 1 g/100 mL. This solution was left to mix for 24 h until it was clear. Unsolved solid particles were removed by centrifugation at 8000 rpm for 10 min. In order to prepare different concentrations of Chitosan:$NaBF_4$ (Ch:$NaBF_4$) hydrogels 10 mL of chitosan solution were separated into beakers and specific amounts of $NaBF_4$ was mixed with chitosan solutions as given in Table 2.

Table 2. Hydrogel synthesis conditions.

Ch:$NaBF_4$ (w/w)	Chitosan (g)	$NaBF_4$ (g)	$NaBF_4$ (mM)	GP (M)	Genipin (mM)
1:0*	0.1	0	0	0.12	1
1:1	0.1	0.1	182.2	0.12	1
1:2	0.1	0.2	364.3	0.12	1
1:3	0.1	0.3	546.5	0.12	1
1:4	0.1	0.4	728.7	0.12	1
1:5	0. 1	0.5	910.8	0.12	1

*Control hydrogel group without $NaBF_4$.

Then, glycerol phosphate (GP) and genipin were added into these solutions as crosslinkers, respectively. Polymer-crosslinker solution kept at 37°C for one day to complete the crosslinking process.

2.7. Characterization of Ch:$NaBF_4$ Hydrogels

Surface morphology of freeze-dried Ch:$NaBF_4$ hydrogels were characterized by Scanning Electron Microscopy (SEM, FEI, Quanta 650, USA) analysis. Samples were coated with Au-Pd for 60 seconds under argon atmosphere using plasma sputter before SEM imaging. The presence of specific chemical groups in the hydrogels were analyzed by Fourier Transform Infrared Spectroscopy (FTIR, PerkinElmer, USA) in the 4000-400 cm^{-1} wavenumber range.

2.8. Agar Disc Diffusion Method

Inhibition of microbial growth by Ch:$NaBF_4$ hydrogels were tested against microorganisms given at Table 1 by using agar disc diffusion method as described previously [30]. Briefly, 0.5 McFarland bacteria, yeast and fungi were prepared from fresh growth cultures. 100 µL of each microbial suspension were inoculated on NA for bacteria, and PDA for yeast and fungi. Ch:$NaBF_4$ hydrogels were cut out with a cork borer (approximately 7 mm diameter hydrogels were obtained) and placed on the inoculated agar. Inoculated plates were incubated for appropriate time and temperature for all microbial species and antimicrobial activity was determined by measuring the inhibition zone diameters.

3. Results

3.1. Antimicrobial Activity of $NaBF_4$

Antimicrobial activity tests were conducted against seven bacteria, one yeast, and two fungi species based on agar disk diffusion assay by measuring the inhibition zones around $NaBF_4$ dopped disks. Zone diameters were obtained for 20 µL of 500 mg/mL $NaBF_4$ solution (Table 3).

Table 3. Agar disk diffusion test results of $NaBF_4$ (mm).

Microorganism	Inhibition zone	PC
E. coli	18	40
P. aeruginosa	16	24
S. typhi	20	36
K. pneumoniae	16	41
A. baumanni	20	10
S. aureus	15	34
MRSA	23	27
C. albicans	16	26
A. niger	14	25
Penicillium sp.	17	25

According to the disk diffusion assay $NaBF_4$ displayed remarkable antimicrobial activity against all microbial species tested. Although there are many studies in the literature that indicate the antimicrobial activities of various boron compounds [31-34], there are few studies that mention the antimicrobial activity of $NaBF_4$. A study conducted by Ghammamy and Keysan (2012) has reported that the synthesized nano-$NaBF_4$ molecules have antibacterial activity against *S. aureus* and Group B *Streptococci* [35]. Another study conducted by Suner et al. (2020) states that protonated polyethyleneimine modified halloysite nanotubes (H-PEI-HNTs) were ion exchanged with $NaBF_4$ ($NaBF_4$-PEI-HNTs) and antimicrobial activity was observed against gram-negative (*E. coli* and *P. aeruginosa*) and gram-positive (*Bacillus subtilis* and *S. aureus*) bacteria, and also a yeast specie (*C. albicans*) [36].

The lowest concentration values of $NaBF_4$ that inhibits the visible growth of the microorganism after overnight incubation (MIC) were determined by the broth microdilution method. The lowest concentration that killed the microorganism was determined by sub-culturing the suspensions onto the agars to look for survivors. Minimum concentration with no microbial growth was evaluated as MBC/MFC. MIC and MBC/MFC results are summarized in Table 4.

Table 4. MIC and MBC/MFC values of $NaBF_4$.

Microorganism	MIC (µg/µL)	MIC (mM)	MBC/MFC (µg/µL)
E. coli	3.906	35.6	3.906
P. aeruginosa	3.906	35.6	3.906
S. typhi	3.906	35.6	3.906
K. pneumoniae	3.906	35.6	3.906
A. baumanni	3.906	35.6	3.906
S. aureus	1.953	17.8	1.953
MRSA	1.953	17.8	15.63
C. albicans	7.813	71.2	7.813
A. niger	7.813	71.2	7.813
Penicillium sp.	7.813	71.2	7.813

MIC results showed that the antifungal and anticandidal efficiency of $NaBF_4$ is lower with respect to its antibacterial efficiency. Moreover, gram-positive bacteria are more susceptible to $NaBF_4$ than gram-negative bacteria. The MBC and MFC values were not different from the MIC values for tested microorganisms except MRSA. MBC was 8 times higher than its MIC value. In literature, there are many studies investigating the MIC values of various boron compounds, however, to the best of author's knowledge there has been no study investigating the MIC values of $NaBF_4$ against any microorganisms. Previously, MIC values of boric acid (BA) and borax were determined by macrodilution method against *S. aureus*, *E. coli*, and *P. aeruginosa* [37]. According to the test results $NaBF_4$ was effective against these microorganisms at 2- and 12-times lower concentrations, compared to BA and borax, respectively. Another study evaluated the MIC values of BA and disodium octaborate tetrahydrate (DOT) against 10 bacterial species. Most susceptible and resistant species are found as *P. aeruginosa* and *S. aureus*, respectively. MIC values of BA and DOT were

determined as 0.385 µg/µL and 0.644 µg/µL against *P. aeruginosa*, 3.09 µg/µL and 10.312 µg/µL against *S. aureus*, respectively [38]. When we compare the MIC results of $NaBF_4$ with DOT and BA, $NaBF_4$ has a higher antibacterial effect than both BA and DOT against *S. aureus*. On the other hand, bactericidal activity of BA and DOT is higher than $NaBF_4$ against *P. aeruginosa*.

The antibacterial activity of $NaBF_4$ for gram-positive bacteria is better than gram-negative bacteria, probably due to their cell wall structure. Cell wall of a gram-positive bacteria is majorly composed of peptidoglycan. On the other hand, a gram-negative bacteria's cell wall is more complex, in addition to the peptidoglycan; polysaccharides, proteins and phospholipids are present in the structure. The charge of the phospholipid is negative, while the peptidoglycan is positively charged [27,39]. When $NaBF_4$ is dissolved in water, it dissociates into Na^+ and BF_4^- ions. Negatively charged BF_4^- ion may interact with positively charged peptidoglycan better than negatively charged phospholipid. As a result of this interaction membrane integrity may be altered and intracellular substances leaked out. This could be the reason why MIC values of $NaBF_4$ for gram-positive bacteria were lower than gram-negative bacteria.

3.2. Cytotoxicity of $NaBF_4$

Cytotoxicity of $NaBF_4$ on L929, mouse fibroblast cell line, was determined by MTT assay and the results are given in Figure 1.

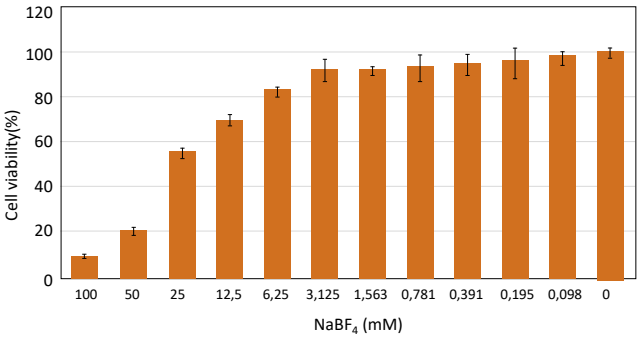

Figure 1. Cytotoxicity of $NaBF_4$ was determined by MTT assay at 24 h culture (n=6).

The cells were cultured in the presence of different concentrations of $NaBF_4$ between 0.098-100 mM for 24 h. The cell viability decreased to 70.26% upon treatment with 12.5 mM $NaBF_4$ and further decreased to 21.25% and 10.33% with 50 mM and 100 mM $NaBF_4$ treatment, respectively. The IC_{50} value of $NaBF_4$ on L929 cells was calculated as 29.3 mM which is a very high concentration. 29.3 mM concentration of $NaBF_4$ corresponds to 3.2 µg/µL concentration. MIC values of *S. aureus* and MRSA with 1.953 µg/µL was lower when compared to the IC_{50} value of L929 cell line. According to these results, MIC values are very close to non-toxic concentration so it can be concluded that $NaBF_4$ can be safely used in tissue engineering studies. In a study, cytotoxicity of $NaBF_4$ was determined with human cervical carcinoma epithelial cells HeLa. The half-maximal effective concentration (EC_{50}) value of $[BF_4]^-$ ion on HeLa cell line was calculated as >25 mM without giving direct concentration [40].

There is a lack of studies investigating the cytotoxicity of $NaBF_4$ in the literature. However, there are some studies investigating the effect of different boron compounds with various cell lines. In a study, IC_{50} value for boric acid on U-87 MG glioblastoma cell line was found as 17 mM, in 48 h culture period [41]. In another study, the combined effect of different concentrations of borax in the presence of 50 µg/mL 5-Fluorouracil (5-FU) on human colorectal cancer cell line, DLD-1 was investigated. 5-FU is a widely used, FDA accepted chemotherapy agent for colorectal cancer. Decreased cell viability and increased early apoptotic cell percentage was shown in the combined application of 5-FU and borax when compared to their application at the same concentrations alone [42]. In a different study, sodium pentaborate pentahydrate (NaB) was used at 15 µg/mL concentration with 10% (v/v) DMSO for freezing. It was concluded that NaB protected viability of A549 cancer cells and L929 cells after 4 freeze-thaw cycles indicating NaB may be a good cryoprotective agent [43].

3.3. Surface Morphology of the Hydrogels

Surface morphologies of the hydrogels were investigated by SEM analysis. Control chitosan surface showed smooth morphology without any roughness. In the $NaBF_4$ modified groups, increased numbers of crystalline particles were found on the surface of the hydrogels with increasing $NaBF_4$ concentration as it is clearly seen from the Figure 2. $NaBF_4$ was dissolved in the chitosan solution before gelation, so this crystallization was triggered during the freeze-drying application. Besides, SEM images obviously shows that $NaBF_4$ crystals were agglomerated during freeze-drying process.

3.4. ATR-FTIR Spectra of the Ch:$NaBF_4$ Hydrogels

The ATR-FTIR spectra of the crosslinked chitosan, $NaBF_4$, and Ch:$NaBF_4$ hydrogels are given in Figure 3. Peaks at 774, 520, 526 and 1332 cm^{-1} are specific for $NaBF_4$ and can be clearly seen in the Ch:$NaBF_4$ hydrogel spectra. These peaks which correspond to characteristic vibrations of $NaBF_4$ [44] were not seen in the spectra of bare chitosan. A broad peak at 3000-3600 cm^{-1}, -OH stretching of the hydroxyl group, was determined for chitosan polymer. The $CONH_2$ and NH_2 groups peaks specific for amide structure of chitosan were recorded at 1651 and 1555 cm^{-1}, respectively [45]. The intensity of the peak at 1555 cm^{-1} was increased with increasing concentrations of $NaBF_4$ indicating the interaction between NH_2 group of chitosan and $NaBF_4$. Sharp peak with broad range at 1055 and 1022 cm^{-1} corresponds to C-O stretching and this peak overlaps with the peak of $NaBF_4$ at 1010 cm^{-1} between the same range.

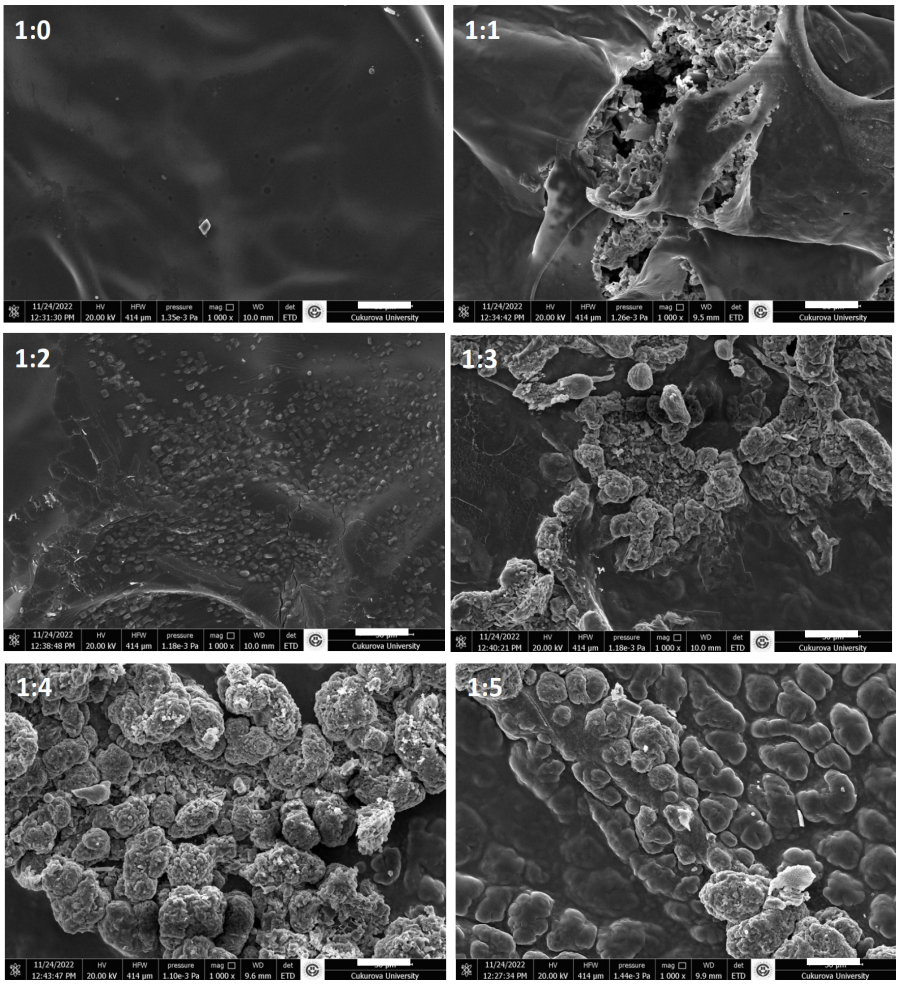

Figure 2. SEM images of Ch:$NaBF_4$ hydrogels with 1000X magnification (Scale bar: 50 µm).

3.5. Agar Disk Diffusion Results of Ch:$NaBF_4$ Hydrogels

Antimicrobial activities of $NaBF_4$ loaded chitosan-based hydrogels were investigated by agar disk diffusion method and, the ratio of the inhibition zone to the sample diameter is given in Table 5, instead of giving the inhibition diameter directly, since each sample could not be obtained at the same diameter. Although chitosan is known as a natural biobased antimicrobial polymer, control groups prepared by using high molecular weight chitosan did not show antimicrobial activity against tested microorganisms. The main reason for the inadequate antimicrobial activity might be related to the molecular weight of chitosan used in this study. Results are coherent with the previous literature studies that support decreasing antimicrobial activity of chitosan with increasing

Table 5. Ratio of inhibition zone diameter to hydrogel diameter.

	Ch:$NaBF_4$					
	1:0	**1:1**	**1:2**	**1:3**	**1:4**	**1:5**
E. coli	N/A*	1.22	2.19	2.22	2.58	2.90
P. aeruginosa	N/A	1.20	3.32	3.82	4.30	4.52
S. typhi	N/A	N/A	N/A	1.85	2.88	3.60
K. pneumoniae	N/A	1.78	2.12	2.19	2.33	2.64
A. baumanni	N/A	N/A	N/A	1.67	1.92	2.16
S. aureus	N/A	N/A	1.36	1.84	2.06	2.26
MRSA	N/A	2.01	2.30	2.44	3.01	3.68
C. albicans	N/A	N/A	N/A	N/A	2.48	3.41
A. niger	N/A	N/A	N/A	1.42	2.04	2.50
Penicillium sp.	N/A	1.60	1.61	2.20	2.51	3.27

*N/A: Not Available.

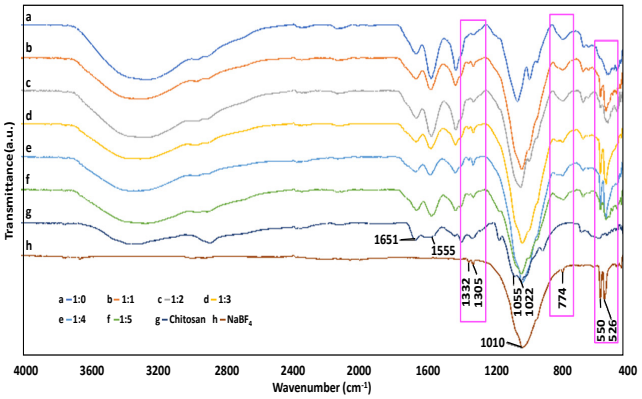

Figure 3. ATR-FTIR spectra of $NaBF_4$ and Ch:$NaBF_4$ hydrogels.

molecular weight [27,46,47]. As described in the previous antimicrobial section, antimicrobial activity could be related to the ionic charge of the biocide itself. Chitosan with positively charged amino groups should interact with the negatively charged cell wall of gram-negative bacteria; however, high molecular weight chitosan have lower pKa and less protonation [27]. This might be the reason why control groups did not show any antimicrobial activity.

Experimental results indicate that inhibition zones increased as the concentration of $NaBF_4$ increased. When we compare the antimicrobial activity among all gram-negative species Ch:$NaBF_4$ hydrogels showed highest antimicrobial activity towards *P. aeruginosa*. Although all gram-negative bacteria, they are different microorganisms from each other, so their susceptibility to any antimicrobial agent may differ from each other. The mode of action of antimicrobial agents such as DNA/RNA inhibition, disturbing enzyme mechanisms etc. may differ according to the type of microorganisms [36]. In a study conducted by Zheng et al. (2003) claimed that increasing molecular weight of chitosan is decreasing the antibacterial activity for gram-negative bacteria while increasing the antibacterial activity for gram-positive bacteria by forming a film which inhibits nutrient adsorption [47]. However, the results obtained from this study could not be associated with the results of the reported study.

Many researchers also used various antimicrobial agents such as metal ions, metal nanoparticles, antibiotics, antifungal drugs, etc. to enhance chitosan's antimicrobial activity [48-51]. In a study by Venkatesan et al. (2014) chitosan-carbon nanotube (CNT) hydrogels were developed by using different CNT concentrations and it was observed that the antimicrobial activity was increased with increasing CNT concentration [46]. In the literature there is no chitosan hydrogel prepared by using $NaBF_4$; however, there are some studies investigating the synergetic effect of boron compounds with chitosan for their potential use as wound care applications. In a study conducted by Huang et al. (2021) chitosan-based hydrogels were prepared by using boric acid or Tris and calcium gluconate containing buffer solutions [52]. According to the results both gels demonstrated tissue repair and anti-infection effects and they were evaluated as potential wound care material for hydrofluoric acid burn therapy. In another study, insufficient antimicrobial activity of chitosan at circumneutral pH of 6.0 was enhanced by using sodium metaborate tetrahydrate and chitosan-borate complexes showed broad spectrum antimicrobial activity against bacteria and fungi [53].

According to the disk diffusion results of this study $NaBF_4$ amount used in 1:3 gels were enough to achieve broad spectrum antimicrobial activity and hydrogels prepared with this formulation can be used as an antimicrobial wound care material (Figure 4).

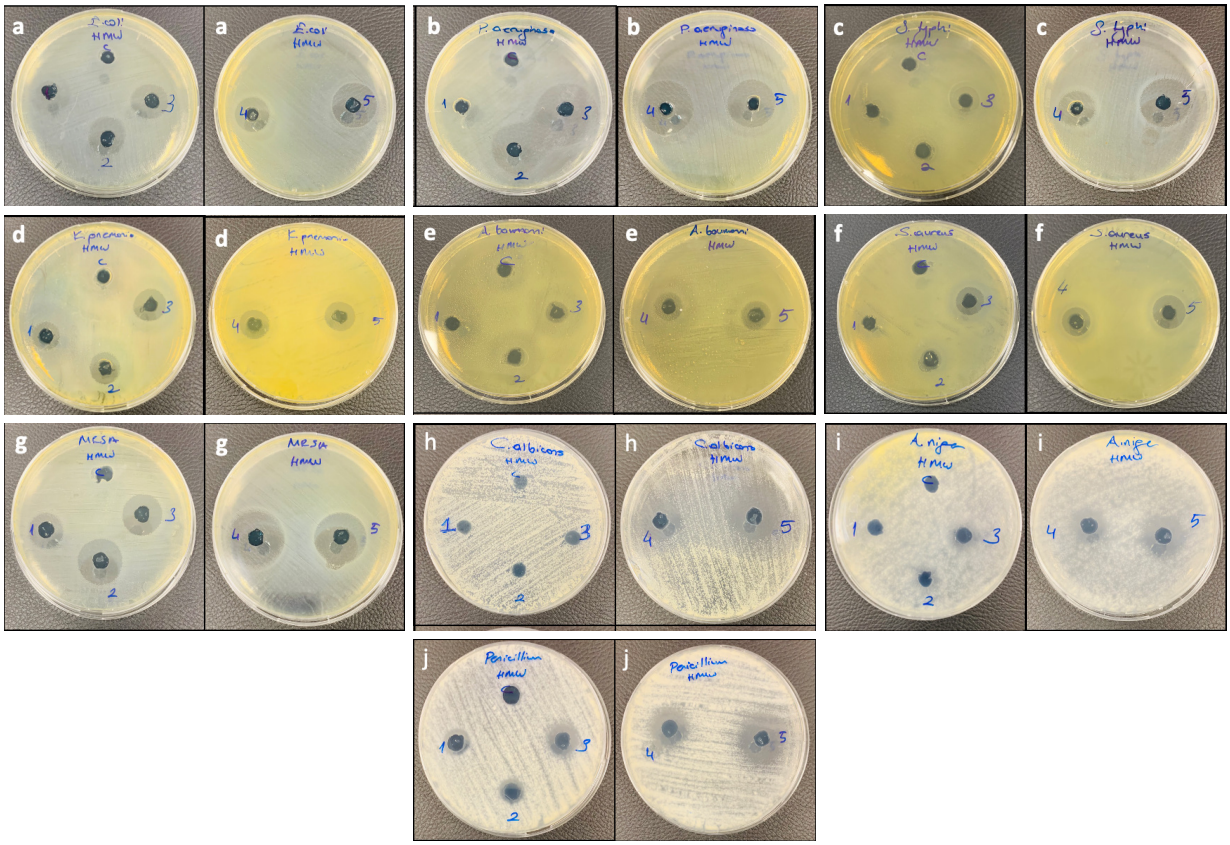

Figure 4. Agar disc diffusion test images of Ch:$NaBF_4$ hydrogels against a. *E. coli*, b. *P. aeruginosa*, c. *S. typhi*, d. *K. pneumoniae*, e. *A. baumanni*, f. *S. aureus*, g. MRSA, h. *C. albicans*, i. *A. niger*, j. *Penicillium* sp.

4. Conclusion

Antimicrobial hydrogels are widely used in wound healing applications due to their numerous advantages. This study is focused on developing antimicrobial chitosan-based hydrogels to be used in topical wound care products. $NaBF_4$ was used as an active agent to enhance the antimicrobial activity of chitosan. The antibacterial properties of $NaBF_4$ were evaluated using *E. coli*, *P. aeruginosa*, *S. typhi*, *K. pneumoniae*, *A. baumanni*, *S. aureus*, MRSA while antifungal properties were evaluated using *C. albicans*, *Penicillium* sp., and *A. niger*. The most effective antimicrobial activity was observed against gram-positive bacteria which are *S. aureus* and MRSA with 1.953 µg/µL MIC value. The IC_{50} value of $NaBF_4$ on the L929 cell line was calculated as 3.2 µg/µL after 24 h culture. Antimicrobial capability of the gels was directly related to the $NaBF_4$ content in hydrogels. Especially, 1:5 ($NaBF_4$ concertation is 910.8 mM) group showed the highest antimicrobial activity against a wide range of microorganisms while the 1:3 ($NaBF_4$ concertation is 546.5 mM) group was sufficient to inhibit microbial growth against all microorganisms used in antimicrobial activity tests. According to the results Ch:$NaBF_4$ hydrogels (1:3, 1:4, 1:5) have the strongest inhibitory effect against *P. aeruginosa* in comparison to the other gram-negative bacteria. Even though the IC_{50} value of $NaBF_4$ on L929 cells was calculated as 29.3 mM which corresponds to 3.2 µg/µL concentration, hydrogels were loaded with higher amount of $NaBF_4$. The reason of this excessive loading is due to the release profile of $NaBF_4$ from the chitosan-based hydrogel which could be discussed in future publication. As a result, the 1:3 sample hydrogel contains a sufficient amount of $NaBF_4$ for preparing an antimicrobial chitosan-based hydrogel which is a promising candidate that can be used as topical wound care product.

Acknowledgement

Author would like to thank Asst. Prof. Merve Capkin Yurtsever for her technical assistance in cell culture studies.

Conflicts of Interest

No conflict of interest was declared by the author.

Kaynaklar (References)

[1] Siddiqui, A. R., & Bernstein, J. M. (2010). Chronic wound infection: Facts and controversies. *Clinics in Dermatology*, *28*(5), 519-526.

[2] Montanaro, L., Campoccia, D., & Arciola, C. R. (2007). Advancements in molecular epidemiology of implant infections and future perspectives. *Biomaterials*, *28*(34), 5155-5168.

[3] Salomé Veiga, A., & Schneider, J. P. (2013). Antimicrobial hydrogels for the treatment of infection. *Biopolymers*, *100*(6), 637-644.

[4] Frieri, M., Kumar, K., & Boutin, A. (2017). Antibiotic resistance. *Journal of Infection and Public Health*, *10*(4), 369-378.

[5] Paul, W., & Sharma, C. P. (2004). Chitosan and alginate wound dressings : A short review. *Trends in Biometerials and Artificial Organs*, *18*(1), 18-23.

[6] Aderibigbe, B. A., & Buyana, B. (2018). Alginate in wound dressings. *Pharmaceutics*, *10*(42), 1-19.

[7] Ulubayram, K., Cakar, A. N., Korkusuz, P., Ertan, C., & Hasirci, N. (2001). EGF containing gelatin-based wound dressings. *Biomaterials*, *22*(11), 1345-1356.

[8] Lin, W. C., Lien, C. C., Yeh, H. J., Yu, C. M., & Hsu, S. H. (2013). Bacterial cellulose and bacterial cellulose-chitosan membranes for wound dressing applications. *Carbohydrate Polymers*, *94*(1), 603-611.

[9] Kofuji, K., Akamine, H., Qian, C. J., Watanabe, K., Togan, Y., … & Kawashima, S. (2004). Therapeutic efficacy of sustained drug release from chitosan gel on local inflammation. *International Journal of Pharmaceutics*, *272*(1-2), 65-78.

[10] Saito, K., Fujieda, T., & Yoshioka, H. (2006). Feasibility of simple chitosan sheet as drug delivery carrier. *European Journal of Pharmaceutics and Biopharmaceutics*, *64*(2), 161-166.

[11] Anjum, S., Arora, A., Alam, M. S., & Gupta, B. (2016). Development of antimicrobial and scar preventive chitosan hydrogel wound dressings. *International Journal of Pharmaceutics*, *508*(1-2), 92-101.

[12] Gaspar, V. M., Moreira, A. F., de Melo-Diogo, D., Costa, E. C., Queiroz, J. A., … & Correia, I. J. (2016). Multifunctional nanocarriers for codelivery of nucleic acids and chemotherapeutics to cancer cells. In *Nanobiomaterials in Medical Imaging: Applications of Nanobiomaterials* (pp. 163-207). Elsevier Inc.

[13] Nunes, C., Maricato, É., Cunha, Â., Nunes, A., da Silva, J. A. L., & Coimbra, M. A. (2013). Chitosan-caffeic acid-genipin films presenting enhanced antioxidant activity and stability in acidic media. *Carbohydrate Polymers*, *91*(1), 236-243.

[14] Delmar, K., & Bianco-Peled, H. (2015). The dramatic effect of small pH changes on the properties of chitosan hydrogels crosslinked with genipin. *Carbohydrate Polymers*, *127*, 28-37.

[15] Kim, I. Y., Seo, S. J., Moon, H. S., Yoo, M. K., Park, I. Y., Kim, B. C., & Cho, C. S. (2008). Chitosan and its derivatives for tissue engineering applications. *Biotechnology Advances*, *26*(1), 1-21.

[16] Agnihotri, S., Mukherji, S., & Mukherji, S. (2012). Antimicrobial chitosan-PVA hydrogel as a nanoreactor and immobilizing matrix for silver nanoparticles. *Applied Nanoscience*, *2*(3), 179-188.

[17] Muzzarelli, R., El Mehtedi, M., Bottegoni, C., Aquili, A., & Gigante, A. (2015). Genipin-crosslinked chitosan gels and scaffolds for tissue engineering and regeneration of cartilage and bone. *Marine Drugs*, *13*(12), 7314-7338.

[18] Moura, M. J., Figueiredo, M. M., & Gil, M. H. (2007). Rheological study of genipin cross-linked chitosan hydrogels. *Biomacromolecules*, *8*(12), 3823-3829.

[19] Kim, G., Kim, N., Kim, D. Y., Kwon, J. S., & Min, B. H. (2012). An electrostatically crosslinked chitosan hydrogel as a drug carrier. *Molecules*, *17*(12), 13704-13711.

[20] Woźniak, A., & Biernat, M. (2022). Methods for

crosslinking and stabilization of chitosan structures for potential medical applications. *Journal of Bioactive and Compatible Polymers*, 37(3), 151-167.

[21] Chenite, A., Chaput, C., Wang, D., Combes, C., Buschmann, M. D., Hoemann, C. D., … F., & Selmani, A. (2000). Novel injectable neutral solutions of chitosan form biodegradable gels in situ. *Biomaterials*, *21*, 2155-2161.

[22] Maiz-Fernández, S., Guaresti, O., Pérez-Álvarez, L., Ruiz-Rubio, L., Gabilondo, N., Vilas-Vilela, J. L., & Lanceros-Mendez, S. (2020). β-Glycerol phosphate/genipin chitosan hydrogels: A comparative study of their properties and diclofenac delivery. *Carbohydrate Polymers*, *248*, 116811.

[23] Kong, M., Chen, X. G., Xing, K., & Park, H. J. (2010). Antimicrobial properties of chitosan and mode of action: A state of the art review. *International Journal of Food Microbiology*, *144*(1), 5163.

[24] Mohamed, N. A., & Abd El-Ghany, N. A. (2012). Synthesis and antimicrobial activity of some novel terephthaloyl thiourea cross-linked carboxymethyl chitosan hydrogels. *Cellulose*, *19*(6), 1879-1891.

[25] Ji, Q. X., Chen, X. G., Zhao, Q. S., Liu, C. S., Cheng, X. J., & Wang, L. C. (2009). Injectable thermosensitive hydrogel based on chitosan and quaternized chitosan and the biomedical properties. *Journal of Materials Science: Materials in Medicine*, *20*(8), 1603-1610.

[26] Niranjan, R., Koushik, C., Saravanan, S., Moorthi, A., Vairamani, M., & Selvamurugan, N. (2013). A novel injectable temperature-sensitive zinc doped chitosan/β-glycerophosphate hydrogel for bone tissue engineering. *International Journal of Biological Macromolecules*, *54*, 24-29.

[27] Chang, H. W., Lin, Y. S., Tsai, Y. D., & Tsai, M. L. (2013). Effects of chitosan characteristics on the physicochemical properties, antibacterial activity, and cytotoxicity of chitosan/2-glycerophosphate/nanosilver hydrogels. *Journal of Applied Polymer Science*, *127*(1), 169-176.

[28] Li, O., Tamrakar, S., Iyigundogdu, Z., Mielewski, D., Wyss, K., Tour, J. M., & Kiziltas, A. (2023). Flexible polyurethane foams reinforced with graphene and boron nitride nanofillers. *Polymer Composites*, *44*(3), 1494-1511.

[29] Iyigundogdu, Z., Kalayci, S., Asutay, A. B., & Sahin, F. (2019). Determination of antimicrobial and antiviral properties of IR3535. *Molecular Biology Reports*, *46*(2), 1819-1824.

[30] Demir, D., Ceylan, S., Gül, G., İyigündoğdu, Z., & Bölgen, N. (2019). Green synthesized silver nanoparticles loaded PVA/Starch cryogel scaffolds with antibacterial properties. *Tehnički Glasnik* [*The Technical Journal*], *13*(1), 1-6.

[31] Iyigundogdu, Z., & Saribas, I. (2022). The effect of various boron compounds on the antimicrobial activity of hardened mortars. *Construction and Building Materials*, *351*, 128958.

[32] Sahin, F., Iyigundogdu, Z., Demir, O., Gulerim, M., & Argin, S. (2022). *Pectin- or Gelatin-Based Antimicrobial Coating* (Patent No. EP 3 494 063 B1).

[33] Reynolds, R. C., Campbell, S. R., Fairchild, R. G., Kisliuk, R. L., Micca, P. L., Queener, S. F., … & Borhani, D. W. (2007). Novel boron-containing, nonclassical antifolates: Synthesis and preliminary biological and structural evaluation. *Journal of Medicinal Chemistry*, *50*(14), 3283-3289.

[34] Benkovic, S. J., Baker, S. J., Alley, M. R. K., Woo, Y., Zhang, Y., Akama, T., … & Shapiro, L. (2005). Identification of borinic esters as inhibitors of bacterial cell growth and bacterial methyltransferases, CcrM and MenH. *Journal of Medicinal Chemistry*, *48*(23), 7468-7476.

[35] Ghammamy, S., & Keysan, S. (2012). Synthesis, characterization, theoretical calculations and biological studies of nano sodium tetrafluoroborate (III). *International Journal of Nano Dimension*, *3*(1), 27-33.

[36] Suner, S. S., Sahiner, M., Akcali, A., & Sahiner, N. (2020). Functionalization of halloysite nanotubes with polyethyleneimine and various ionic liquid forms with antimicrobial activity. *Journal of Applied Polymer Science*, *137*(6), 48352.

[37] Yilmaz, M. T. (2012). Minimum inhibitory and minimum bactericidal concentrations of boron compounds against several bacterial strains. *Turkish Journal of Medical Sciences*, *42*(8), 1423-1429.

[38] Sayin, Z., Ucan, U. S., & Sakmanoglu, A. (2016). Antibacterial and antibiofilm effects of boron on different bacteria. *Biological Trace Element Research*, *173*(1), 241-246.

[39] Dutta, P. K., Tripathi, S., Mehrotra, G. K., & Dutta, J. (2009). Perspectives for chitosan based antimicrobial films in food applications. *Food Chemistry*, *114*(4), 1173-1182.

[40] Stepnowski, P., Skladanowski, A. C., Ludwiczak, A., & Laczyńska, E. (2004). Evaluating the cytotoxicity of ionic liquids using human cell line HeLa. *Human & Experimental Toxicology*, *23*(11), 513-517.

[41] Aydin, H. E., Gunduz, M. K., Kizmazoglu, C., Kandemir, T., & Arslantas, A. (2021). Cytotoxic effect of boron application on glioblastoma cells. *Turkish Neurosurgery*, *31*(2), 206-210.

[42] Kirlangic, Ö. F., Kaya-Sezginer, E., Oren, S., Gur, S., Yavuz, Ö., & Ozgurtas, T. (2022). Cytotoxic and apoptotic effects of the combination of borax (Sodium tetraborate) and 5-fluorouracil on DLD-1 human colorectal adenocarcinoma cell line. *Turkish Journal of Pharmaceutical Sciences*, *19*(4), 371-376.

[43] Hayal, T. B. (2020). Boron increases the viability of human cancer and murine fibroblast cells after long time of cryopreservation. *Trakya University Journal of Natural Sciences*, *21*(2), 11.

[44] Nigoghossian, K., Miyashita, T., Omura, A., Yeroslavsky, G., Kim Dung, D. T., Okubo, K., … & Soga, K. (2020). Infrared to visible upconversion luminescence of trivalent erbium tetrafluoroborate complexes. *Optical Materials Express*, *10*(7), 1749.

[45] Lustriane, C., Dwivany, F. M., Suendo, V., & Reza, M. (2018). Effect of chitosan and chitosan-nanoparticles on post harvest quality of banana fruits. *Journal of Plant Biotechnology*, *45*(1), 36-44.

[46] Venkatesan, J., Jayakumar, R., Mohandas, A., Bhatnagar, I., & Kim, S.-K. (2014). Antimicrobial activity of chitosan-carbon nanotube hydrogels. *Materials*, *7*(5), 3946-3955.

[47] Zheng, L. Y., & Zhu, J. F. (2003). Study on antimicrobial

activity of chitosan with different molecular weights. *Carbohydrate Polymers*, *54*(4), 527-530.

[48] Wang, X., Du, Y., & Liu, H. (2004). Preparation, characterization and antimicrobial activity of chitosan-Zn complex. *Carbohydrate Polymers*, *56*(1), 21-26.

[49] Rhim, J.-W., Hong, S. I., Park, H. M., & Ng, P. K. W. (2006). Preparation and characterization of chitosan-based nanocomposite films with antimicrobial activity. *Journal of Agricultural and Food Chemistry*, *54*(16), 5814-5822.

[50] Ke, C. L., Deng, F. S., Chuang, C. Y., & Lin, C. H. (2021). Antimicrobial actions and applications of chitosan. *Polymers*, *13*(6), 904.

[51] Tyliszczak, B., Drabczyk, A., Kudłacik-Kramarczyk, S., Bialik-Wąs, K., Kijkowska, R., & Sobczak-Kupiec, A. (2017). Preparation and cytotoxicity of chitosan-based hydrogels modified with silver nanoparticles. *Colloids and Surfaces B: Biointerfaces*, *160*, 325-330.

[52] Huang, S. W., Yeh, F. C., Ji, Y. R., Su, Y. F., Su, Y. S., Chiang, M. H., … & Lee, Y. T. (2021). Chitosan-based hydrogels to treat hydrofluoric acid burns and prevent infection. *Drug Delivery and Translational Research*, *11*(4), 1532-1544.

[53] Saita, K., Nagaoka, S., Shirosaki, T., Horikawa, M., Matsuda, S., & Ihara, H. (2012). Preparation and characterization of dispersible chitosan particles with borate crosslinking and their antimicrobial and antifungal activity. *Carbohydrate Research*, *349*, 52-58.

BOR DERGİSİ
JOURNAL OF BORON
https://dergipark.org.tr/boron

Investigation of mechanical properties of Al/Al-B_4C circular hybrid composites

Abdullah Göçer [1,*], **Fehmi Nair** [1]

[1]*Erciyes University, Engineering Faculty, Department of Mechanical Engineering, Kayseri, 38280, Turkiye*

ARTICLE INFO

Article history:
Received May 13, 2023
Accepted April 20, 2023
Available online June 30, 2023

Research Article

DOI: 10.30728/boron.1116270

Keywords:
B_4C
Circular hybrid composite
Extrusion
MMC
Powder in tube (PIT)

ABSTRACT

Hybrid composites are material types obtained by combining two different composite structures. This study focused on investigating the mechanical properties of a hybrid composite material produced in a circular shape with aluminum sheath and metal matrix composite core (Al-Ceramic mixture). Mechanical properties were determined by compression, bending, and hardness tests. Ceramic reinforcement improves the basic mechanical properties of metal matrix composites (MMC). However, some features such as strain ability are adversely affected. It was aimed to improve such properties by producing MMC material with sheath. Al7075 was used as the sheath material and Al2124-B_4C MMC material was used as the core material in this hybrid material. Composite rods were produced by extruding the billets prepared by the PIT (powder in tube) method. With this method, the core material in powder form was compressed into Al tube materials. In the core material, three different ratios of B_4C were used as 5, 10, and 15% by volume fraction. The extrusion process was carried out at 500°C degrees and with an extrusion rate of R=14. According to the test results, the strain ability, which decreased with the B_4C reinforcement, improved in materials produced with sheath.

1. Introduction

Composite materials are material types obtained by combining two or more materials and have the superior properties of these materials [1,2]. Today, many reasons such as developing technology, energy consumption, and material costs reveal the need for composite materials and the studies in this field are increasing day by day. Composite materials consist of the matrix phase that generates the main structure and the reinforcement phase called the secondary phase being in the matrix [3,4]. According to the situation of the reinforcement phase, composite materials can be classified as fiber and particulate reinforced or layered and hybrid composite [5,6]. Hybrid composite materials can find a wide usage area because of the their advantages [7]. Although hybrid composite materials are generally in the form of sheet, they are also produced in circular form such as bars and pipes or other special forms [8,9,10]. Materials used on the inside and outside of the circular hybrid composites vary according to the requirements. Creating a new structure by combining the properties of two different materials or achieving different properties inside and outside of the material is an example of these requirements. When the general structures of circular composites are looked;

- Copper(Cu)-aluminum(Al) material pairs to obtain conductivity, lightness, and cost properties [11-13],

- Al-Al, steel-steel material pairs because of the requirement of the different properties on inside and outside of the composite material [14-16],

- Cu-conductive powder pairs to obtain superconductive material [17],

are the most common circular metal composite materials. In the production of these materials, different methods are used such as extrusion, rolling, and explosive coating [18-20]. In this study, the circular form of Al/Al-B_4C hybrid composite was studied. In this material, while Al-B_4C forms the core of the hybrid composite material, Al forms the sheath. Aluminum has intensive use in the fields of machinery, automotive, and aerospace because of its high strength/density ratio and good machinability properties [21]. At the same time, the studies to improve the properties of composite materials are multiplying. Ceramic reinforced composite is one of these areas in which aluminum is used as the matrix phase [22]. The core of the circular hybrid composite that formed as Al-B_4C, is an MMC material and its density is reduced and some mechanical properties are increased with B_4C reinforcement. However, its toughness, namely the ability of plasticity, decreases.

In this study, materials were produced with a ceramic-free sheath on their outer surfaces in order to eliminate some of the negative results that occur with ceramic

*Corresponding author: abdullahgocer@erciyes.edu.tr

reinforcement in ceramic reinforced metal matrix composite materials. The decrease in surface quality and toughness values is the most important of these negative results. By producing the Al-B_4C composite material with the same or a different aluminum alloy sheath on the outside, the ceramic reinforcement will be prevented from being on the outer surface, and since the aluminum ratio in the material cross-section will be high, its deformation ability will be partially preserved. This material can be preferred in areas where surface quality is at the forefront with its high strength properties.

2. Materials and Methods

The production of circular hybrid rods was carried out by the extrusion method (Figure 1). In this method, the circular cross-section material (billet) was pushed through a die system with high forces. The first stage of production is the preparation of billets. They were prepared with the powder in tube method [23]. Al-B_4C powders mixed homogeneously were compressed into Al tubes in this method (Figure 2).

In these composite materials, the outer of the material is called "sheath" and the inner is called "core". Al7075 alloy as sheath material, Al2124-B_4C powder mixture with an average size of 30 µm Al2124 and 20 µm B_4C as core material was used in these composites. The dimensions of Al tubes (sheath of billet) were presented in Figure 2 and were obtained by drilling the rod-shaped Al7075 alloy. Al2124/B_4C powder mixture was prepared with 5%, 10%, and 15% B_4C volume fractions to be used as core material in these sheaths. The powder mixture was mixed for 2 hours with a three-dimensional mechanical mixer. The powder mixture was compressed into aluminum tubes at an average pressure of 500 kPa. The billets were extruded after the sintering process at 500°C for 1 hour. The diameter of billets was reduced from 30 mm to 8 mm with an extrusion rate of R=14. In each extrusion process, billets, extrusion sleeve and die were spray coated with graphite. In Table 1, the material structure of 9 different billets and products was given in detail. The outer and core diameters of circular hybrid composites were achieved at 8 mm and 5.33 mm respectively.

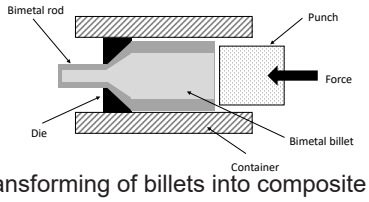

Figure 1. Transforming of billets into composite bars by extrusion method.

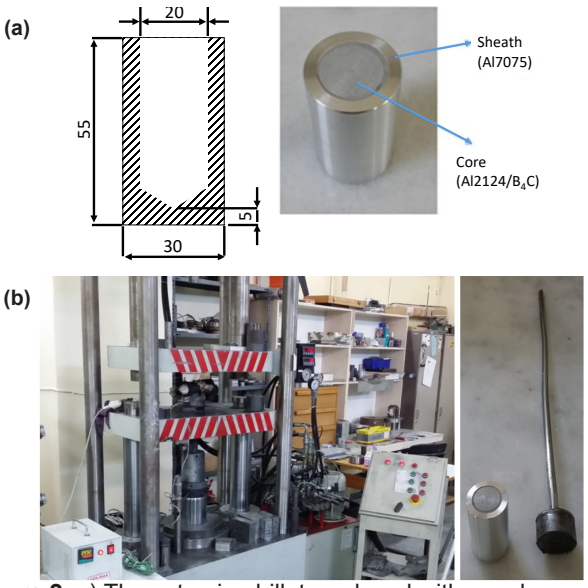

Figure 2. a) The extrusion billet produced with powder in tube method, b) Extrusion press and product (circular hybrid bar).

The samples taken from the composite materials were first mounted and then prepared for micro structural examination. Polishing process was carried out with 600, 1200 and 2000 numbered paper grinding discs and woven polishing cloth. In etching, a general purpose etchant (1,5% Hydrofluoric Acid(HF)-98,5% pure water) was used. On the other hand, bending tests were carried out according to the ISO 7438 standard, and the distance between the supports was determined as 50 mm and the sample length was determined as 80 mm. The test speed was applied as 0.02 mm/sec [24]. Compression tests were carried out according to ASTM E9-09 standard, and compression samples were

Table 1. Technical details of nine different extrusion billets and products.

Samples	Sheath	Core	D_{outlet}-Billet (mm)	D_{inlet}-Billet (mm)	Doutlet-Rod (mm)	D_{inlet}-Rod (mm)
1	Al7075		30	-	8	-
2	Al7075	Al2124	30	20	8	2,66
3	Al7075	Al2124-B_4C(5%)	30	20	8	2,66
4	Al7075	Al2124-B_4C(10%)	30	20	8	2,66
5	Al7075	Al2124-B_4C(15%)	30	20	8	2,66
6	Al2124		30	-	8	-
7	Al2124-B_4C(5%)		30	-	8	-
8	Al2124-B_4C(10%)		30	-	8	-
9	Al2124-B_4C(15%)		30	-	8	-

prepared as 16 mm length by taking L/D=2. The tests were carried out at speeds of 0.02 mm/s [25]. Also, hardness measurements were carried out separately in the sheath and core regions at the cross section perpendicular to the material axis In the tests carried out with the Vickers microhardness measurement method for 5 seconds at 100 g load, at least 3 healthy measurements were obtained at appropriate intervals and the hardness values were determined by taking the average of them. The densities of the materials were measured according to the Archimedes principle [26]. For this, Presica precision balance (with precision of 0,0001 g) and density measurement kit were used.

3. Results and Discussion

When the sheath-core boundaries of hybrid circular composites were examined with a micro-scale, it was observed that the sheath and core were very well bonded to each other, and there was no separation or gap in the boundaries (Figure 3). It was seen that B_4C distribution was homogeneous in B_4C reinforced core (Figure 3b, c, d). In addition, it was observed that the linearity disappeared at the sheath-core boundary with increasing in the B_4C ratio in the core material. The increase in the bond strength between sheath-core could be attributed to the fact that the sheath and core materials crossed each other's boundaries (Figure 3c, d).

The bending test is used to specify the mechanical properties of materials under loads that force them to bend. In this test, a bending force is applied to the middle of the material placed between two supports and the material is deformed. As a result of this experiment, values such as bending moment, bending strength, modulus of elasticity, and bending displacement can be calculated [27]. According to the bending tests, first of all, the bending strengths of the aluminum materials used in this study were compared with each other. The Al7075 rod was produced by extrusion from a rod product with a diameter of 30 mm. Al2124 rod was produced by extruding of billets obtained by compressing the Al2124 powder used in MMC production. According to the bending test graphics, Al2124 has lower bending strength and strain rate than Al7075 (Figure 4a). When the material was layered as Al7075-Al2124, although the deformation did not increase, a significant increase in bending strength was achieved.

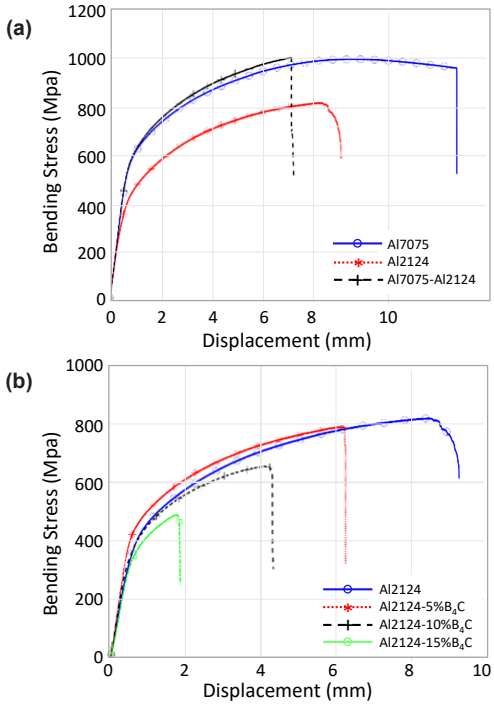

Figure 4. a) Bending stress-displacement (σ-δ) curves of Al7075 and Al2124 rods and Al7075/Al2124 circular composite, b) Changing of σ-δ curves with B_4C ratio in circular composites.

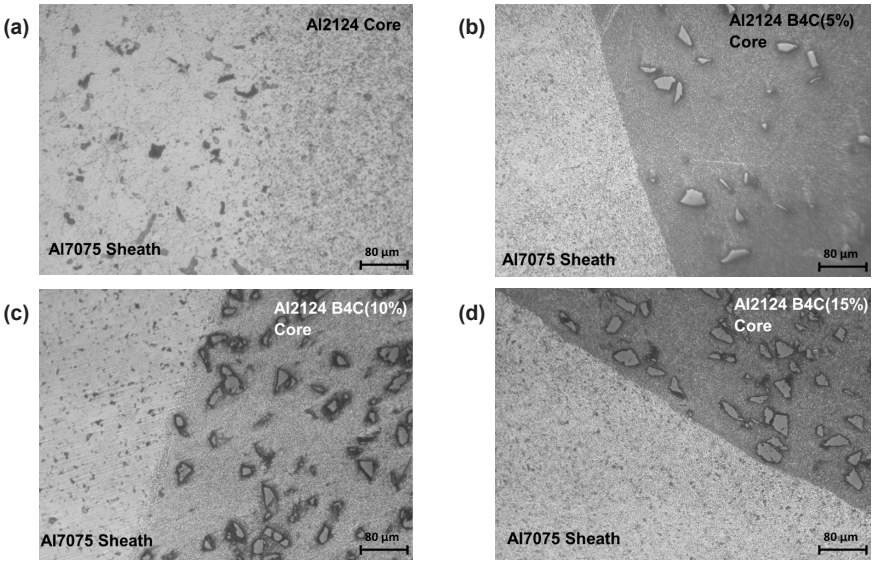

Figure 3. Optical microscope images of sheath-core boundary in hybrid composite materials, a) Al7075-Al2124 sheath-core boundary, b) Al7075-Al2124/B_4C (5%) sheath-core boundary, c) Al7075-Al2124/B_4C (10%) sheath- core boundary, d) Al7075-Al2124/B_4C (15%) sheath-core boundary.

In ceramic reinforced composites, the strength values of the materials can be improved considerably by optimum adjustment of the reinforcement ratio. However, high ceramic ratios increase the brittleness of the material as well as decrease the strength values [28]. As can be seen in Figure 4b, the material with B_4C ratio of 5% provided superiority in terms of yield strength compared to Al2124, while the material rapidly loosed its strength and deformability with an increase in this ratio to 15%. The poor wettability between Al and B_4C is also an important factor in this situation [29,30].

When the rods containing B_4C of 5%, 10%, and 15% were turned into hybrid composites with Al 7075 sheath, significant changes occurred in their mechanical properties, with an increase of approximately 25%, 45%, and 90% in yield and breaking points, respectively. In other words, the bending strengths of MMCs could be improved with the hybrid composite structure. And this improvement rate increased with increasing in B_4C ratio (Figure 5a, b, c, d).

The analysis of the bending samples reveals that the fracture cross-sections were shaped in different structures depending on the bending rate and the bending ability of the material. Al7075 was the material that have the most strain, and it showed a brittle fracture surface because of its structure (Figure 6a). On the other hand, Al2124 displayed multiple fractures with a smooth surface because of its ductility (Figure 6a). The fracture surface in Al2124-B_4C composites was quite rough and brittle because of the separation that occurred at the B_4C-Al grain interfaces (Figure 6b). The limited bending deformation observed in Al2124-B_4C composites reinforced B_4C of 5% was almost never observed in composites containing 10% and 15% B_4C, and their fracture types were quite similar to the type of brittle fracture encountered in tensile tests (Figure 6b). The fracture behavior of the materials changed with the Al7075 sheath. In Al7075-Al2124 material, the bending deformation of both layers decreased (Figure 6a). In Al7075/Al2124-B_4C sheathed composites, the Al7075 sheath increased the bending strength and the bending strain rates of the composites significantly (Figure 6c). In the bending tests, the punch forces to separate the interfaces of sheathed composites because of the application type. However, no separation was observed between the sheath and core in the tests of the Al7075/Al2124-B_4C composites.

According to the compression test results, the yield strengths of the materials increased with the increase of B_4C ratio in Al2124-B_4C composites, but the compression strength and strain rate decreased (Figure 7b). It was observed that Al7075 material was better than Al2124 in terms of strength values (Figure 7a). The yield strength of the composites, which was produced in Al7075/Al2124 form with sheath, reached the Al7075. In the circular hybrid composite materials, the yield strengths increased in each one. However, these hybrid composite materials lost some of their strain rates compared to the MMC ones. In terms of compression strength, the hybrid composite materials containing 5% B_4C was very close to the unsheathed one. However, hybrid composites containing 10% and 15% B_4C exceeded the unsheathed form of these materials in terms of compression strength. The tensile strengths of hybrid composites were above those of unsheathed ones (Figure 7c, d, e).

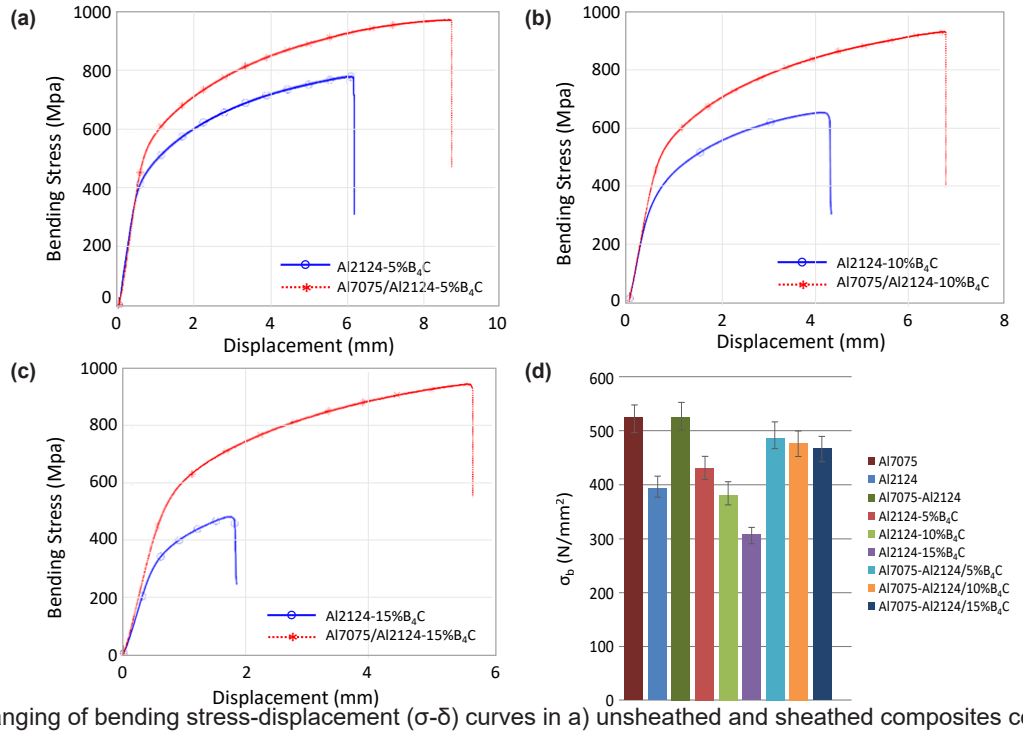

Figure 5. Changing of bending stress-displacement (σ-δ) curves in a) unsheathed and sheathed composites containing 5% B_4C, b) unsheathed and sheathed composites containing 10% B_4C, c) unsheathed and sheathed composites containing 15% B_4C, d) changing of bending strength of sheathed and unsheathed composites.

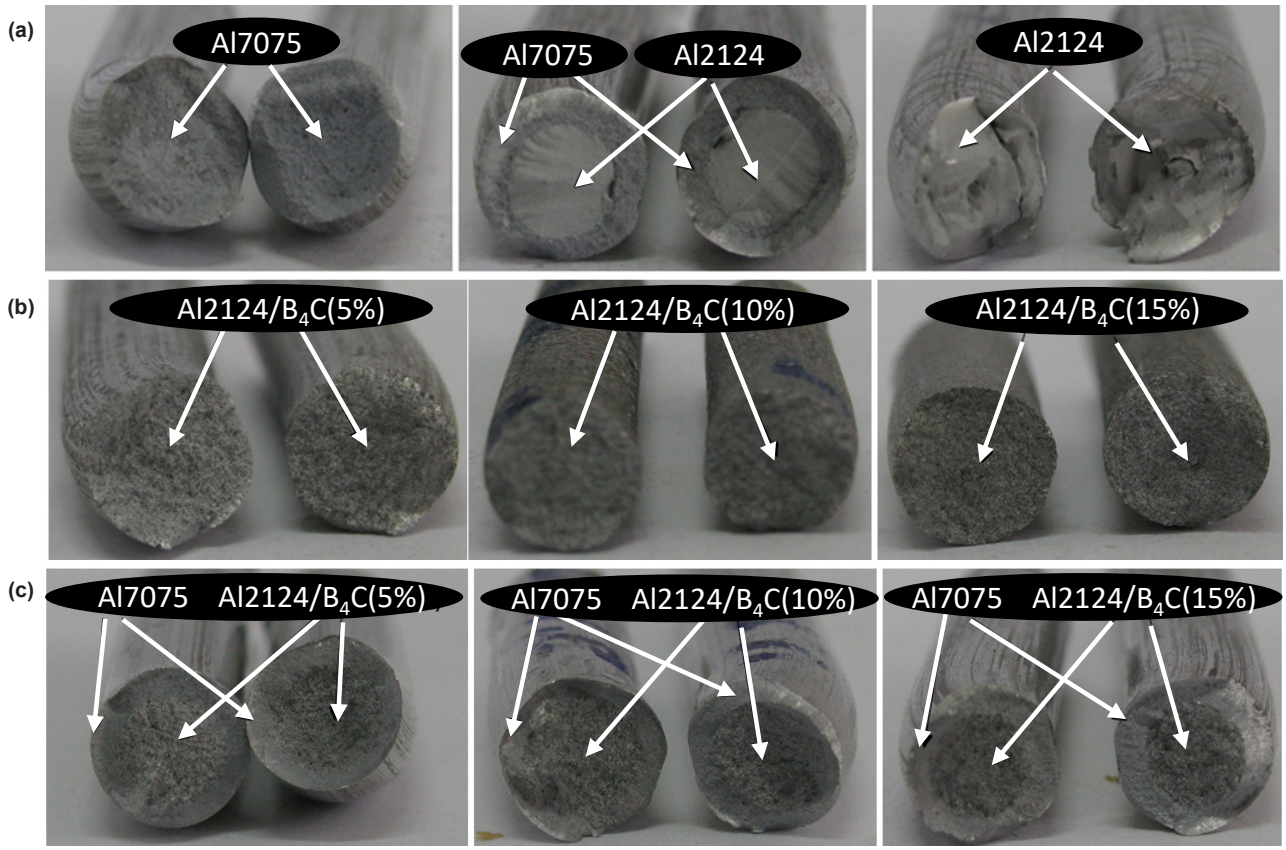

Figure 6. The fracture types of materials subjected to bending test, a) Al7075, Al7075-Al2124 and Al2124, b) Al2124-B_4C (5%), Al2124-B_4C (10%) and Al2124-B_4C (15%). c) Al7075-Al2124-B_4C (5%), Al7075-Al2124-B_4C (10%) and Al7075-Al2124 (15%).

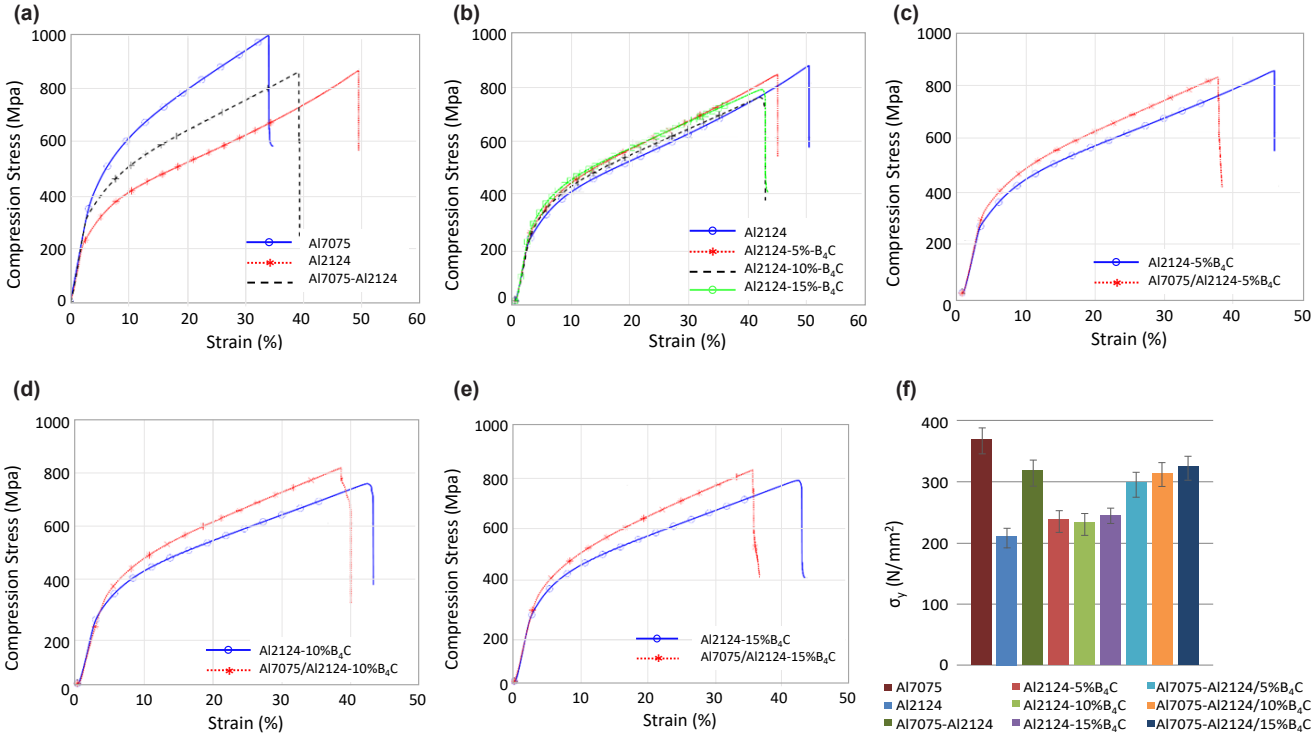

Figure 7. The changing of compression stress-strain % (σ-ε%) curves in a) Al7075, Al2124, and Al7075/Al2124 MM composites b) MM composite materials with B_4C ratio, c) Hybrid and MM composites containing 5% B_4C, d) Hybrid and MM composites containing 10% B_4C, e) Hybrid and MM composites containing 15% B_4C, f) changing of yield strength of sheathed and unsheathed composites.

According to the fracture types seen in the compression samples [31], an evaluation can be made on the deformation ability of the materials (Figure 8).

Figure 8. Fracture types seen at compression tests a) Failure by barreling, b) Brittle fracture, c) Semi-brittle fracture.

From the observation of the fracture structures of the compression test specimens, it was noticed that Al2124 and Al2124-B_4C (5%) materials showed semi-brittle fracture behavior (Figure 9a). Al7075 is a popular aluminum alloy with high strength and brittle structure. Therefore, the fracture behavior of Al7075 and Al7075 sheathed composites was in the brittle type (Figure 9b). In Al2124-B_4C composites, the semi-brittle fracture type turned into brittle fracture with increasing in B_4C ratio from 5% to 10% and 15% (Figure 9c). Also, the fracture behavior of materials and σ-ε curves were compatible with each other.

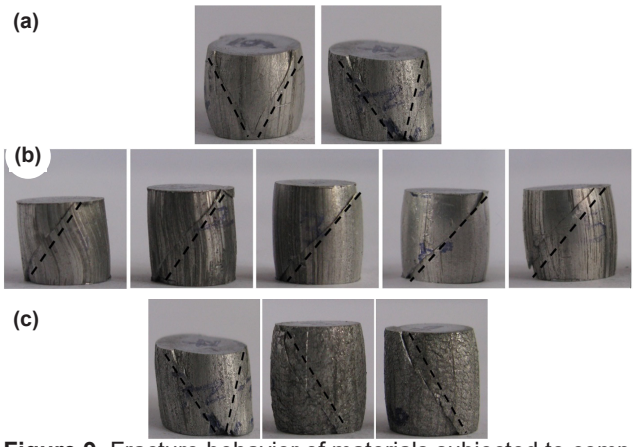

Figure 9. Fracture behavior of materials subjected to compression test, a) Semi-brittle fracture behavior of Al2124 and Al2124-B_4C (5%), b) Brittle fracture behavior of Al7075, Al7075-Al2124, Al7075-Al2124-B_4C (5%), Al7075-Al2124-B_4C (10%) and Al7075-Al2124 (15%), c) Fracture behavior of Al2124-B_4C (5%), Al2124-B_4C (10%) and Al2124-B_4C (15%).

Aluminum, MM composite, and laminated composite bars were subjected to tests after the extrusion process and any heat treatment did not apply to them after extrusion. When the hardness tests of these materials were examined, it was seen that Al7075 had a higher hardness value than Al2124 and A2124-B_4C composites because of its alloy structure (Figure 10b). In Al2124-B_4C composites, the hardness values of MM composites increased with increasing in B_4C ratio (Figure 10a) [32]. In the hardness tests performed on hybrid composite materials, the hardness values of the sheath and core material were different from unsheathed materials. The sheath and core hardness of Al7075-Al2124 material were slightly higher than other hybrid composites. In Al7075-Al2124/B_4C composites, the hardness of sheath and core increased with the increase in the B_4C ratio in the core material (Figure 10b). When the density of the materials was examined, the density decreased with B_4C reinforcement and with increasing the B_4C ratio [33]. In materials that became hybrid composite with Al7075 sheath, the densities increased slightly compared to MMC materials (Figure 10c).

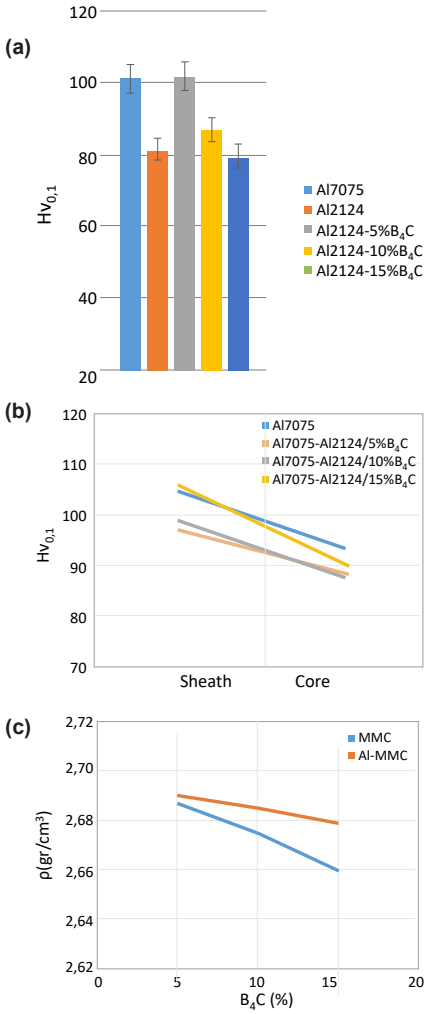

Figure 10. a) Changing of hardness values of Al7075, Al2124 and Al2124-B_4C materials, b) Sheath-core hardness changing of sheath-core materials in hybrid composites, c) Density changing in Al2124-B_4C and Al7075-Al2124/B_4C composites depending on the B_4C ratio.

4. Conclusions

According to the bending and compression tests of metal matrix composites (MMC) and hybrid composites;

- The composite materials produced in Al7075/Al2124 form had better strength values under bending loads

compared to Al2124.

- While the B_4C ratio was 5% in Al2124/B_4C MMC materials, it was found that the bending strength increased and the strain rate decreased compared to Al2124. With the increase of the B_4C ratio to 10% and 15%, both strength values and strain rates decreased rapidly.

- The bending strength and strain ability of circular hybrid composites increased considerably compared to unsheathed ones, and the highest increase occurred in composite material containing 15% B_4C.

- With the increase of the B4C ratio in MM composites, the yield strength values of the materials increased, but the compression strength and strain rate decreased.

- It was observed that the Al7075 material was better than Al2124 in compression strength values. The yield strengths of the composite materials produced in Al7075/Al2124 form approached to the strength of the Al7075.

- The yield strengths of the hybrid composite materials increased in each form. Hybrid composite materials loosed some of their strain rates compared to unsheathed ones. In the compression strength, the hybrid material containing 5% B_4C was very close to the unsheathed one. However, the compression strength of hybrid composites containing 10% and 15% B_4C exceeded unsheathed ones.

- Microstructurally, the materials were examined to see the sheath-core boundary region. Microstructure images showed that Al7075 and Al2124 alloys fully bonded with each other and a gapless boundary region was formed. From these images, it was determined that the B_4C dispersion in the core region is generally homogeneous.

- Hardness tests shown that the hardness of the Al7075 sheath material is higher than the Al2124 core matrix material. In addition to this, it was observed that the hardness of the core region increased with the B_4C reinforcement and the increasing of the reinforcement ratio. The density value of the core material, whose density decreased with the B_4C reinforcement and increasing the reinforcement ratio, continued to decrease with the Al7075 sheath. However, the density decrease in these materials was more limited compared to the unsheathed material.

References

[1] Ramanathan, A., Krishnan, P. K., & Muraliraja, R. (2019). A review on the production of metal matrix composites through stir casting-Furnace design, properties, challenges, and research opportunities. *Journal of Manufacturing Processes*, *42*, 213-245. https://doi.org/10.1016/j.jmapro.2019.04.017.

[2] Nedelcu, D., & Carcea, I. (2013). Technology for obtaining samples of layered composite materials with metallic matrix. *Metals and Materials International*, *19*(1), 105-112. https://doi.org/10.1007/s12540-013-1017-2.

[3] Garg, P., Jamwal, A., Kumar, D., Sadasivuni, K. K., Hussain, C. M., & Gupta, P. (2019). Advance research progresses in aluminium matrix composites: manufacturing & applications. *Journal of Materials Research and Technology*, *8*(5), 4924-4939. https://doi.org/10.1016/j.jmrt.2019.06.028.

[4] Liao, Z., Abdelhafeez, A., Li, H., Yang, Y., Diaz, O. G., & Axinte, D. (2019). State-of-the-art of surface integrity in machining of metal matrix composites. *International Journal of Machine Tools and Manufacture*, *143*(February), 63-91. https://doi.org/10.1016/j.ijmachtools.2019.05.006.

[5] Rajak, D. K., Pagar, D. D., Kumar, R., & Pruncu, C. I. (2019). Recent progress of reinforcement materials: A comprehensive overview of composite materials. *Journal of Materials Research and Technology*, *8*(6), 6354-6374. https://doi.org/10.1016/j.jmrt.2019.09.068.

[6] Saidi, H., Roudini, G., & Afarani, M. S. (2015). High-volume-fraction Cu/Al2O3–SiC hybrid interpenetrating phase composite. *Applied Physics A: Materials Science and Processing*, *121*(1), 109-113. https://doi.org/10.1007/s00339-015-9392-9.

[7] Garg, A., & Chalak, H. D. (2019). A review on analysis of laminated composite and sandwich structures under hygrothermal conditions. *Thin-Walled Structures*, *142*(March), 205-226. https://doi.org/10.1016/j.tws.2019.05.005.

[8] Priel, E., Ungarish, Z., & Navi, N. U. (2016). Co-extrusion of a Mg/Al composite billet: A computational study validated by experiments. J*ournal of Materials Processing Technology*, *236*, 103-113. https://doi.org/10.1016/j.jmatprotec.2016.05.007.

[9] Lee, K. S., Yoon, D. H., Kim, H. K., Kwon, Y. N., & Lee, Y. S. (2012). Effect of annealing on the interface microstructure and mechanical properties of a STS-Al-Mg 3-ply clad sheet. *Materials Science and Engineering A*, *556*, 319-330. https://doi.org/10.1016/j.msea.2012.06.094.

[10] Tanks, J., Sharp, S., & Harris, D. (2016). Charpy impact testing to assess the quality and durability of unidirectional CFRP rods. *Polymer Testing*, *51*, 63-68. https://doi.org/10.1016/j.polymertesting.2016.02.009.

[11] Sapanathan, T., Khoddam, S., & Zahiri, S. H. (2013). Spiral extrusion of aluminum/copper composite for future manufacturing of hybrid rods: A study of bond strength and interfacial characteristics. *Journal of Alloys and Compounds*, *571*, 85-92. https://doi.org/10.1016/j.jallcom.2013.03.210.

[12] Lee, K. S., & Kwon, Y. N. (2013). Solid-state bonding between Al and Cu by vacuum hot pressing. *Transactions of Nonferrous Metals Society of China (English Edition)*, *23*(2), 341-346. https://doi.org/10.1016/S1003-6326(13)62467-X.

[13] Khosravifard, A., & Ebrahimi, R. (2010). Investigation of parameters affecting interface strength in Al/Cu clad bimetal rod extrusion process. *Materials and Design*, *31*(1), 493-499. https://doi.org/10.1016/j.matdes.2009.06.026.

[14] Son, I. S., Lee, S. P., Lee, J. K., Kim, W. C., Moon, J. S., Lee, S., Lee, J. S., Kim, Y. B., Lee, G. A., & Bae, D. S. (2014). Effect of hydro co-extrusion on

microstructure of duo-cast Al 3003/Al 4004 clad materials. *Transactions of Nonferrous Metals Society of China*, *24*(SUPPL. 1), s75-s80. https://doi.org/10.1016/S1003-6326(14)63291-X.

[15] Zhang, S., Xiao, H., Xie, H., & Gu, L. (2014). The preparation and property research of the stainless steel/iron scrap clad plate. *Journal of Materials Processing Technology*, *214*(6), 1205-1210. https://doi.org/10.1016/j.jmatprotec.2014.01.006.

[16] Lee, J. S., Son, H. T., Oh, I. H., Kang, C. S., Yun, C. H., Lim, S. C., & Kwon, H. C. (2007). Fabrication and characterization of Ti-Cu clad materials by indirect extrusion. *Journal of Materials Processing Technology*, *187-188*, 653-656. https://doi.org/10.1016/j.jmatprotec.2006.11.144.

[17] Chou, I., & Hung, C. (1999). The finite-element study on extrusion of powder_solid composite clad rods-*ScienceDirect*. *96*, 124-132.

[18] Berski, S., Dyja, H., Maranda, A., Nowaczewski, J., & Banaszek, G. (2006). Analysis of quality of bimetallic rod after extrusion process. *Journal of Materials Processing Technology*, *177*(1-3), 582-586. https://doi.org/10.1016/j.jmatprotec.2006.04.107.

[19] Guo, X., Tao, J., Wang, W., Li, H., & Wang, C. (2013). Effects of the inner mould material on the aluminium-316L stainless steel explosive clad pipe. *Materials and Design*, *49*, 116-122. https://doi.org/10.1016/j.matdes.2013.02.001.

[20] Chen, G., Li, J. T., Yu, H. L., Su, L. H., Xu, G. M., Pan, J. S., You, T., Zhang, G., Sun, K. M., & He, L. Z. (2016). Investigation on bonding strength of steel/aluminum clad sheet processed by horizontal twin-roll casting, annealing and cold rolling. *Materials and Design*, *112*, 263-.274. https://doi.org/10.1016/j.matdes.2016.09.061

[21] Asgari, M., & Fereshteh-Saniee, F. (2016). Production of AZ80/Al composite rods employing non-equal channel lateral extrusion. *Transactions of Nonferrous Metals Society of China (English Edition)*, *26*(5), 1276-1283. https://doi.org/10.1016/S1003-6326(16)64228-0.

[22] Malaki, M., Tehrani, A. F., & Niroumand, B. (2020). Fatgiue behavior of metal matrix nanocomposites. *Ceramics International*, *46*(15), 23326-23336. https://doi.org/10.1016/j.ceramint.2020.06.246.

[23] Zhao, K.N., Xu, D.X., Li, H.X., Zhang, J.S., Chen, D.L. (2019). Microstructure and mechanical properties of Mg/Mg bimetal composites fabricated by hot-pressing diffusion and co-extrusion. *Materials Science & Engineering A*, *764*. https://doi.org/10.1016/j.msea.2019.138194.

[24] Taherishargh, M., Vesenjak, M., Belova, I. V., Krstulović-Opara, L., Murch, G. E., & Fiedler, T. (2016). In situ manufacturing and mechanical properties of syntactic foam filled tubes. *Materials and Design*, *99*, 356-368. https://doi.org/10.1016/j.matdes.2016.03.077.

[25] Aherwar, A., Patnaik, A., & Pruncu, C. I. (2020). Effect of B4C and waste porcelain ceramic particulate reinforcements on mechanical and tribological characteristics of high strength AA7075 based hybrid composite. J*ournal of Materials Research and Technology*, *9*(5), 9882-9894. https://doi.org/10.1016/j.jmrt.2020.07.003.

[26] De Terris, T., Andreau, O., Peyre, P., Adamski, F., Koutiri, I., Gorny, C., & Dupuy, C. (2019). Optimization and comparison of porosity rate measurement methods of Selective Laser Melted metallic parts. *Additive Manufacturing*, *28*(June), 802-813. https://doi.org/10.1016/j.addma.2019.05.035.

[27] Javdanil, A., & Daei-Sorkhabi, A. H. (2018). Microstructural and mechanical behavior of blended powder semisolid formed Al7075/B4C composites under different experimental conditions. *Transactions of Nonferrous Metals Society of China*, *28*(7), 1298-1310. https://doi.org/10.1016/S1003-6326(18)64767-3.

[28] Ghasali, E., Alizadeh, M., Ebadzadeh, T., Pakseresht, A. H., & Rahbari, A. (2015). Investigation on microstructural and mechanical properties of B4C-aluminum matrix composites prepared by microwave sintering. *Journal of Materials Research and Technology*, *4*(4), 411-415. https://doi.org/10.1016/j.jmrt.2015.02.005.

[29] Rıfat, Y., & Nilhan, Ü. T. (2019). Production of AA5754/B4C composite materials by the semi-solid stirring method. *Technological Applied Sciences*, *14* (22018), 57-67. https://doi.org/10.12739/NWSA.2019.14.2.2A0169.

[30] Wu, H., Zeng, F., Yuan, T., Zhang, F., & Xiong, X. (2014). Wettability of 2519Al on B4C at 1000-1250 C and mechanical properties of infiltrated B4C-2519Al composites. *Ceramics International*, *40*(1 PART B), 2073-2081. https://doi.org/10.1016/j.ceramint.2013.07.120.

[31] Erdem, Y. (2010). *Çelik Talaşı/Silikon Kompozit Malzeme Üretimi ve Düşük Hızlı Darbe Özelliklerinin Deneysel İncelenmesi*. [Yüksek Lisans Tezi, Selçuk Üniversitesi].

[32] Deuis, R. L., Subramanian, C., & Yellup, J. M. (1996). Abrasive wear of aluminium composites-A review. *Wear*, *201*(1-2), 132-144. https://doi.org/10.1016/S0043-1648(96)07228-6.

[33] Canakci, A., & Arslan, F. (2012). Abrasive wear behaviour of B4C particle reinforced Al2024 MMCs. *International Journal of Advanced Manufacturing Technology*, *63*(5-8), 785-795. https://doi.org/10.1007/s00170-012-3931-8.

BOR DERGİSİ
JOURNAL OF BORON
https://dergipark.org.tr/boron

Aktif karbon destekli ucuz ve kullanışlı katalizörün amonyak bor hidrolizinde incelenmesi

Hatice Beştaş [1], Erhan Onat [1], Ömer Şahin [2], Sevilay Demirci [3,*], Orhan Baytar [1], Mehmet Sait İzgi [1]

[1]*Siirt Üniversitesi, Mühendislik Fakültesi, Kimya Mühendisliği Bölümü, Siirt, 56100, Türkiye*
[2]*İstanbul Teknik Üniversitesi, Mühendislik Fakültesi, Kimya Mühendisliği Bölümü, İstanbul, 34467, Türkiye*
[2]*Kafkas Üniversitesi, Mühendislik Mimarlık Fakültesi, Kimya Mühendisliği Bölümü, Kars, 36000, Türkiye*

MAKALE BİLGİSİ

Makale Geçmişi:
İlk gönderi 23 Eylül 2022
Kabul 25 Nisan 2023
Online 30 Haziran 2023

Araştırma Makalesi

DOI: 10.30728/boron.1179156

Anahtar kelimeler:
Amonyak boran
CuMoB
Hidrojen
Hidroliz

ÖZET

Bu çalışmada ilk kez kahve çekirdeği atığından (kahve telvesinden) elde edilen aktif karbon kullanılarak CuMoB/AC katalizörü sentezlenmiştir. Burada en iyi katalitik performanslarını belirlemek amacıyla; Cu:Mo oranı, Metal/AC oranı, optimum NaOH oranı, katalizör miktarı, en uygun NH_3BH_3 oranı ve farklı sıcaklıklarda yapılan deneyler sonucunda da reaksiyon kinetiği çıkarılarak reaksiyonun derecesinin n. dereceden (0.9) olduğu ve aktivasyon enerjisinin de 34,89 kJ/mol olduğu belirlenmiştir. Aynı zamanda katalizörün karakterizasyonu SEM-EDS, XRD ileri analitiksel yöntemlerle yapılarak SEM-EDS analizlerinde Cu ve Mo metallerinin aktif karbona başarıyla tutunduğu görülmüştür.

Investigation of cheap and useful activated carbon supported catalyst in ammonia boron hydrolysis

ARTICLE INFO

Article History:
Received September 25, 2022
Accepted April 25, 2023
Available online June 30, 2023

Research Article

DOI: 10.30728/boron.1179156

Keywords:
Ammonia borane
CuMoB
Hydrogen
Hydrolysis

ABSTRACT

In this study, CuMoB/AC catalyst was synthesized for the first time by using activated carbon obtained from coffee bean waste (coffee grounds). In order to determine the best catalytic performances; Cu:Mo ratio, Metal/AC ratio, optimum NaOH ratio, catalyst amount, optimum NH_3BH_3 ratio and reaction kinetics were determined as a result of experiments performed at different temperatures. It was determined that the degree of the reaction was n. degree (0.9) and the activation energy was 34.89 kJ/mol. At the same time, the catalyst was determined using SEM-EDS, XRD advanced analytical methods to determine the characterization.

1. Giriş (Introduction)

Son yıllarda artan enerji krizi ile birlikte fosil yakıtların çevreye verdiği zararlar göz önüne alındığında temiz ve yenilenebilir enerjinin önemi günden güne artmaktadır [1-3]. Bu bağlamda temiz ve yenilenebilir enerjiler arasında hidrojen, en iyi alternatif enerji taşıyıcılarından biri olarak kabul edilmektedir. Hidrojen evrende en bol bulunan elementtir. Ancak yeryüzünde kendi başına bulunmadığı halde başka kaynaklardan üretilmesi gerekecektir. Bu nedenle hidrojen bir enerji taşıyıcısı olarak kabul edilir. Doğal gaz, kömür, su ve yenilenebilir enerji kaynakları gibi çeşitli bol öncülerden üretilebilir. Hidrojen çeşitli enerji kaynaklarından üretilir, depolanır, taşınır ve endüstrilerde kullanılır. Hidrojen, yakıt hücreleri kullanılarak tekrar faydalı enerjiye dönüştürülebilir [4-9]. Hidrojen kaynakları arasında da son zamanlarda bor hidrürler öne çıkmaktadır. Son zamanlarda amonyak boran (AB) gelecek vaat eden bir hidrojen kaynağı olarak kabul edilmiştir [10-15]. Bunun en önemli özelliklerden bazıları; hidrojen içeriğinin ağırlıkça %19,6 olması, toksik olmaması ve aynı zamanda oda sıcaklığında kararlı olması nedeniyle öne çıkmaktadır. Borhidrürlerden

*Corresponding author: incesevilay@gmail.com

sodyum borhidrür ile ilgili birçok çalışma yapılmasına karşın amonyak boran ile ilgili pek fazla bir çalışma mevcut değildir [16]. Amanyok boranın hidroliziyle oda sıcaklığında hidrojen üretim hızı yüksek ve ucuz katalizörler geliştirmek oldukça önemlidir [15,17-25].

Literatürde yapılan çalışmalara bakıldığında genellikle Rh, Pd, Pt gibi değerli metallerle katalizörler geliştirilerek çalışmalar yapılmıştır [15,21-24]. Ancak, bu değerli metallerin ekonomik açıdan maliyetleri bakımından kullanımları sınırlı olduğundan ucuz, kullanışlı ve aktiviteleri bu değerli metallere yakın katalizörlerin geliştirilmesi gerekmektedir. Bunlardan bazıları Ni, Co, Cu, Cr, Mo gibi metallerden oluşan katalizörlerdir [5,26-31]. Bu metallerden Co-B, Ni-B, Co-Cu-B, Co-Cr-B gibi ucuz kullanışlı ve katalitik aktiviteleri yüksek katalizörler sentezlenerek bunların amonyak boran ile hidrolizindeki hidrojen üretimleri incelenmiştir. Bununla birlikte son yıllarda katalizördeki partiküllerin homojen dağılmasını sağlamak için destek malzemesi kullanılmaktadır. Bu sayede hem katalizörün yüzey alanı artar hem de katalizörün katalitik aktivitesini artırarak hidrojen üretim hızını artırır. Destek malzemeleri arasında; Karbon nanotüp (CNT), Alüminyum oksit (Al_2O_3), aktif karbon (AC), grafen (G), polimer yapılı malzemeler (Eupergit), metal organik yapılı (MOF) ve Karbon kuantum noktaları (CQD) gibi malzemeler kullanılmaktadır [5,16,32-36]. Bununla birlikte metallere desteklerin eklenmesi ile ekonomik açıdan daha ucuz ve kullanışlı olur [37].

Bu çalışmada ilk kez kahve çekirdeği atığından elde edilen aktif karbon kullanılarak CuMoB/AC katalizörü sentezlenmiştir. Burada katalizörün yapısına eklenen Molibdenin (Mo), katalizörün amonyak boran ile hidrolizinden elde edilen hidrojen üretimini arttırdığı belirlenmiştir. Burada en iyi katalitik performanslarını belirlemek amacıyla; Cu:Mo oranı, Metal/AC oranı, optimum NaOH oranı, katalizör miktarı, en uygun NH_3BH_3 oranı ve farklı sıcaklıklarda yapılan deneyler sonucunda da reaksiyon kinetiği çıkarılarak reaksiyonun derecesi ve aktivasyon enerjisi belirlenmiştir. Aynı zamanda katalizörün karakterizasyonu için XRD, SEM gibi ileri teknikler kullanılmıştır.

2. Malzemeler ve Yöntemler (Materials and Methods)

2.1. Katalizör Sentezi (Catalyst Synthesis)

Kahve telvesinden iki kademeli H_3PO_4 aktifleştiricisi kullanılarak kimyasal aktivasyon yöntemiyle aktif karbon sentezlenmiştir. İmpragnasyon oranı; 70°C impragnasyon(ön işlem) sıcaklığı, 3 saat impragnasyon süresi, 400°C aktivasyon sıcaklığı ve 30 dk aktivasyon süresi parametreleri varlığında incelenmiş ve impragnasyon oranının iyot sayısı ile belirlenmiştir. Ön işlem sıcaklığı ise; 8 impragnasyon oranı, 3 saat impragnasyon süresi, 400°C aktivasyon sıcaklığı ve 30 dk aktivasyon süresi parametreleri varlığında incelenmiş ve ön işlem sıcaklığının iyot sayısı ile değişimi belirlenmiştir. Elde edilen aktif karbon alınarak deneylerde kullanılmak üzere farklı oranlarda emdirme yöntemiyle metaller eklenmiştir.

Katalizör hazırlamanın 2. aşamasında ise 50 ml etanol içerisine (X_M=M/(Cu+M)) molar cinsinden olacak şekilde $CuSO_4.5H_2O$ ve $(NH_4)_6Mo_7O_{24}$ koyduktan sonra çözününceye kadar farklı oranlarda karıştırılmıştır. Sonrasında farklı oranlarda AC eklenmiş ve 24 saat karıştırmaya bırakılmıştır. 24 saat sonunda alkol uçurularak elde edilen çamurumsu karışıma 50 ml saf su ilave edilerek buz banyosuna alınmış ve 0-5°C dereceye kadar sıcaklığı düşürülmüştür. Daha sonra azot ortamında önceden hazırlanan $NaBH_4$ çözeltisi yavaş yavaş damlatılmıştır. Reaksiyon sonunda elde edilen Cu-Mo-B/AC katalizörü süzülmüştür. Etanol ve saf su ile birkaç kez yıkandıktan sonra 80°C'de azot gazı ortamında 2 saat kurutulmuştur. NH_3BH_3 hidrolizinde kullanılmak üzere kapalı kapta muhafazaya alınmıştır.

2.2. Katalizörün Karakterizasyonu (Characterization of the Catalyst)

Elde edilen katalizör numunesi için; SEM görüntüleme, FEI marka QUANTA FEG 250 ESEM model çevresel taramalı elektron mikroskobunda, 25 kV voltaj ve 6 spot değerlerinde ETD dedektörü ile yüksek vakumda yapılmıştır. Yüzey alanları azot izotermi üzerinden Brunauere EmmetteTeller (BET) yöntemi kullanılarak hesaplanmış ve gözenek boyutu dağılımları, Barrett Joyner Halenda (BJH) yöntemine göre belirlenmiştir. Örneklerin mikro yapılarını ve bileşimlerini analiz etmek için geçirimli elektron mikroskobu (TEM, Tecnai F20, Philips) ve karşılık gelen enerji dağılımlı X-ışını spektroskopisi (EDX) uygulandı. X-ışını kırınımı (XRD), Cu Kα radyasyonu (α=1.54056 Å) ile bir Rigaku RINT-2000 X-ışını kırınım ölçer üzerinde gerçekleştirilmiştir. Debby-Scherrer eşitliği [38] kullanılarak Cu-Mo-B/AC katalizörünün ortalama partikül boyutu hesaplanmıştır.

3. Sonuçlar ve Tartışma (Results and Discussion)

3.1. Malzeme Karakterizasyonu (Material Characterization)

3.1.1. BET karakterizasyonu (BET characterization)

Sentezlenen CuMoB/AC katalizörün yüzey alanı Bruauner-Emmett-Teller (BET) metodu ile yaklaşık -196°C'de adsorbsiyonu ile belirlenerek hem aktif karbonun hem de destekli katalizörün yüzey alanı belirlenmiştir. Burada aktif karbonun yüzey alanı 4,74 m^2/g iken desteksiz CuMoB katalizörün 33,873 m^2/g, destekli CuMoB/AC katalizörün yüzey alanı 13,655 m^2/g olduğu görülmektedir. Bunun muhtemel sebebi, elde edilen aktif karbonun gözeneklerinin mikro yapıda olmasından dolayı CuMoB katalizörünün buradaki mikro gözenekleri kapatmasından kaynaklanmaktadır. Destekli katalizörlerle yapılan çalışmaların çoğunda bu durum gözlenmektedir. Yani; bazı destek malzemeleri üzerine Co ilave edilerek, eklenen Co partiküllerinin destek malzemesinin gözeneklerini doldurarak destek malzemesinin yüzey alanını küçültüldüğü belirtilmektedir [39].

3.1.2. SEM karakterizasyonu (SEM characterization)

Bu çalışmada üretilmiş olan katalizörün morfolojik yapısını belirlemek amacıyla SEM analizi yapılmıştır. Şekil 1'de aktif karbon ve buna bağlı olarak CuMoB/AC katalizörünün görüntüsü verilmiştir. Şekilden görüleceği üzere CuMoB katalizörünün aktif karbon üzerinde düzensiz ve pürüzlü olarak dağıldığını ayrıca buradaki mikro gözenekli olan aktif karbon boşluklarını homojen olarak doldurduğu görülmektedir. Bu görüntüler aynı zamanda yukarıdaki BET sonuçlarını da desteklediği görülmüştür.

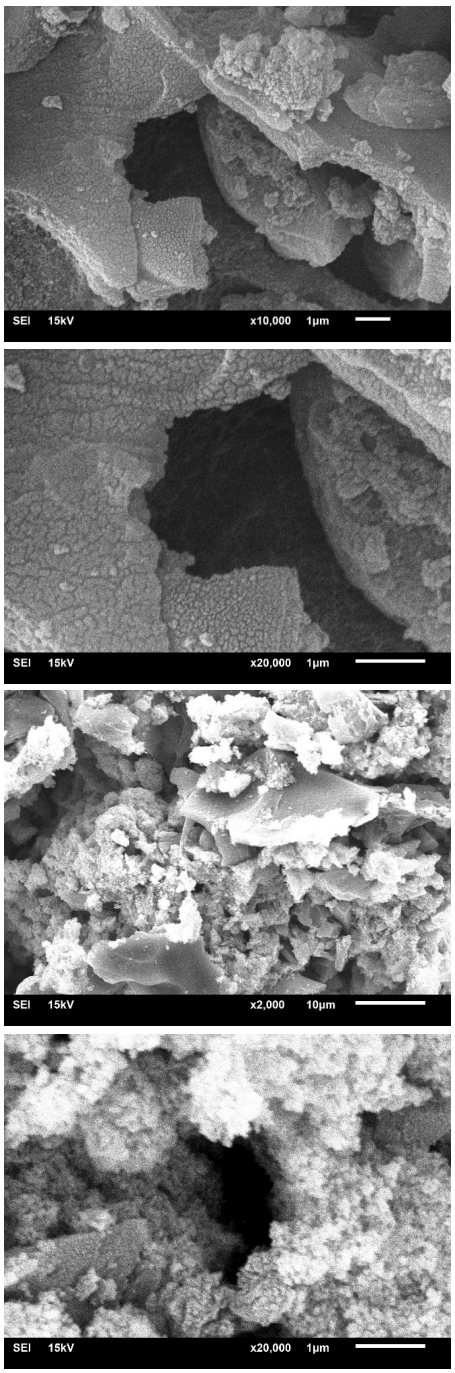

Şekil 1. AC aktif karbon (a ve b) ve CuMoB/AC (c ve d) katalizörünün SEM görüntüsü (SEM image of AC activated carbon (a and b) and CuMoB/AC (c and d) catalyst).

3.1.3. EDS karakterizasyonu (EDS characterization)

Şekil 2'de malzemelerin enerji dağılımlı X-ışını spektrumlarını (EDX) analiz sonuçları verilmiştir. Şekilden görüleceği gibi ilk grafiğin büyük kısmını karbon (C) elementi oluşturmakta, sağdaki grafiğe bakıldığında ise Cu metalinin aktif karbon yüzeyine başarıyla tutunduğu görülmektedir.

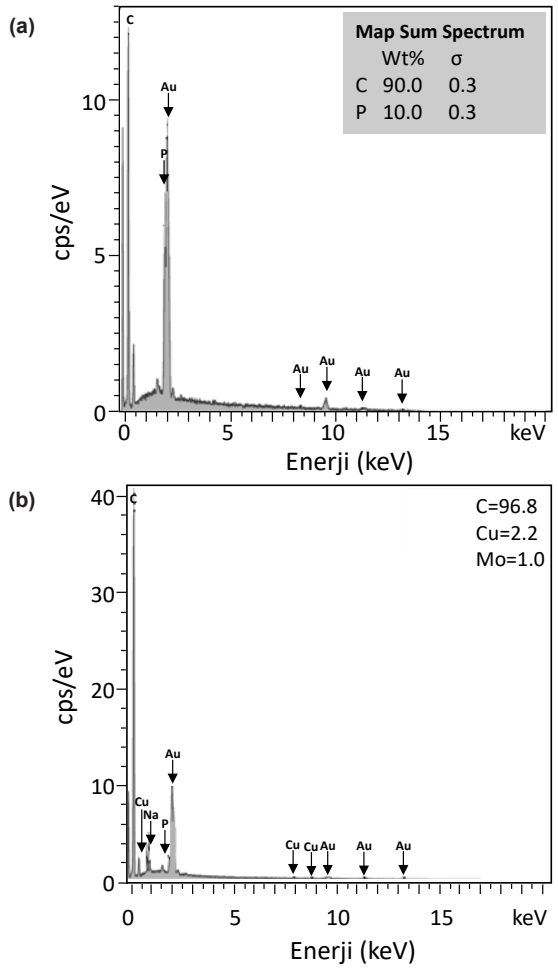

Şekil 2. a) AC aktif karbon ve b) CuMoB/AC katalizörünün EDS Grafiği (EDS Graph of a) AC activated carbon and b) CuMoB/AC catalyst).

3.1.4. XRD karakterizasyonu (XRD characterization)

Şekil 3'de, sırasıyla kahve telvesinden elde edilen aktif karbonu AC ve aktif karbon destekli CuMoB/AC katalizörünün XRD desenleri, Tablo1'de de XRD verileri gösterilmiştir. Burada Şekil 2a'da görülen 2Θ=25° bazı kırınım tepe noktalarının yoğunluğu kahve atığının bileşimini, göstermektedir. Bununla birlikte Şekil 2b'de görülen grafikte ise bu piklere karşılık gelen kristal indeksler, kırınım açıları (2θ), kristal fazların aydınlatılması için kullanılan JCPDS kartlarının numaraları aşağıdaki tabloda derlenmiştir. Katalizörümüzün partikül boyutu ilgili formül (Debby-Scherrer eşitliği) ile 2 nm gibi çok küçük bir boyutta olduğu hesaplanmıştır.

Tablo 1. CuMoB katalizörüne ait XRD verileri.

Kristal Faz	Dizin No	2θ	JCPDS Kart No
Cu	111	43.26	01-085-1326
CuO	111	38.96	01-072-0629
MoO_3	021	25.82	05-0508
CuMo	111	43.33	01-085-1326

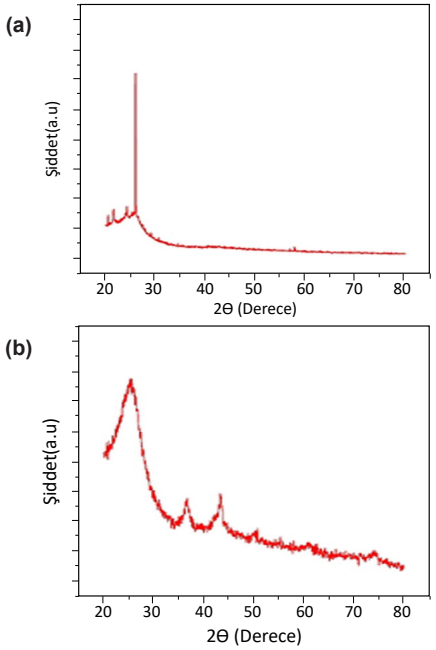

Şekil 3. a) AC aktif karbon ve b) CuMoB/AC katalizörünün XRD grafiği (XRD graph of a) AC activated carbon and b) CuMoB/AC catalyst).

3.2. Deneysel Sonuçlar (Experimental Results)

Bu çalışmada; kahve atığından elde edilen aktif karbon ile ilk defa destek malzemesi olarak Cu-Mo-B katalizörünün amonyak boranın hidrolizinde incelenmiştir. Bilindiği üzere heterojen katalizör hazırlamada taşıyıcı olarak kullanılması düşünülen bir malzemede en önemli özelliklerden birisi uygulanacak olan proseste herhangi bir aktivite göstermemesidir. Bu bağlamda önce farklı yüzdelerde Cu-Mo-B katalizörü aktif karbon yüzeyine adsorplanarak amonyak boran hidrolizi incelendi ve elde edilen hidrojen hacimlerinin zamanla değişimi Şekil 4'te verilmiştir. Şekilde görüleceği gibi AC destek malzemesi üzerine yüklenen metal miktarı Cu-Mo-B katalizörünün miktarı artıkça hidroliz reaksiyonu daha uzun sürede sonlanmaktadır. Şekil içinde verilen başlangıç hızlarının metal oranı grafiğine bakıldığında desteksiz katalizörün hızının 1500 mL/dak.gr olduğu, %10 metal varlığında ise bunun yaklaşık 1700 mL/dak.gr kadar çıktığı görülmektedir. Daha yüksek metal eklenmesi durumunda hızın tekrar düştüğü gözlemlenmiştir. Bunun muhtemel sebebinin fazla metal yüklenmesiyle gözeneklerin kapanmasına ve aktivitesinin düşmesine sebep olduğu düşünülmektedir. Burada optimum metalin destek malzemesi olarak kullanılan aktif karbona oranı %10 olarak belirlenmiştir [40].

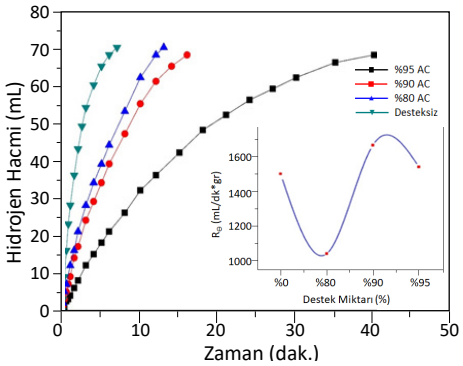

Şekil 4. Aktif karbon destek malzemesine yüklenen farklı CuMoB katalizörünün NH_3BH_3 hidrolizinde incelenmesi (30ºC, 1mmol NH_3BH_3, %1 NaOH, 50 mg Katalizör) (Investigation of different CuMoB catalyst loaded on activated carbon support material in NH_3BH_3 hydrolysis).

3.2.1. NaOH etkisi (NaOH effect)

Bilindiği üzere borhidrürlerin katalitik hidrolizi incelenirken incelenmesi gereken diğer bir parametrede sodyum borhidrür çözeltisinin kendi kendine bozunmasını engelleyen çözeltideki baz konsantrasyonudur. Bu bağlamda Şekil 5'de farklı NaOH konsantrasyonlarının amonyak boran ile hidrolizi incelenmiştir ve şekil içinde başlangıç hızlarının NaOH konsantrasyonu grafiği verilmiştir.

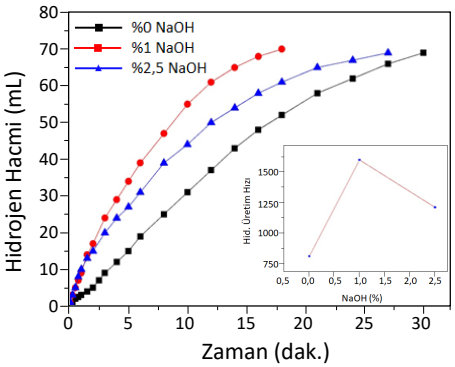

Şekil 5. Farklı NaOH konsantrasyonlarının katalizöre etkisi (The effect of different NaOH concentrations on the catalyst).

Buradan da görüleceği gibi %0 NaOH varlığındaki başlangıç hızı, 630 $mL^{-1}dk.g^{-1}$ iken %1 NaOH varlığında ise 1666 $mL^{-1}dk.g^{-1}$ olduğu görülmektedir. Burada NaOH konsantrasyonunun artmasıyla aktivitenin azalmasının nedeni; ortam pH'ının artmasıyla hidroliz reaksiyonunu engellediği görülmüştür. Hidroksil iyonlarının doğrudan adsorpsiyonu sırasında çözeltide mevcut olan bu katalizörün yüzeyine, hem hidrojen hem de hidroksil iyonlarının adsorpsiyonunu içeren iki işlevli bir yüzey reaksiyonu beklenebilir. Muhtemelen, optimal seviyenin üzerinde çok fazla OH konsantrasyonu bu hidroliz reaksiyonunu olumsuz etkiler. Bu nedenle Cu-Mo-B/AC katalizörü varlığında AB'nin hidrolizi ile elde edilen H_2 üretimi için diğer parametreleri incelerken çözelti ortamında NaOH konsantrasyonu katalizör aktivitesinin en yüksek olduğu %1 alınacaktır.

3.2.2. NH_3BH_3 etkisi (NH_3BH_3 effect)

Şekil 6'da Cu-Mo-B/AC katalizörü varlığında farklı (0,5 mmol, 1 mmol, 2 mmol, 3 mmol) amonyak bor hidrür konsantrasyonlarında çözeltilerin hidrolizi sonucu elde edilen hidrojen hacimlerinin zamanla değişimi verilmiştir. Şekilden görüleceği üzere AB konsantrasyonu arttıkça elde edilen hidrojen üretiminin düzenli bir şekilde arttığı görülmektedir. Bunun muhtemel sebebi; Amonyak boran hidrolizinde elde edilen yan ürünün, diğer borhidrürlerde oluşan yan ürüne göre daha az viskoz olmasından kaynaklandığı ve bunun da yüksek AB konsantrasyonlarında hidrojen üretim hızının düzenli bir şekilde artmasına sebep olduğu görülmüştür. Yani 0,5 mmol AB konsantrasyonu varlığındaki hidrojen üretim hızı 700 mL/dak.grkat iken 3 mmol AB hidrolizi varlığında ise başlangıç hızının 2100 mL/dak.gr kat kadar çıktığı belirlenmiştir [12].

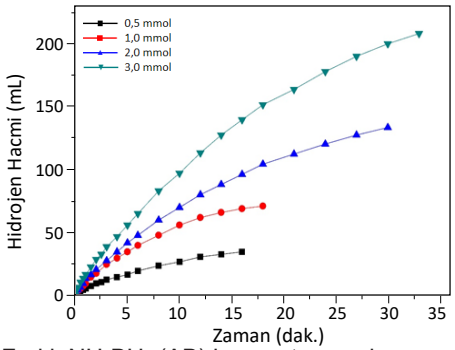

Şekil 6. Farklı NH_3BH_3 (AB) konsantrasyonlarının CuMoB/AC katalizörü varlığında hidrolizin incelenmesi (Investigation of hydrolysis of different NH_3BH_3 (AB) concentrations in the presence of CuMoB/AC catalyst).

3.2.3. Sıcaklık etkisi (Temperature effect)

Cu-Mo-B/AC katalizörünün farklı sıcaklıklarda amonyak boran hidrolizine etkinliği incelenmiş ve bu amaçla 30-60°C arasındaki 4 farklı sıcaklıkta açığa çıkan hidrojen hacimlerinin zamanla değişimi incelenmiş ve elde edilen sonuçlar Şekil 7'de verilmiştir. Şekilden görüldüğü gibi sıcaklık artıkça hidrolizin arttığı ve hidrojen üretim hızının arttığı görülmektedir.

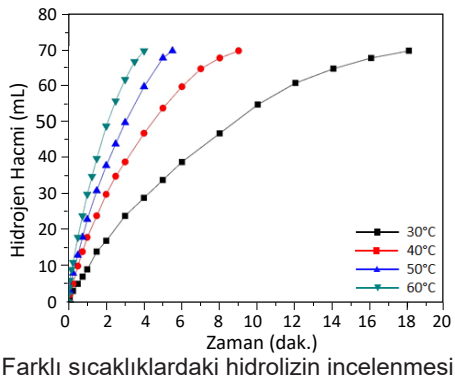

Şekil 7. Farklı sıcaklıklardaki hidrolizin incelenmesi (%1 NaOH, 1mmol AB, 50 mg Katalizör) (Investigation of hydrolysis at different temperatures).

3.2.4. Kinetik (Kinetic)

Şekil 7'de elde edilen farklı sıcaklıklardaki değerler kullanılarak n. derecede hız eşitliğine uygulanmıştır. Bu eşitliğe göre $1/CA^{n-1}$'e karşın çizilen zaman, t grafiğinde farklı sıcaklıklar için en uygun reaksiyon hız derecesi, n dereceden olduğu belirlenmiş ve en uygun reaksiyon hız mertebesi, n değeri 0,9 olarak bulunmuştur. Bu hız mertebesi için elde edilen doğruların reagrasyon katsayılarının 0,99'un üzerinde olması seçilen "n" değerinin doğruluğunu göstermesi bakımında önemlidir. Bu değerlerden yola çıkarak her bir sıcaklıkta elde edilen doğru denklemlerin eğiminde bulunan reaksiyon hız sabitleri, k değerlerinin Arrhenius eşitliğine uygulanması ile elde edilen grafik Şekil 8'de verilmiştir.

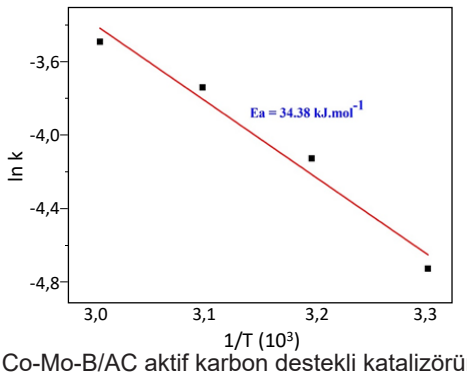

Şekil 8. Co-Mo-B/AC aktif karbon destekli katalizörün Arhenius grafiği (Arhenius graph of Co-Mo-B/AC activated carbon supported catalyst).

Tablo 2'de $NaBH_4$'ün hidrolizi için farklı Co bazlı aktif karbon destekli katalizörlerin hidrojen üretim hızları ve olduğu pH'larında aktivasyon enerjilerinin literatür verileriyle çalışmada elde edilen verilerinin karşılaştırılması verilmiştir

Tablo 2. $NaBH_4$'ün hidrolizi için farklı Co bazlı aktif karbon destekli katalizörlerin karşılaştırılması (Comparison of different Co-based activated carbon supported catalysts for the hydrolysis of $NaBH_4$).

Katalizör	Ea (kJ/mol)	Sıcaklık (°C)	Hidrojen Üretim Hızı ($L.g^{-1}.min^{-1}$.catalyst)	Referans
CoB/C	57.8	-	2.073	[41]
CoB/Kil	56.32	30	3.350	[42]
CoB/C	44,1	-	-	[43]
Al_2O_3/CoB	56.8	20	5.495	[44]
Co-Cr-B	37	-	3.400	[45]
Bu çalışma	34.38	30	2.100	-

4. Sonuçlar (Conclusions)

Amonyak bor hidroliz reaksiyonundan hidrojen üretimi için Cu-Mo metalleri aktif karbon üzerine

emdirilerek Cu-Mo-B/AC katalizörü hazırlandı. Elde edilen katalizörörün katalitik performansı; farklı pH çözeltilerinde, farklı katalizör miktarı, farklı metal oranları ve farklı amonyak boran konsantrasyonlarında karşılaştırılarak incelenmiştir. Cu:Mo optimum karışımı (97:3) oranında elde edilen katalizör en iyi performansı sergilediği görülmüştür. Öte yandan aktif karbon üzerine tutturulan %10 oranında bimetalik (Cu ve Mo), Cu-Mo/AC katalizörünün NH_3BH_3 hidrolizi ile hidrojen üretimi için kullanılabileceği sonucuna varılabilir

Teşekkür (Acknowledgement)

Bu çalışma Siirt Üniversitesi tarafından desteklenmiştir (Proje no: 2019-SİÜFEN-004).

Kaynaklar (References)

[1] Patel, N. & Miotello, A. (2015). Progress in Co-B related catalyst for hydrogen production by hydrolysis of boron-hydrides: A review and the perspectives to substitute noble metals. *International Journal of Hydrogen Energy*, *40*(3), 1429-1464.

2. Han, M., Qu, J., & Guo, Q. (2015). Corn stalk activated carbon based Co catalyst prepared by one-step method for hydrogen generation. *Procedia Engineering*, *102*, 450-457.

3. Du, Y., Shen, Y. B., Zhan, Y.-L., Ning, F.D., Yan, L.-M. & Zhou, X.C. (2017). Highly active iridium catalyst for hydrogen production from formic acid. *Chinese Chemical Letters*, 28(8), 1746-1750.

4. Keskin, M.S., Agırtaş, M.S., Baytar, O., Izgi, M.S. & Horoz, S. (2022). High hydrogen production rate from potassium borohydride hydrolysis with an efficient catalyst: CNT@ Ru(0). *Desalination and Water Treatment*, *250*, 189-196.

5. Sahin, O., Izgi, M.S., Tayboğa, S. & Kazıcı, H. (2021). Effect of plasma pretreatment of Co-Cu-B catalyst on hydrogen generation from sodium borohydride methanolysis. *Reaction Kinetics, Mechanisms and Catalysis*, *133*(2), 851-861.

6. Kazıcı, H.Ç., M.S. İzgi, and Ö. Şahin, (2022). Co-Mn-B nanoparticles supported on epoxy-based polymer as catalyst for evolution of H2 from ammonia borane semi-methanolysis. *Journal of Electronic Materials*, *51*(5), 2356-2368.

7. Erhan, O., Aslan, M. and İzgi, M.S., (2021). Kobalt bazli bimetalik nanokatalizörün potasyum borhidrür hidroliz tepkimesi üzerindeki katalitik etkisinin incelenmesi. *Konya Mühendislik Bilimleri Dergisi*, *9*, 200-212.

8. Onat, E., Cevik, S., Sahin, O., Horoz, S., and İzgi, M.S., (2021) Investigation of high catalytic activity catalyst for high hydrogen production rate: Co-Ru@ MOF. *Journal of the Australian Ceramic Society*, *57*, 1389-1395.

9. Chou, C.C., C.H. Hsieh, and B.H. Chen, (2015). Hydrogen generation from catalytic hydrolysis of sodium borohydride using bimetallic Ni-Co nanoparticles on reduced graphene oxide as catalysts. *Energy*, *90*, 1973-1982.

10. Peng, B. & Chen, J. (2008). Ammonia borane as an efficient and lightweight hydrogen storage medium. *Energy & Environmental Science*, *1*(4), 479-483.

11. Karkamkar, A., Aardahl, C. & Autrey, T. (2007). Recent developments on hydrogen release from ammonia borane. *Material Matters*, *2*, 6-9.

12. Izgi, M.S., Sahin, O. & Saka, C. (2019). gamma-Al2O3 supported/Co-Cr-B catalyst for hydrogen evolution via NH3BH3 hydrolysis. *Materials and Manufacturing Processes*, *34*(14), 1620-1626.

13. Izgi, M.S., Sahin, O., Onat, E., & Saka, C. (2020). Epoxy-activated acrylic particulate polymer-supported Co-Fe-Ru-B catalyst to produce H-2 from hydrolysis of NH3BH3. *International Journal of Hydrogen Energy*, *45*(43), 22638-22648.

14. Jiang, H.-L. & Xu, Q. (2011). Catalytic hydrolysis of ammonia borane for chemical hydrogen storage. *Catalysis Today*, *170*(1), 56-63.

15. Kazici, H.C., Yıldız, F., Izgi, M.S., Ulas, M., & Kıvrak, H. (2019). Novel activated carbon supported trimetallic PdCoAg nanoparticles as efficient catalysts for the hydrolytic dehydrogenation of ammonia borane. *International Journal of Hydrogen Energy*, *44*(21), 10561-10572.

16. Sahin, O., Bozkurt, A., Yayla, M., Kazici, H.C. & Izgi, M.S. (2020). As a highly efficient reduced graphene oxide-supported ternary catalysts for the fast hydrogen release from NaBH4. *Graphene Technology*, *5*(3), 103-111.

17. Heldebrant, D.J., Karkamkar, A., Linehan, J.C. & Autrey, T. (2008). Synthesis of ammonia borane for hydrogen storage applications. *Energy & Environmental Science*, *1*(1), 156-160.

18. Himmelberger, D.W., Yoon, C.W., Bluhm, M.E., Carroll, J.P. & Sneddon, L.G. (2009). Base-promoted ammonia borane hydrogen-release. *Journal of the American Chemical Society*, *131*(39), 14101-14110.

19. Alpaydın, C.Y., Gülbay, S.K. & Colpan, C.O. (2020). A review on the catalysts used for hydrogen production from ammonia borane. *International Journal of Hydrogen Energy*, *45*(5): p. 3414-3434.

20. Kazici, H.C., Izgi, M.S. & Sahin, O. (2021).A comprehensive study on the synthesis, characterization and mathematical modeling of nanostructured Co-based catalysts using different support materials for AB hydrolysis. *Chemical Papers*, *75*(6), 2713-2725.

21. Akbayrak, S., Tonbul, Y. & Ozkar, S. (2016). Ceria supported rhodium nanoparticles: superb catalytic activity in hydrogen generation from the hydrolysis of ammonia borane. *Applied Catalysis B: Environmental*, *198*, 162-170.

22. Akbayrak, S. & Özkar, S. (2012). Ruthenium (0) nanoparticles supported on multiwalled carbon nanotube as highly active catalyst for hydrogen generation from ammonia-borane. *ACS Applied Materials & Interfaces*, *4*(11), 6302-6310.

23. Akbayrak, S. & Özkar, S. (2021). Magnetically isolable Pt0/Co3O4 nanocatalysts: outstanding catalytic activity and high reusability in hydrolytic dehydrogenation of ammonia borane. *ACS Applied Materials & Interfaces*, *13*(29), 34341-34348.

24. Tunç, N. & Rakap, M. (2020) Preparation and

characterization of Ni-M (M: Ru, Rh, Pd) nanoclusters as efficient catalysts for hydrogen evolution from ammonia borane methanolysis. *Renewable Energy*, *155*, 1222-1230.

25. Abay, B. & Rakap, M. (2020). Eco-friendly synthesis of carboxymethyl cellulose-stabilized Ru0.57Co0.43 nanoclusters as extremely efficient and durable catalysts for hydrolytic dehydrogenation of methylamine borane. *ACS Sustainable Chemistry & Engineering*, *8*(43), 16197-16204.

26. Kazici, H.C., Izgi, M.S. & Sahin, O. (2022). Co-Mn-B Nanoparticles Supported on Epoxy-Based Polymer as Catalyst for Evolution of H-2 from Ammonia Borane Semi-Methanolysis. *Journal of Electronic Materials*, *51*(5), 2356-2368.

27. Izgi, M.S., Ece, M.S., Celik, K.H., Sahin, O. & Onat, E. (2020). Hydrogen production by using Ru nanoparticle decorated with Fe3O4@SiO2-NH2 core-shell microspheres. *International Journal of Hydrogen Energy*, *45*(55), 30415-30430.

28. Izgi, M.S., Onat, E., Celik, K.H. & Sahin, O. (2019). Hydrogen production through the cooperation of a catalyst synthesized in ethanol medium and the effect of the plasma. *Energy Sources Part a-Recovery Utilization and Environmental Effects*.

29. Onat, E., Aslan, M. & İzgi, M.S. (2021). Kobalt bazli bimetalik nanokatalizörün potasyum borhidrür hidroliz tepkimesi üzerindeki katalitik etkisinin incelenmesi. *Konya Mühendislik Bilimleri Dergisi*. *9*, 200-212.

30. Onat, E., Sahin, O., Izgi, M.S. & Horoz, S. (2021). An efficient synergistic Co@CQDs catalyst for hydrogen production from the hydrolysis of NH3BH3. *Journal of Materials Science-Materials in Electronics*, *32*(23), 27251-27259.

31. Onat, E., Cevik, S., Sahin, O., Horoz, S. & Izgi, M.S. (2021). Investigation of high catalytic activity catalyst for high hydrogen production rate: Co-Ru@MOF. *Journal of the Australian Ceramic Society*, *57*(5), 1389-1395.

32. Lu, Y.C., Chen, M.-S. & Chen, Y.W. (2012). Hydrogen generation by sodium borohydride hydrolysis on nanosized CoB catalysts supported on TiO2, Al2O3 and CeO2. *International Journal of Hydrogen Energy*, *37*(5), 4254-4258.

33. Baytar, O., Izgi, M.S., Horoz, S., Sahin, O. & Nar, S. (2019). Al2O3 supported Co-Cu-B (Co-Cu-B/Al2O3) catalyst for hydrogen generation by hydrolysis of aqueous sodium borohydride (NaBH4) solutions. *Digest Journal of Nanomaterials and Biostructures*, *14*(3), 673-681.

34. Izgi, M.S., Baytar, O., Sahin, O. & Horoz, S. (2019). Studies on catalytic behavior of Co-Cr-B/Al2O3 in hydrogen generation by hydrolysis of NaBH4. *Digest Journal of Nanomaterials and Biostructures*, *14*(4), 1005-1012.

35. Zhang, X., Sun, X., Xu, D., Tao, X., Dai, P.,Guo, Q. & Liu, X. (2019). Synthesis of MOF-derived Co@ C composites and application for efficient hydrolysis of sodium borohydride. *Applied Surface Science*, *469*, 764-769.

36. Zorer, C., Baytar, O., Sahin, O., Horoz, S. & Izgi, M.S. (2020) Synthesis of an efficient photocatalyst (activated carbon supported Zns) for methylene blue degradation. *Digest Journal of Nanomaterials and Biostructures*, *15*(3), 629-636.

37. Kazici, H.C., Salman, F., Izgi, M.S. & Sahin, O. (2020). Synthesis of metal-oxide-supported triple nano catalysts and application to H-2 production and H2O2 oxidation. *Journal of Electronic Materials*, *49*(6), 3634-3644.

38. Jenkins, R. and J.L. De Vries, Worked examples in X-ray analysis. 1978: Macmillan London.

39. Rahemi, N., Haghighi, M., Babaluo, A.A. & Jafari, M.F. (2013). Synthesis and physicochemical characterizations of Ni/Al2O3-ZrO2 nanocatalyst prepared via impregnation method and treated with non-thermal plasma for CO2 reforming of CH4. *Journal of Industrial and Engineering Chemistry*, *19*(5), 1566-1576.

40. Saka, C., Eygi, M.S. & Balbay, A. (2021). Cobalt loaded organic acid modified kaolin clay for the enhanced catalytic activity of hydrogen release via hydrolysis of sodium borohydride. *International Journal of Hydrogen Energy*, *46*(5), 3876-3886.

41. Zhu, J., Li, R., Niu, W. & Wu, Y. (2012). Facile hydrogen generation using colloidal carbon supported cobalt to catalyze hydrolysis of sodium borohydride. *Journal of Power Sources*, *211*, 33-39.

42. Tian, H., Guo, Q. & Xu, D. (2010). Hydrogen generation from catalytic hydrolysis of alkaline sodium borohydride solution using attapulgite clay-supported Co-B catalyst. *Journal of Power Sources*, *195*, 2136-2142.

43. Xu, D., Dai, P., Liu, X., Cao, C. & Guo, Q. (2008). Carbon-supported cobalt catalyst for hydrogen generation from alkaline sodium borohydride solution. *Journal of Power Sources*, *182*, 616-620.

44. Lu, Y., Chen, M. & Chen, Y. (2012). Hydrogen generation by sodium borohydride hydrolysis on nanosized CoB catalysts supported on TiO2, Al2O3 and CeO2. *International Journal of Hydrogen Energy*, *37*(5), 4254-4258.

45. Fernandes, R., Patel, N. & Miotello, A. (2009). Hydrogen generation by hydrolysis of alkaline NaBH4 solution with Cr-promoted Co-B amorphous catalyst. *Applied Catalysis B: Environmental*, *92*(1-2), 68-74.

BOR DERGİSİ
JOURNAL OF BORON
https://dergipark.org.tr/boron

Interaction of betacoronavirus and *S. aureus* with boron nitride nanoparticles (BNNPs)

Gizem Aytoğu [1], Yapıncak Göncü [2], Belma Nural Yaman [2], Berfin Kadiroğlu [3], Özer Ateş [4], Mustafa Erdem Üreyen [5], Nuran Ay [6,*], Kadir Yeşilbağ [1,*]

[1]*Bursa Uludag University, Faculty of Veterinary Medicine, Department of Virology, Bursa, 16059, Turkiye*
[2]*Eskisehir Osmangazi University, Faculty of Engineering and Architecture, Department of Biomedical Engineering, Eskisehir, 26040, Turkiye*
[3]*Dicle University, Faculty of Veterinary Medicine, Department of Virology, Diyarbakır, 21200, Turkiye*
[4]*Afyon Kocatepe University, Faculty of Veterinary Medicine, Department of Laboratory Animals Science, Afyonkarahisar, 03204, Turkiye*
[5]*Eskisehir Technical University, Department of Fashion and Textile Design, Eskisehir, 26555, Turkiye*
[6]*Eskisehir Technical University, Faculty of Engineering, Department of Materials Science and Engineering, Eskisehir, 26555, Turkiye*

ARTICLE INFO

Article history:
Received March 7, 2023
Accepted May7, 2023
Available online June 30, 2023

Research Article

DOI: 10.30728/boron.1261594

Keywords:
Bovine coronavirus
Cell viability
Hexagonal boron nitride
in-vitro analysis
S. aureus

ABSTRACT

Investigations on the advanced effects of boron-containing compounds have gained attention in the last decade. This study was carried out to investigate the effect of hexagonal boron nitride nanoparticles (BNNPs) on Bovine Coronavirus (BCoV) and *Staphylococcus aureus* (*S. aureus*) by different methods. First, the biological effects of different BNNPs concentrations lower than 0.5 mg/mL were examined on HRT-18 (Human Rectal Tumor) for 5 days. Different concentrations of hBN were mixed with BCoV in liquid, on a membrane, or directly on cells and examined for differences in titers or replications. Moreover, Bacterial Filtration Efficiency (BFE) test of hBN powders coated on polypropylene fabric by spray method was applied against *S. aureus*. The compound was found slightly toxic on the HRT-18 cell line by live cell counting, while no remarkable morphological difference was observed. BNNPs treatment with 0.025 or 0.3 mg/mL concentrations did not reduce the infective titer and created no inhibitory effect on in vitro replication. The stability of the virus titer after treatment of BNNPs coated fabric also indicated no antiviral efficiency. But hBN-applied fabric formed a barrier of ≥90.3%, while non hBN-applied fabric formed a≥64.6% barrier for *S. aureus*. The present study demonstrates that BNNPs alone are not a good candidate for disinfectant or drug for BCoVs, while it could be valuable to use as coated fabric in areas needing easy sanitation, especially for *S. aureus*.

1. Introduction

Boron-containing compounds (BCCs) are ubiquitous in nature. It is known that boron, which is mainly used in chemical compounds, is significant in plant nutrition and takes place in the diets of mammals [1,2]. The discovery and widespread research of the biological uses of boron compounds gained attention in the twentieth century. Although the mechanism of action is still mostly not clarified, recent researchers reveal the increasing role of boron in medicinal chemistry and drug design. BCCs have broad application areas in preventative (as an antiseptic and vector disease control), diagnostic, and therapeutic applications [3]. BCCs can be used as biomolecules in boron neutron capture therapy (BNCT) and in detecting biological markers of diseases [1,4]. The high adsorption rate of boron increases its use in drug development, diagnosis, and treatment [3,5]. As an antibiotic and antiseptic, boron has also other therapeutic properties such as anti-fungal, anti-coagulant, anti-diabetic, anti-hypertensive, anti-nociceptive, anti-parasitic and antiviral [1,3-7].

On the other hand, nanotechnology has also gained potential in biomedical applications. Nanoparticles (NPs) are complex molecules used for clinical diagnosis, treatment of diseases, and biomedical imagining, known as nanomedicine [8]. While copper and silver NPs demonstrated as toxic to microorganisms, boron has been suggested as functional in host defense [8].

Boron nitride (BN) is one of those boron-containing nanomaterials which has multiple purpose features. BN has different polymorphisms as; cubic BN (cBN), hexagonal BN (hBN), wurtzite BN and rhombohedral

*Corresponding author: kyesilbag@uludag.edu.tr, nay@eskisehir.edu.tr

BN (rBN) [9]. Among them, hBN has potential and several successes in drug carrier systems, increasing drug or biomolecule delivery, gene delivery, biosensors, and tissue engineering [9]. There are many studies on the use of hBN in the form of nanotubes, nanosheets, nanocages, and nanoparticles. While BNNPs have many layers, nanosheets have a few layers. Typically, lengths in one of the three dimensions of nanoparticles have a size between 1 and 100 nm, it plays a primary role in their longer circulation half-life, biodistribution, and clearance [10]. Recent studies have shown that the antibacterial activity of BN nanosheets doped with zirconium (0.5, 1.0 mg/50μL) enhanced against *Escherichia coli* (*E. coli*) and (*Staphylococcus aureus*) *S. aureus* [11]. Additionally, hBNNPs have been indicated high biofilm activity and inhibiting bacterial growth for *Staphylococcus pasteuri* (*S. pasteur*i) M3, *Staphylococcus mutans* (*S. mutans*) ATTC 25175, S. mutans 3.3, and Candida sp. M25 agents [12]. The antimicrobial activity of BN nano flake-polymer composite samples has been investigated against *E. coli, Pseudomonas aeruginosa, Staphylococcus epidermidis* (*S. epidermidis*), and *S. aureus*. The results have indicated that BN nano flakes physically interact with the bacterial cellular envelope, leading to irreparable physical damage, and also BN can minimize infections that may be associated with biomedical devices [13].

Due to the impact of the SARS-CoV2 pandemic raised in 2020, the activities of nanomaterials on viruses have become more important. The effects of BNNPs on viruses have not been studied yet. In this study, it was aimed to investigate the efficacy of hexagonal boron nitride nanoparticles on Bovine Coronavirus (BCoV), as a model of betacoronaviruses. Also, their biological compatibility on the Human rectal tumor (HRT-18) cell line and bacterial filtration efficiency for determination of bacterial permeability were studied.

2. Materials and Methods

2.1. Materials

Polypropylene (PP) non-woven fabric has an average of 100 g/m^2 and 0.55 mm thickness, provided from Mogul Company (Gaziantep, Türkiye). hBN powder (99.97% purity) was supplied from BORTEK Inc. (Eskişehir, Türkiye). Trimethyl methoxysilane (TMS) used as the bonding and adherent agent were purchased from Sigma Aldrich. ORGAL 430, the acrylic resin used as a binder, was obtained from Organic Chemicals Ltd. Sti. All chemicals used are of analytical purity.

2.2. Methods

2.2.1. Preparation of BNNPs and BNNPs coated fabrics

The dispersed BNNPs were obtained through continually stirring for 24 h in distilled water and after that sonication process (SONICS 750) for an hour. After the dispersion process (3.0 wt.%), a certain amount of trimethyl methoxysilane (2 vol%) dissolved in a suspension by stirring. The mixture was stirred at room temperature for 2 h, followed by adding a binder (1g/100mL). The prepared solution was filled into pressurized spray cans and applied to fabrics. Thermal treatment was applied at 110°C for 2 h to form covalent bonds between the silane coupler and nanosheets besides fixation to the fabric.

2.2.2. Characterizations

The density of hBN was calculated using the Helium pycnometer (Quanthachrome Multipycnometer). The grain size distribution was determined using the Malvern Mastersizer Hydro G2000 grain size measuring device. Fourier transforms infrared (FT-IR) spectroscopy in the attenuated total reflectance (ATR) mode (Bruker, Tensor 27) was utilized to measure whether raw materials, fabric, and silane grafted BNNSs were successfully coated onto the fabric surface. The measurements were done in a spectral range from 700 to 4000 cm^{-1} with a resolution of 4 cm^{-1} and 32 scans. The data were collected and processed using OPUS Software. The microstructure and morphology of BNNPs, silane grafted BNNs, and coated fabrics were identified by X-Ray diffraction patterns (XRD, Rigaku, Miniflex 600, Japan, Cu Kα radiation, λ=0.15406 nm) and scanning electron microscope images (SEM, ZEISS Supra 50VP). Before observation, the samples were coated with gold/palladium using a sputtering coater.

2.2.3. Virus, bacteria and cell line

BCoV, Mebus strain was used for testing the antiviral activities of hBN. While the virus used had an early passage (5p) level, the infective titer (50% tissue culture infectivity dose, $TCID_{50}$) for the test virus was $10^{6,25}$. The virus was obtained from our stock of laboratory. Human Rectal Tumor (HRT-18) cell line was used to propagate and titrate the viruses. Cells were maintained in Dulbecco's Modified Eagles Medium (DMEM) supplemented with heat-treated 10% fetal calf serum (FCS), 100 UI/mL Penicillin/Streptomycin, and 250 μL/mL Amphotericin B solution. Cells were incubated at 37°C, in a 5% CO_2 atmosphere. *S. aureus* ATCC 6538 was used for the bacterial filtration efficiency test. The bacterium was enabled from Biotechnology Laboratory, Eskişehir Osmangazi University, and was grown in a Brain Heart Infusion medium. *S. aureus* was grown up at optimum at 37°C.

2.2.4. Preparation of BNNPs for experiments

The BNNPs were dispersed in PBS to be adjusted as 1mg/mL. The pH was not balanced during preparation. When the measurement was made, it was determined that the pH of the prepared solution was 7.0. To eliminate the negative effects that may occur in cell cultures, the compound was autoclaved at 121°C for 15 minutes. After autoclaving, the solution was rotated

on a magnetic stirrer for 24 h to obtain a homogeneous mixture. Just before the experiments, this mixing process was carried out at 100°C for 10 minutes. Then, the solution was used in the experiments when it was cooled-down to 37°C.

2.2.5. Cell viability assay

HRT-18 cells were prepared at a concentration of 100,000 cells/mL in 24-well plates one day before the assays. For cell viability assay, the culture fluids were collected from morphologically healthy cells with fully covered wells. Seven concentrations (0.5, 0.4, 0.3, 0.2, 0.1, 0.05, 0.025 mg/mL) were prepared by diluting the BNNPs dispersed with sterile PBS and were added to the allocated wells for each dose. The well plates were incubated at 37°C with a 5% CO_2 atmosphere for 5 days and were examined daily by inverted light microscopy. During the test period, cells from individual wells were collected by trypsinization and centrifuged at 1500 rpm for 10 min. Cells were stained with trypan blue after the cell pellet was diluted with 1mL of DMEM. The viability rate, calculated as the percentage of living cells to total cells, was recorded with 24 h intervals.

2.2.6. Experimental application on BCoV

2.2.6.1. Effects of BNNPs on free virus particles in a liquid environment

For this experiment, equal volumes of BNNPs at different concentrations and 100 $TCID_{50}$ BCoV diluted in DMEM were mixed in a glass tube at room temperature. Also, an equal volume of 100 $TCID_{50}$ viruses and PBS were mixed for BNNPs-free conditions as negative (blanc) control. This experimental design was applied for two concentrations (0.025, 0.3 mg/mL hBN) selected according to predetermined cell viability analyses. However, this experiment was also carried out with a little modification for a higher concentration whose effect on the cell was not determined (1mg/mL). The BNNPs/virus mixtures prepared in glass tubes were incubated at room temperature 23±1°C for 0, 1, 2, and 6 h. During this period, the mixture was homogenized using a vortex every hour, even before sampling. At each represented hour, 100 µL of suspension was taken and used for the titration assays.

The mixture prepared in high concentration (1mg/mL) and its negative-control tube, were incubated at room temperature for 1 h. In order to exclude the adverse effect of the precipitated excessive amount of BNNPs during the microscopic examination, suspensions were centrifuged at 1500rpm before sampling. Then, 100 µL of suspension was used for the titration assays. The experimental setup was repeated twice for each condition.

2.2.6.2. Effect of BNNPs on virus replication

For analyzing the antiviral activity of BNNPs on infected cells, 24-well plates were used. Wells coated with 100,000 cells/mL were prepared 24 h before the assay. The next day, when the cells covered almost the entire well, cell culture fluids were removed and cells were infected with 100 $TCID_{50}$ virus suspensions. The plates were incubated for an hour at 37°C for virus adsorption. The inoculum was removed and monolayers were washed with PBS. Serum-free medium containing different pre-determined concentrations of BNNPs (0.025, 0.3 mg/mL) was added to the cells. Cells were daily examined for morphological changes for 5 days. And also, titration assays were conducted to collect samples from the relevant wells each day during this period. The experimental setup was repeated twice.

2.2.6.3. Effect of BNNPs on serial virus passages

In this test design, the collected samples from the previous experiment were used to identify the BNNPs effect on the sensitivity of viral replication in recurrent infections. For this purpose, 24-well plates were coated with HRT-18 cells with a concentration of 100,000 cells/mL. Cells culture media was removed and 200 µL of each sample was inoculated on a different well without dilution. The plates were incubated for an hour at 37°C and the virus growth medium (DMEM without FCS) was added. In this experiment, only a microscopic examination was carried out. And it was investigated whether there were cytopathogenic changes (CPE) due to the virus replication.

2.2.6.4. Exposure of BCoV on BNNPs coated fabric

BNNPs coated fabrics were cut in 2*2 cm^2 sizes and placed in petri dishes were sterilized by autoclaving at 121°C for 15 minutes prior to use. Three dishes were used for experimental conditions.

- *Petri dish A:* 100 $TCID_{50}$ BCoV with a volume of 200 µL was placed on the BNNPs coated fabric and incubated at room temperature. Consecutive samples were taken at the 2^{nd}, 8^{th} and 24^{th} hours after adding the virus suspension to the fabric.

- *Petri dish B:* 100 $TCID_{50}$ viruses with a volume of 200 µL was added to the BNNPs -free fabric and incubated at room temperature. The sample was taken only at the 8^{th} hour after adding the virus suspension.

- *Petri dish C:* 100 $TCID_{50}$ virus with a volume of 200 µL was added to an empty petri dish as control and similar conditions are provided.

Each of the fabrics was collected from dishes at designated times and placed in falcon tubes. After adding 3.8 mL of DMEM to it, it was vortexed for 5 minutes, allowing the viral particles on the fabrics to pass into the liquid phase. This obtained virus suspension was filtered using 0.2 nm PES filters (ISOLAB, Türkiye) and then titrated for the number of live virus particles.

2.2.6.5. Virus titration assay

To measure the antiviral activity of BNNPs, the $TCID_{50}$ was determined for each concentration for every sampling period of the experiments. For this purpose, serial dilutions (10-fold) of samples were made in DMEM. For each sampling 4 replicate wells of 96-well tissue culture plate were used. The virus diluent of 50 µL and an equal amount of cell suspension (2×10^5 cells/mL) was added to all the test wells and incubated at 37°C, 5% CO_2 atmosphere. Cells were observed daily by an inverted light microscope and the $TCID_{50}$ per milliliter was calculated according to the Spearman-Kârber method.

2.2.7. Bacterial filtration efficiency experiment

The Bacterial Filtration Efficiency (BFE) test of hBN powders coated on polypropylene fabric by spray method was applied according to standards including ISO11737-1 and TSE-EN 14683+AC. It has been made compatible with the requirements of ASTM (American Society of Testing and Materials) F2101. This test was performed in a sterile cabin under aseptic conditions. PP blank and PP-hBN fabrics were measured using *S. aureus* ATCC 6538 in airflow of 14 L/min. The bacterium suspension was applied as an aerosol by a nebulizer on the outside of two materials. The concentration of *S. aureu*s was diluted as 1700-2700 cfu/ml (colony-forming unit) mentioned in the standard procedure. BHI (Brain Heart Infusion) agar and normal saline (NaCl, 0,9%) were used for the growing bacteria and dilutions, respectively. The aerosol sample was sprayed from one side (from the outside of the mask), and the bacteria passing through the other side (to the inside of the mask) were collected onto a petri dish. Planted petri dishes were incubated at 37ºC overnight then the growing colonies were counted. The mean values obtained in duplicate experiments were used to calculate the BFE [14,15].

Positive control was a bacteria suspension that was sprayed directly without materials onto a petri dish. After the incubation, the colonies were counted. Equation 1 was used for the calculation of BFE %. 1% was accepted as low limit detection, and 99% was accepted as high limit detection [15].

$$BFE\ (\%) = \frac{Positive\ control\ (CFU) - Test\ Sample\ (CFU)}{Positive\ control\ (CFU)} x100 \qquad (1)$$

3. Results

3.1. Characterization of Hexagonal Boron Nitride

In a previous study, the characterization of commercial hBN powder was done and similar results were obtained [16]. Briefly, it was determined that the density of hBN powder used in experimental studies was 2.01 g/cm^3 and the tap density of the powder was in the range of 0.4-0.5 g/cm^3. The specific surface area of the hBN powder was measured as 22 m^2/g. The average particle size distribution of hBN was measured and D_{10}, D_{50}, and D_{90} values were 0.050 µm, 0.098 µm, and 0.210 µm, respectively. The mineralogical analysis of hBN was determined by the x-ray method (Figure 1a) and the sharp peaks in the diffraction pattern are characteristic peaks of hBN with lattice parameters a=2.57Å, c=6.70Å (JCPDS No: 034-0421). It was determined that hBN was well crystallized and free of impurities.

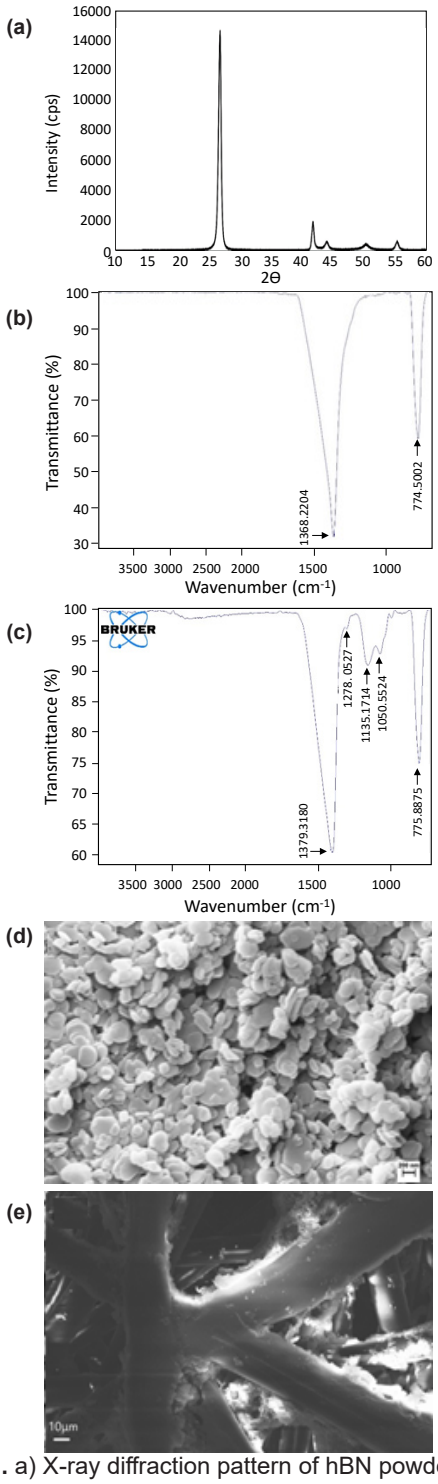

Figure 1. a) X-ray diffraction pattern of hBN powder, FTIR spectrum of b) hBN powder and c) silane modified BNNPs. SEM images of d) hBN nanoparticles and e) Fabric after silane decorated BNNPs coating.

FTIR technique allows the chemical composition and bonding arrangement of the components in the powder to be determined. To verify the purity of the BN powder, FTIR analysis was performed (Figure 1b). The bands detected at 774.5 cm^{-1} with 1368 cm^{-1} belong to the hexagonal phase of BN. While the peak at 774.5 cm^{-1} corresponds to B-N-B vibrations, the band at 1368 cm^{-1} was caused by stretching vibrations of B-N. No other bands were observed, which means that there is no bonding on the particle surface. Its morphological structure is shown in Figure 1d, e. The SEM image revealed that BN particles had diameter of 50-200 nm and thickness of 50-75 nm with a rounded shape.

3.2. Characterization of BNNPs Coated Fabric

Since silane coupling agent TMS have unique chemical composition, they act as binders between BNNPs and PP fabric. Figure 1c also shows the FTIR analysis of the suspension after drying at 100°C. While 1379 cm^{-1} and 775.8 cm^{-1} bands show hBN characteristic binding, the bands located at 1278.05, 1135.17, 1050.5, and 970 cm^{-1} in the fingerprint region show that the silane agent interacts with BN. The reason for BN characteristic peaks shifting may be the introduction of chemical groups of silane agents in the BN network. 1278 cm^{-1} is possibly from C-N stretching of amines that of 1050 cm^{-1} may be due to asymmetric stretching of Si-O-C [17]. There are peaks found at 1130 cm^{-1} and 970 cm^{-1} that could be assigned to Si-O-Si [17,18].

Silane modified BNNPs coated and uncoated PP fabrics were examined by FTIR to investigate what chemical interaction happens at the surface of the polymer (Figure 2). All dominant bands observed in PP fabrics (red line) were characteristic bands showing the isotactic structure of PP. Asymmetric stretching vibrations of CH_3 and CH_2 groups were observed in the spectrum corresponding to wavenumbers of 2958 and 2919 cm^{-1}, respectively. While symmetric stretching of CH_3 (methyl group) was observed at 2875 cm^{-1}, symmetrical and asymmetrical scissoring vibrations were observed at 1458 and 1375 cm^{-1} wavenumbers, respectively [19,20]. As 1376 cm^{-1} and 777 cm^{-1} bands show hBN characteristic bonding, the vibration bands located at 1278.05 and 1135.17 in the fingerprint region supports that the silane agent formed a bond with BN. A new absorption band was found at 1731 cm^{-1} in the treated fabric. It was probably caused by C=O stretching vibration. According to FTIR analysis, silane decorated BNNPs successfully formed a barrier film on PP fabric.

The surface morphology of the polypropylene fabric after silan decorated BNNPs coating is shown in Figure 1d, e. It can be said that the coating thickness is not homogeneous depending on the spray application. BNNPs were distributed on PP fibers and at fiber intersections, and BNNPs were also found to penetrate into the PP fabric.

3.3. Cytocompatibility of BNNPs to HRT-18 Cells

Biocompatibility of BNNPs in *in-vitro* cultures, determined by treating HRT-18 cell line with seven different concentrations (0.5, 0.4, 0.3, 0.2, 0.1, 0.05, 0.025 mg/mL) of the BNNPs. Cell viability rate was analyzed over 5 days. All concentrations remained above 50% viability during the evaluation period (Figure 3). In all the data obtained during 5 days, it was determined that death cell rates varied between 0.2% and 38%. On the fifth day of the treatment, viable cell count rates for concentrations from 0.5% to 0.025% were as follows; 91.89, 89.65, 93.5, 89, 84.4, 84.6, 90.4% for treatments and 94.4% for non-treated cells, respectively. It was observed that the maximum cell deaths were on the 2nd day for most concentrations and decreased in the following days.

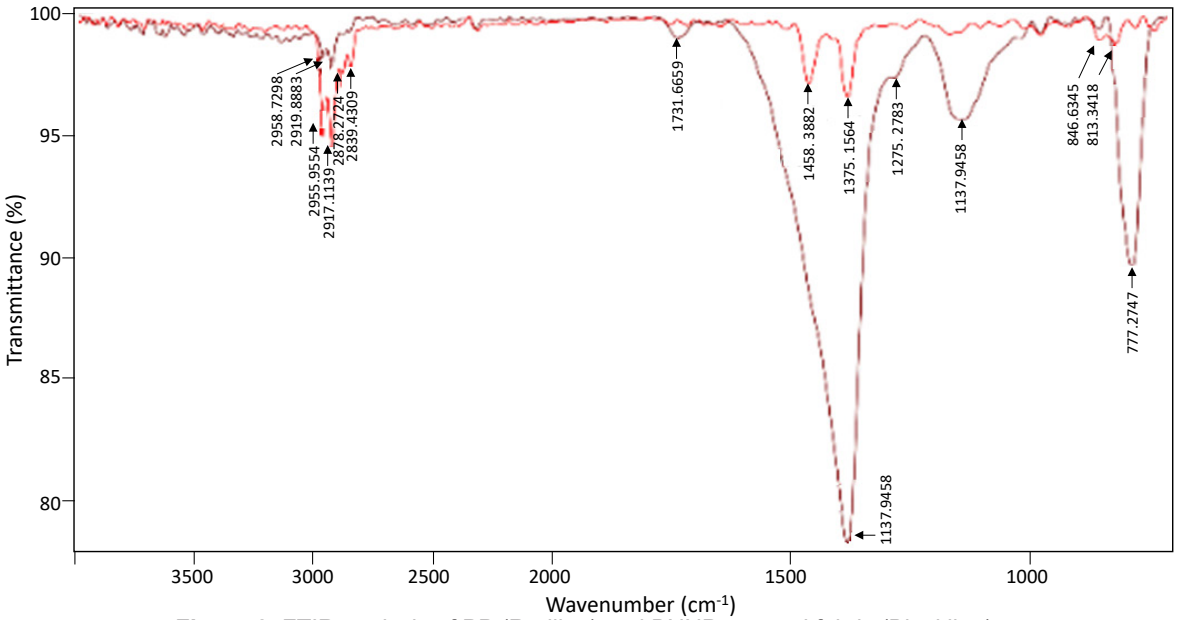

Figure 2. FTIR analysis of PP (Redline) and BNNPs coated fabric (Blackline).

Also, it was determined that the BNNPs in the medium did not have a negative effect on the cells in following days, and even the number of cells increased at all concentrations. In the evaluation of the 5th day, it was observed that the rate of cell death varied between 0.9-10 percent

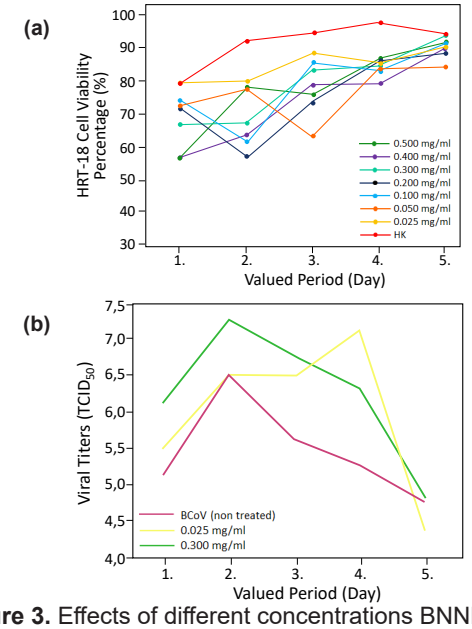

Figure 3. Effects of different concentrations BNNPs on cell viability and BCoV infectivity.

3.4. In Vitro Microscopic Analyses

Apart from cell viability rates, cells were further examined for morphological changes under an inverted microscope on all the days of the sampling period designed for the cell viability assay. No toxic effects or morphological differences were observed at the evaluated concentrations. However, it was observed that the BNNPs accumulated extensively at the cell-cell boundaries at concentrations of ≥0.2 mg/mL. Especially at the concentrations of 0.4 and 0.5 mg/mL, accumulation of the product was at a level that might be made it difficult to microscopically examine the CPE development led by virus growth (Figure 4). For this reason, in order to accurately evaluate the morphological changes in virus infected cultures, it was decided to study with concentrations of 0.3 mg/mL and below in cell-related experiments.

3.5. The Effect of BNNPs on Free Virus Particles in a Liquid Environment

In this experimental design, the inactivation activity of BNNPs was examined by combining both BNNPs and BCoV particles in the liquid phase and keeping them at room temperature for whether there was a difference in virus titer by time. Virus titer values of samples taken at 1, 2, and 6 hours for 0.025 and 0.3 mg/mL concentrations compared with values from untreated BCoV determined not even a half-log difference at either concentration or across all sampling periods (Table 1). On the other hand, when values of 1 mg/mL concentration were compared with BNNPs-free virus suspension, there was also no significant difference at all time intervals as well.

Table 1. Titer values at different time intervals of boron-treated BCoV in liquid phase.

Sampling hours	Viral titers (Log10 $TCID_{50}$)		
	BNNPs-free BCoV	0,025 mg BNNPs	0,3 mg BNNPs
0.	$10^{1,75}$	$10^{1,75}$	$10^{1,5}$
1.	$10^{1,75}$	$10^{2,0}$	$10^{1,75}$
2.	$10^{1,75}$	$10^{1,75}$	$10^{1,5}$
6.	$10^{0,75}$	$10^{1,75}$	$10^{1,5}$

3.6. The Effect of BNNPs on Virus Replication

Effect of BNNPs on BCoV replication was examined by adding BNNPs containing medium after virus

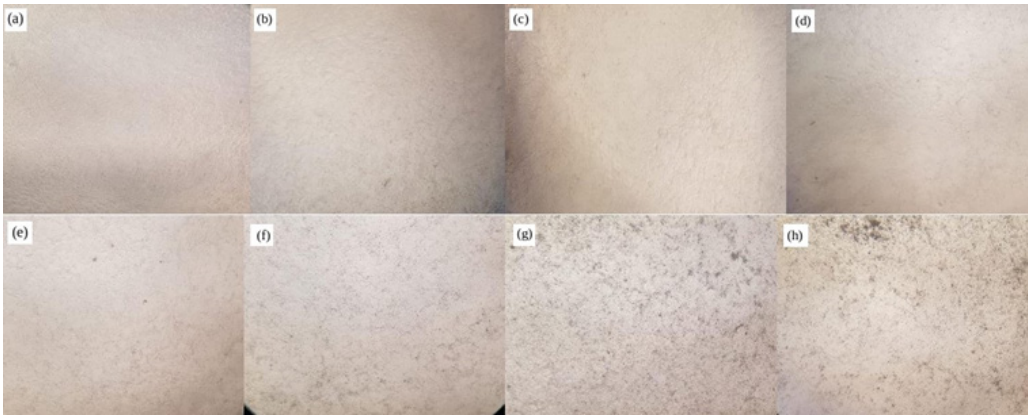

Figure 4. Microscopic images obtained from cell viability assay on the 3rd day treated with different concentrations of BNNPs (4x magnification): a) BNNPs free cell, b) 0.025 mg/mL treated cells, c) 0.05 mg/mL treated cells, d) 0.1 mg/mL treated cells, e) 0.2 mg/mL treated cells, f) 0.3 mg/mL treated cells, g) 0.4 mg/mL treated cells, h) 0.5 mg/mL treated cells. Accumulation on the cell which limits differentiation of slightly occurred CPE effects in the culture.

attachment. According to the mean values of the test results, both concentrations (0.025, 0.3 mg/mL) did not inhibit the virus replication until the 4th day of the experiment, even an enhancer effect on virus replication has been determined. When the titer values of BNNPs non-treated virus were compared with the titer values of virus grown in the presence of both concentrations (0.025, 0.3 mg/mL) of BNNPs, it was seen that the increase both in the 3rd day and 4th day values were higher than one log (Figure 3). It was observed that the mentioned effect disappeared on the 5th day. Virus titers (log 10) of BNNPs free, 0.025, and 0.3 mg/mL treated virus suspensions were evaluated as 4.75, 4.4, and 4.8, respectively. The obtained results were very close to each other, though shows that the treatments are not effective on BCoV replication. Although the experimental setup was carried out in 2 repetitions, after the results were obtained, the titration process was repeated for confirmation, and similar results were obtained.

3.7. The Effect of BNNPs on Serial Virus Passages

Samples obtained from both BNNPs-treated virus suspensions (0.025 and 0.3 mg/mL) and BNNPs free virus suspension as a control in the previous experiment were further passaged. This process was repeated twice. In both replicates, it was observed that effective virus replication could be yielded not only in the BNNPs-free, but also BNNPs treated experiment at both 0.025 and 0.3 mg/mL concentrations.

3.8. The Effect of Membrane Coated BNNPs Against BCoV

To determine whether BNNPs-containing compound inhibited the infectivity of BCoV particles when they came together on a fabric, infective virus particles were perfused on a BNNPs coated fabric and treated for 24 hours. The data obtained from this combination were compared with the infectivity of both pure virus and virus particles suspended on the uncoated fabrics. Results of BCoV (pure control virus) were detected as $10^{5.75}$ while BCoV titers collected over; membrane free of BNNP at 8th hour, membrane coated with BNNPs at 2th, 8th and 24th hour were all $10^{4.25}$. More than 1 log (Log 10) decrease between the titers of pure BCoV and the virus collected from the uncoated fabric. However, the titer of virus suspensions treated with the BNNPs-coated and uncoated fabrics were at the same level after incubation for 2, 8, and 24 hours.

3.9. Bacterial Filtration Efficiency Analyses

S. aureus aerosol was only applied on the coated surface. According to the using direction of the fabric, bacteria permeability from the outside to the inside has been tested. BFE % was calculated by using Eq.1. As a result of the tests, it has been determined that the PP blank sample creates a barrier of ≥64.6% and the PP-hBN sample a barrier of ≥90.3% in the application made from the outside to the inside. It can be said that the hBN applied to the fabric surface protects by reducing bacterial permeability.

4. Discussion

According to recent findings, boron containing compounds have low toxicity for humans and animals similar to table salt [1]. BNNPs are a unique boron compound that have recently attracted attention in medical practice. But their use as a medical material is related to their properties such as size, shape, form, and surface area [9].

Despite the fact that only limited reports are available on the effects of BNNPs to date, there are various studies describing the antiviral effects of BCCs [21-30]. For instance, proteasomal inhibitor, 0.1 μM Bortezomib was found to inhibit Influenza A (IAV) virus at over 100-fold (2 fold at Log 10). However, the compound was found to be highly toxic on MDCK cells and expressed to have no practical utility to inhibit IAV replication in this in vitro system [31]. Horváth et al. evaluated that a concentration of 2 μg/mL BNNT was cytotoxic for all the cell types (lung alveoli and human embryonic kidney cells) studied for 5 days [32]. In another study, 0.4 μg/mL BNNPs revealed low cytotoxicity in MDCK cells but a significant reduction with the same concentration in normal human skin fibroblast cells on the second day [12]. Therefore, it is possible to mention that the toxicity values for BCCs vary in different cell lines. Differences were associated with physical forms, coatings, dispersion procedures of BNNP, preferred cell types, and toxicological assays in *in-vitro* studies Kıvanç et al. showed that BNNPs nanoparticles could be considered as a potentially safe oral care product up to 0.1 mg/mL concentration [12].

Comparing the previous investigations this study presents a longer evaluation (5 days) for toxicity by exposing HRT-18 cells to low concentrations of BNNPs. As <20% reduction in the number of live cells referred to as slight cytotoxic in a previous study [12], in the present study, we determined all the tested concentrations as slightly toxic on the HRT-18 cell line and no remarkable difference in cell morphology was observed. But BNNPs accumulation observed on cell monolayer can create a negative effect on the visuality of cell morphology or may be deterring on *in-vitro* studies performed for determining the virus replications by microscopic analyses of the cell cultures.

Nevertheless, it was preferred to study concentrations of BNNPs, where 0.025% was the lowest concentration tested in cytotoxicity assay and also 0.3% was the highest concentration where the relatively low level of BNNPs accumulation on cells was determined by microscopic evaluations. However, according to the results obtained from viable cell numbers for both of the selected concentrations, the cumulative accumulation did not lead to cell death, and the proliferation rate seen in BNNPs-treated cells was similar to non-treated ones.

A dipeptide-boronic acid analog (Bortezomib/PS-341), has a proteasome inhibitor nature, and had shown a significant reduction of progeny *Severe fever with thrombocytopenia syndrome virus* (SFTSV) titers in infected cells [30]. Virus replication inhibition for *Hepatitis B virus* as long as 6 days with a single intravenous dose of 1 mg of bortezomib/kg was also accomplished *in vivo* [29]. The protease inhibitor effectiveness of BCCs has also expressed for *Vesicular stomatitis virus, Venezuelan equine enceph* [21-28].

Recently, Cetiner et al., demonstrated the possible suitability of BCCs as an antiviral agent against SARS-CoV-2, by molecular docking [33]. A BCCs binding site in the M^{pro} region of SARS-CoV-2 was also reported [34]. Moreover, it is clear to mention the necessity for confirmation of the molecular docking studies by in vitro testing of the molecule-virus interaction. Despite there is no previous molecular docking study on compatibility between BNNPs and BCoV, we performed a direct treatment of BNNPs to BCoV suspension, which resulted in no significant effect on the BCoV titer, suggesting there is no direct antiviral effect of BNNPs. These data show that the possibility to use of BNNPs as a disinfectant is limited.

Interaction of BCCs with drug molecules makes the therapeutic agents more favorable and efficient [35]. At a treatment study, the combination of bortezomib and acyclovir, an anti-herpes drug, inhibited *Herpes Simplex* infection more effectively comparing treatment with drug alone, and also had reduced the infectivity of acyclovir resistant HSV-1 strains [36]. In the present study, BNNPs are tested alone (without interaction with an antiviral drug) and no inhibitory effect on BCoV replication presented by viral infectivity assay was demonstrated. This result represents that BNNPs do not limit virus growth in vitro and are not successful drug candidates alone. But, in analogy to previous studies [36], it is an open area to test, in the case of combined use, the effect of BNNPs on the efficiency of antiviral drugs which already exist in the market.

Coating the material surfaces and fabrics by an antiviral preparation could serve as an efficient approach for preventing from some contact infections [37]. The efficiency of BNNPs as well as other BCCs as a fabric coating material in various fields has already been reported [38,39].

In the present study, hexagonal boron nitride nanoparticles were investigated for inhibition of BCoV with direct contact either on nanoparticle coated fabric or in liquid form. The BNNPs concentrations of 0.3 and 0.025 mg/mL did not make changes in the virus titers in liquid phase analyses. Despite the concentration of 1 mg/mL BNNPs was not evaluated in cell viability test, it was included in the analyzing the inhibitory effect by direct treatment. Similarly, no significant reduction in virus titer was observed by using 1 mg/mL BNNPs in liquid form. No inhibitor effect of those of tested concentrations on BCoV replication was observed either.

With the Covid-19 pandemic, the research on face mask materials has increased. There are many studies conducted with different mask materials including PP which is the most preferred [40,41]. PP is one of the most preferred materials for mask manufacturing because of its rare allergen characteristics [42]. Studies on the mask materials like cotton, polyester, nylon, and silk have shown around 5-25% bacteria filtration efficiencies [40]. Medical masks manufactured with different techniques including non-woven spun-bonded and Meltblown have shown >99 % BFE [43]. The mask materials associated with spun-bonded PP showed low filtration efficiency [41,43]. The masks composed using one layer or less than three layers of polypropylene spun bond have better breathability than others, but the BFE of these masks has remained below the threshold set by the standards [43]. Therefore, masks manufactured with a combination of different techniques including non-woven spun-bonded and Meltblown have shown >99 % BFE [43]. The coated materials have been studied and shown a positive effect on BFE %. While the BFE of PP fabrics coated with mangosteen extract was measured as >95% [44], the BFE of PP coated with alginate copper (II) was not reported as the characteristics of viral inactivation were reported [45]. Although no antiviral effect was found in this article, it was evaluated that BNNP can be used successfully in face masks, especially because it increases bacterial filtration efficiency.

5. Conclusions

Advances in boron chemistry expanded the field of research and the use of this element in medical chemistry. However, there is an insufficient number of studies on hBNNPs, especially on viruses, among the extensive studies of boron-containing compounds. The present study demonstrates that low dose BNNPs alone is not a good candidate to use as a disinfectant or drug on BCoV but coated materials have been studied shown a positive effect on *S. aureus*. However, it could be valuable to use as coated fabric in areas needing easy sanitation. The non-cytotoxic effect obtained in this study indicates that research evaluating the role of BNNPs as a carrier rather than the antiviral activity would be favorable in future work.

Conflict of interest

The authors declare that they have no conflicts of interest.

Funding information

This study was supported by Eskişehir Technical University, Scientific Research Projects Commission (Project No: 20GAP072).

References

[1] Soriano-Ursúa, M. A., Das, B. C., & Trujillo-Ferrara, J. G. (2014). Boron-containing compounds: Chemico-biological properties and expanding medicinal potential in prevention, diagnosis and therapy. *Expert Opinion on Therapeutic Patents*, (24), 485-500. https://doi.org/10.1517/13543776.2014.881472.

[2] Pizzorno, L. (2015). Nothing boring about boron. *Integrative Medicine*, 14(4), 35-48.

[3] Nielsen, F. H. (2014). Update on human health effects of boron. *Journal of Trace Elements in Medicine and Biology*, (28), 383-387. https://doi.org/10.1016/j.jtemb.2014.06.023.

[4] Farfán-García, E. D., Castillo-Mendieta, N. T., Ciprés-Flores, F. J., Padilla-Martínez, I. I., Trujillo-Ferrar, J.G., & Soriano-Ursúa, M. A. (2016). Current data regarding the structure-toxicity relationship of boron-containing compounds. *Toxicology Letters*, (258), 115-125. https://doi.org/10.1016/j.toxlet.2016.06.018.

[5] Baker, S. J., Tomsho, J. W., & Benkovic, S. J. (2011). Boron-containing inhibitors of synthetases. *Chemical Society Reviews*, *40*(8), 4279-4285. https://doi.org/10.1039/c0cs00131g.

[6] Dembitsky, V. M., Al Quntar, A. A. A., & Srebnik, M. (2011). Natural and synthetic small boron-containing molecules as potential inhibitors of bacterial and fungal quorum sensing. *Chemical Reviews*, *111*(1), 209-237. https://doi.org/10.1021/cr100093b.

[7] Fernandes, G. F. S., Denny, W. A., & Dos Santos, J. L. (2019). Boron in drug design: Recent advances in the development of new therapeutic agents. *European Journal of Medicinal Chemistry*, *179*, 791-804. https://doi.org/10.1016/j.ejmech.2019.06.092.

[8] Munir, M., Hussain, S., Anwar, R., Waqas, M., & Ali, J. (2020). The role of nanoparticles in the diagnosis and treatment of diseases. *Scientific Inquiry and Review*, *4*, 14-26. https://doi.org/10.32350/sir.

[9] Sharker, SM. (2019). Hexagonal boron nitrides (White graphene): A promising method for cancer drug delivery. *International Journal of Nanomedicine*, *14*, 9983-9993. https://doi.org/10.2147/IJN.S205095.

[10] Adamo, G., Campora, S., & Ghersi, G. (2017). Functionalization of nanoparticles in specific targeting and mechanism release. In F. Denisa, G. A. Mihai, (Eds.). *Nanostructures for Novel Therapy* (1st ed, pp. 57-80). Elsevier Inc. https://doi.org/10.1016/B978-0-323-46142-9.00003-7.

[11] Ikram, M., Jahan, I., Haider, A., Hassan, J., Ul-Hamid, A., Imran, M., Haider, J., Shahzadi, A., Shahbaz, A., & Ali, S. (2020). Bactericidal behavior of chemically exfoliated boron nitride nanosheets doped with zirconium. *Applied Nanoscience*, 10, 2339-2349. https://doi.org/10.1007/s13204-020-01412-z.

[12] Kıvanç, M., Barutca, B., Koparal, A. T., Göncü, Y., Bostancı, S. H., & Ay, N. (2018). Effects of hexagonal boron nitride nanoparticles on antimicrobial and antibiofilm activities, cell viability. *Materials Science and Engineering: C*, *91*, 115-124. https://doi.org/10.1016/j.msec.2018.05.028.

[13] Pandit, S., Gaska, K., Mokkapati, V. R. S. S., Forsberg, S., Svensson, M., Kádár, R., & Mijakovic, I. (2019). Antibacterial effect of boron nitride flakes with controlled orientation in polymer composites. *RSC Advances*, *9*, 33454-33459. https://doi.org/10.1039/C9RA06773F.

[14] Rengasamy, S., Shaffer, R., Williams, B., & Smit, S. (2017). A comparison of facemask and respirator filtration test methods. *Journal of Occupational and Environmental Hygiene*, *14*, 92-103. https://doi.org/10.1080/15459624.2016.1225157/SUPPL_FILE/UOEH_A_1225157_SM2604.DOC.

[15] Leonas, K., Jones, C. R., & Hall, D. (2003). The relationship of fabric properties and bacterial filtration efficiency for selected surgical face masks. J*ournal of Textile and Apparel, Technology and Management*, *3*, 1-8.

[16] Kar, F., Hacıoğlu, C., Göncü, Y., Söğüt, İ., Şenturk, H., Burukoğlu Dönmez, D., … & Ay, N. (2020). In vivo assessment of the effect of hexagonal boron nitride nanoparticles on biochemical, histopathological, oxidant and antioxidant status. *Journal of Cluster Science*, *322*(32), 517-529. https://doi.org/10.1007/S10876-020-01811-W.

[17] Teresa, O. H., & Choi, C. K. (2010). Comparison between SiOC thin films fabricated by using plasma enhance chemical vapor deposition and SiO2 thin films by using fourier transform infrared spectroscopy. *Journal of the Korean Physical Society*, *56*, 1150-1155. https://doi.org/10.3938/JKPS.56.1150.

[18] Ahmed, G. S., Gilbert, M., Mainprize, S., & Rogerson, M. (2013). FTIR analysis of silane grafted high density polyethylene. *Plastics, Rubber and Composites*, *38*(1), 13-20. https://doi.org/10.1179/174328909X387711

[19] Fang, J., Zhang, L., Sutton, D., Wang, X., & Lin, T. (2012). Needleless melt-electrospinning of polypropylene nanofibres. *Journal of Nanomaterials*, *2012*, 1-9. 382639, https://doi.org/10.1155/2012/382639.

[20] Abdel-Hamid, H. M. (2005). Effect of electron beam irradiation on polypropylene films-dielectric and FT-IR studies, *Solid-State Electronics*, *49*, 1163-1167. https://doi.org/10.1016/J.SSE.2005.03.025.

[21] Nocentini, A., Supuran, C. T., & Winum, J. Y. (2018). Benzoxaborole compounds for therapeutic uses: a patent review (2010-2018). *Expert Opinion on Therapeutic Patents*, *28*, 493-504. https://doi.org/10.1080/13543776.2018.1473379.

[22] Ghosh, A. K., Xia, Z., Kovela, S., Robinson, W. L., & Johnson, M. E. (2019). Potent HIV-1 protease inhibitors containing carboxylic and boronic acids: Effect on enzyme inhibition and antiviral activity and protein-ligand xray structural studies. *ChemMedChem*, *14*, 1863-1872. https://doi.org/10.1002/cmdc.201900508.

[23] Maynard, A., Crosby, R. M., Ellis, B., Hamatake, R., & Hong, Z. (2014). Discovery of a potent boronic acid derived inhibitor of the HCV RNA-dependent RNA polymerase. *Journal of Medicinal Chemistry*, *57*, 1902-1913. https://doi.org/10.1021/jm400317w.

[24] Neznanov, N., Dragunsky, E. M., Chumakov, K. M., Neznanova, L., & Wek, R. C. (2008). Different effect of proteasome inhibition on vesicular stomatitis virus and poliovirus replication. *PLoS One*, *3*, (4). e1887. https://doi.org/10.1371/journal.pone.0001887.

[25] Amaya, M., Keck, F., Lindquist, M., Voss, K., & Scavone, L. (2015). The ubiquitin proteasome system plays a role in Venezuelan equine encephalitis virus infection. *PLoS One*, *30*, 10(4), e0124792. https://doi.org/10.1371/journal.pone.0124792.

[26] Choy, M. M., Zhang, S. L., Costa, V. V., Tan, H. C., & Horrevorts, S. (2015). Proteasome inhibition suppresses dengue virus egress in antibody dependent infection. *PLOS Neglected Tropical Diseases*, *9*(11), e0004058. doi: 10.1371/journal.pntd.0004058.

[27] Barrows, N. J., Campos, R. K., Powell, S. T., Prasanth, K. R., & Schott-Lerner, G. (2016) A screen of FDA-approved drugs for inhibitors of zika virus infection. *Cell Host Microbe*, *20*, 259-270. https://doi.org/10.1016/j.chom.2016.07.004.

[28] Barrado-Gil, L., Galindo, I., Martínez-Alonso, D., Viedma, S., & Alonso, C. (2017). The ubiquitin-proteasome system is required for African swine fever replication. *PLoS One*, *12*(12), e0189741. https://doi.org/10.1371/journal.pone.0189741.

[29] Bandi, P., Garcia, M. L., Booth, C. J., Chisari, F. V., & Robek, M. D. (2010). Bortezomib inhibits Hepatitis B virus replication in transgenic mice. *Antimicrobial Agents and Chemotherapy*, *54*(2), 749-756. https://doi.org/10.1128/AAC.01101-09.

[30] Liu, S., Liu, H., Zhang, K., Li, X., & Duan, Y. (2019). Proteasome inhibitor PS-341 effectively blocks infection by the severe fever with thrombocytopenia syndrome virus. *Virologica Sinica*, *34*, 572-582. https://doi.org/10.1007/s12250-019-00162-9.

[31] Shahiduzzaman, M., Ezatti, P., Xin, G., & Coombs, K. M. (2014). Proteasomal serine hydrolases are up-regulated by and required for influenza virus infection. *Journal of Proteome Research*, *13*, 2223-2238. https://doi.org/10.1021/pr5001779.

[32] Horváth, L., Magrez, A., Golberg, D., Zhi, C., & Bando, Y. (2011). In vitro investigation of the cellular toxicity of boron nitride nanotubes. *ACS Nano*, *5*, 3800-3810. https://doi.org/10.1021/nn200139h.

[33] Cetiner, E., Sayin, K., Tuzun, B., & Ataseven, H. (2021). Could boron-containing compounds (BCCs) be effective against SARS-CoV-2 as antiviral agent. *Bratislava Medical Journal*, *122*, 263-269. https://doi.org/10.4149/BLL_2021_044.

[34] Vega Valdez, I. R., Melvin, R. N., José, S. Q. M., Eunice, F. G. E. D., & Marvin, S. U. A. (2020). Docking simulations exhibit bortezomib and other boron-containing peptidomimetics as potential inhibitors of SARS-CoV-2 main protease. *Current Chemical Biology*, *14*, 279-288. https://doi.org/10.2174/2212796814999201102195651.

[35] Soliman, K. A., & Aal, S. A. (2021). Theoretical investigation of favipiravir antiviral drug based on fullerene and boron nitride nanocages. *Diamond and Related Materials*, *117*, 108458. https://doi.org/10.1016/j.diamond.2021.108458.

[36] Schneider, S. M., Pritchard, S. M., Wudiri, G. A., Trammell, C. E., & Nicola, A. V. (2019). Early steps in herpes simplex virus infection blocked by a proteasome inhibitor. *MBio*, *10*(3): e00732-e00719. https://doi.org/10.1128/mBio.00732-19.

[37] Wang, W., Yim, S. L., Wong, C. H., & Kan, C. W. (2021) Study on the development of antiviral spandex fabric coated with poly(hexamethylene biguanide) hydrochloride (PHMB). *Polymers (Basel)*, *13*(13), 2122. https://doi.org/10.3390/POLYM13132122.

[38] Bentis, A., Boukhriss, A., & Gmouh, S. (2020). Flame-retardant and water-repellent coating on cotton fabric by titania–boron sol–gel method. *Journal of Sol-Gel Science and Technology*, *94*, 719-730. https://doi.org/10.1007/S10971-020-05224-Z.

[39] Akbar, W., Karagoz, A., Basim, G. B., Noor, M., Syed, T., Lum, J., & Unluagac, M. (2015). Nano-boron as an antibacterial agent for functionalized textiles. *MRS Online Proceedings Library*, *1793*, 53-57. https://doi.org/10.1557/OPL.2015.728.

[40] Kwong, L. H., Wilson, R., Kumar, S., Crider, Y.S., & Sanchez, Y. R. (2021). Review of the breathability and filtration efficiency of common household materials for face masks. *ACS Nano*. *15*(4). 5904-5924. https://doi.org/10.1021/ACSNANO.0C10146.

[41] Ju J. T. J., Boisvert L. N., & Zuo Y. Y. (2021). Face masks against COVID-19: Standards, efficacy, testing and decontamination methods. *Advances in Colloid and Interface Science*, *292*, 102435. https://doi.org/10.1016/J.CIS.2021.102435.

[42] Yu, De J., Goldminz, A., Chisolm, S., Jacob, S. E., Zippin, J. H., Wu, P. A., ... & Atwater, A. R. (2021) Facial personal protective equipment: materials, resterilization methods, and management of occupation-related dermatoses. *Dermatitis*, *32*(2), 78-85. https://doi.org/10.1097/DER.0000000000000699.

[43] Tessarolo, F., Nollo, G., Benedetti, L., Helfer, F., & Rovati, L. (2022). Measuring breathability and bacterial filtration efficiency of face masks in the pandemic context: A round robin study with proficiency testing among non-accredited laboratories. *Measurement*, *189*, 110481. https://doi.org/10.1016/J.MEASUREMENT.2021.110481.

[44] Ekabutr, P., Chuysinuan, P., Suksamrarn, S., Sukhumsirichart, W., & Hongmanee, P. (2019). Development of antituberculosis melt-blown polypropylene filters coated with mangosteen extracts for medical face mask applications. *Polymer Bulletin*. *76*, 1985-2004. https://doi.org/10.1007/S00289-018-2468-X/FIGURES/7.

[45] Bataglioli, R. A., Rocha Neto, J. B. M., Calais, G. B., Lopes, L. M., & Tsukamoto, J. (2022). Hybrid alginate-copper sulfate textile coating for coronavirus inactivation, *Journal of the American Ceramic Society*, *105*, 17481752. https://doi.org/10.1111/JACE.17862.

BOR DERGİSİ
JOURNAL OF BORON
https://dergipark.org.tr/boron

Toz metalurijisi ile üretilen hegzagonal bor nitrür takviyeli AZ91 magnezyum kompozitlerin tribolojik özelliklerinin incelenmesi

Cevher Kürşat Macit [1,*], Turan Gürgenç [2], Muhammet Gökhan Albayrak [3], Cihan Özel [1]

[1]*Fırat Üniversitesi, Mühendislik Fakültesi, Makine Mühendisliği Bölümü, Elazığ, 23000, Türkiye*
[2]*Fırat Üniversitesi, Teknoloji Fakültesi, Otomotiv Mühendisliği Bölümü, Elazığ, 23000, Türkiye*
[3]*Fırat Üniversitesi, Mühendislik Fakültesi, Metaluriji ve Malzeme Mühendisliği Bölümü, Elazığ, 23000, Türkiye*

MAKALE BİLGİSİ

Makale Geçmişi:
İlk gönderi 19 Mart 2023
Kabul 19 Nisan 2023
Online 30 Haziran 2023

Araştırma Makalesi

DOI: 10.30728/boron.1267756

Anahtar kelimeler:
AZ91 Magnezyum alaşımı
Hegzagonal bor nitrür
Kompozit
Toz metalurijisi
Triboloji

ÖZET

Bu çalışmada, AZ91 magnezyum alaşımı ve AZ91 alaşımına ağırlıkça %10 hegzagonal bor nitrür (hBN) nanoparçacıkları takviye edilerek homojen kompozit malzemeler üretilmiştir. Hazırlanan tozlar, soğuk presleme yöntemiyle 400 MPa basınç ile preslenmesi ve 590°C sıcaklıkta argon atmosferinde sinterlenmiştir. Numunelerin mikroyapıları taramalı elektron mikroskobu (SEM) ve enerji dağılımlı X-ışını (EDX) analizleri ile incelenmiştir. Numunelerin 20 saniye yükleme süresinde 5 farklı noktadan sertlik değerleri alınmış ve bu sertlik değerlerinin ortalaması alınarak ortalama sertlik değerleri belirlenmiştir. Aşınma testleri pin-on-disk deney cihazında farklı yük değerlerinde (5 N, 10 N ve 15 N) toplam 300 m kayma mesafesinde, 50 mm/sn kayma hızında ve kuru şartlarda yapılmıştır. Sürtünme katsayısı değerleri ile aşınma sonucundaki ağırlık kayıpları incelenmiştir. AZ91 kompozitinin sertlik değeri 62 HB iken hBN takviyesiyle 93 HB olarak ölçülmüştür. Benzer şekilde, yapılan aşınma deneylerinde hBN katkısıyla aşınma direnci 10 kat daha fazla bir kompozit elde edilmiştir. Özetle, hBN katkısının metal matrisli malzemelerin mekanik ve tribolojik özelliklerini olumlu yönde etkileme potansiyeline sahip olduğu görülmüştür.

Investigation of tribological properties of hexagonal boron nitride reinforced AZ91 magnesium composites produced by powder metallurgy

ARTICLE INFO

Article History:
Received March 19, 2023
Accepted April 19, 2023
Available online July 30, 2023

Research Article

DOI: 10.30728/boron.1267756

Keywords:
AZ91 Magnesium alloy
Hexagonal boron nitride
Wear
Powder metallurgy
Microstructure

ABSTRACT

In this study, homogeneous composite materials were produced by supplementing AZ91 magnesium alloy and AZ91 alloy with 10% by weight hexagonal boron nitride (hBN) nanoparticles. The prepared powders were pressed by cold pressing method with 400 MPa pressure and sintered at 590°C in argon atmosphere. Microstructures of the samples were investigated by scanning electron microscopy (SEM) and energy dispersive X-ray (EDX) analysis. The hardness values of the samples were taken from 5 different points during the 20 second loading time and the average hardness values were determined by taking the average of these hardness values. Wear tests were carried out in a pin-on-disc test device at different load values (5 N, 10 N and 15 N) at a total sliding distance of 300 m, at a sliding speed of 50 mm/sec and in dry conditions. The friction coefficient values and the weight losses as a result of wear were examined. The hardness value of AZ91 composite was 62 HB, while it was measured as 93 HB with hBN reinforcement. Similarly, in the wear tests, a composite with 10 times higher wear resistance was obtained with hBN additive. In summary, it has been observed that hBN additive has the potential to positively affect the mechanical and tribological properties of metal matrix materials.

1. Giriş (Introduction)

Magnezyum (Mg) özellikle düşük yoğunluğu ve yüksek spesifik dayanımı nedeniyle 21. yüzyılda ve ilerleyen yıllarda daha geniş bir kullanım alanı bulmaktadır. Mg matrisli kompozitler, diğer metal matrisli kompozitlere göre daha hafif olmaları, yüksek özgül mukavemetleri ve sertlikleri nedeniyle geniş çapta çalışmalarda tercih edilmektedir [1-3]. Hafif metal kompozitler sınıfında oldukları için havacılık ve otomobil endüstrileri için yapısal malzemeler olarak büyük potansiyel sunmaktadır. Mg ve alaşımlarının

*Corresponding author: macitkursatcevher@gmail.com

olumlu özelliklerinin yanında olumsuz özellikleri de bulunmaktadır. Bunlardan en önemlisi metal matrisli diğer kompozit malzemelere göre daha üstün mekanik özellikleri sağlayamamasıdır. Bu sebeple hala araştırmacılar magnezyum alaşımları üzerinde çalışmaları sürdürmektedir. Endüstriyel uygulamalarda hafif mühendislik malzemelerine olan talep sürekli artmaktadır. Mg ve alaşımlarının özelliklerinin iyileştirilmesi için uygulanan imalat yöntemlerinden birisi de mg esaslı kompozit malzeme üretilmesidir. Mg esaslı kompozit malzeme üretiminde magnezyumun kristal kafes yapısı nedeniyle haddeleme ve ekstrüzyon gibi geleneksel yöntemlerle şekillendirilebilirliğinin kısıtlı olması bu alaşımların farklı yöntemlerle şekillendirilmesi konusunda çalışmalar yapılmasını gerekli hale getirmiştir [4,5]. Farklı üretim yöntemleri ile bu zorlukların üstesinden gelmek mümkündür. Bunun için kullanılabilecek yöntemlerden biri Toz Metalurjisi (TM) ile üretimdir. TM yöntemi partikül haline getirilmiş olan metal veya alaşımların basınç altında şekillendirilmesi ve ergime sıcaklıklarının altındaki bir sıcaklıkta tutulması ve birleştirilmesi esasına dayanır [6]. TM yöntemi diğer geleneksel imalat yöntemlerine göre nispeten daha yeni bir üretim yöntemidir ve üreticilerin enerji ve hammadde giderlerinden büyük miktarda tasarruf etmesini sağlar [7].

Mg ve alaşımlarının TM yöntemiyle üretilmesi esnasında çözülmesi gereken bazı temel zorluklar bulunmaktadır. Mg ve alaşımlarının TM ile üretimindeki temel zorluk, Mg ve alaşımların oksijenle reaksiyona girmesi çok kolay olduğundan tozların yüzeyinde oluşması muhtemel ince magnezyum oksit (MgO) tabakası, sinterlenme sırasında difüzyonu önlemekte, tozlar arasında zayıf ve kırılgan tane sınırlarının oluşmasına dolayısıyla düşük mekanik özelliklere neden olmaktadır. Bu durumu önlemek amacıyla Mg ve alaşımlarının toz metalurijisindeki bütün aşamaları sırasında numunelerin argon gazı akışı ile oksitlenmeden korunması gerekmektedir [8-10]. Magnezyumun endüstriyel anlamda geniş kullanım alanı bulmasının önündeki diğer engeller ise düşük dayanım özelliği, şekillendirilebilirliği, korozyon ve aşınma dayanımının oldukça düşük olmasıdır [11]. Mg ve alaşımlarına farklı takviyeler katılarak üretilen kompozit malzemelerde mekanik, aşınma ve mikroyapı özelliklerinin geliştirilmesi üzerine çalışmalar yapılmıştır [2,3,12-19].

Hegzagonal bor nitrür (hBN), bor nitrürün (BN) kristal yapılarından biridir ve geniş bir sıcaklık aralığında mükemmel katı yağlama kabiliyetine sahiptir [20]. Grafit ve molibden disülfid gibi, hBN de bor ve nitrojen atomları arasında güçlü bir kovalent bağa sahip altıgen tabaka katmanlarından oluşan katmanlı bir yapıya sahiptir. Levha katmanları, zayıf Van der Waals kuvvetleri tarafından bir arada tutulur. Bu yapı, kuvvet katmanlara paralel uygulandığında kesmeye izin verir. Böylece beklenen sürtünme azalmasını sağlar ve çok verimli yağlama sağlar. hBN ilavesiyle bakır ve nikel bazlı kendi kendini yağlayan kompozitlerin oda ve yüksek sıcaklıklardaki tribolojik özellikleri üzerine birçok çalışma yapılmıştır. hBN içeren sinterlenmiş kompozitlerin temel matristen daha düşük bir sürtünme katsayısı verdiği ve hBN takviyeli numunelerde yüksek sertlik değerleri bulunmuştur [21-23].

Magnezyum alaşımları ve hBN takviyeli kompozitlerin mekanik ve tribolojik özellikleri ile ilgili daha önce yapılan çalışmalar bulunmaktadır. Yan ve ark., yapmış oldukları çalışmada, saf magnezyum tozuna çinko takviyesinin kompozit numunenin mekanik özelliklerini iyileştirdiği görülmüştür [24]. Rashad ve ark. çalışmalarında saf magnezyum tozuna alüminyum ve kalay takviyeli kompozitler toz metalurijisi ile üretimi gerçekleştirilmiştir. Üretilen numunelerin saf magnezyum tozuna göre alüminyum ve kalay takviyesinin mekanik özellikleri iyileştirdiği görülmüştür [25]. Lingaraju ve ark., AZ91 magnezyum alaşımına TiC, B_4C ve hBN takviyeleriyle nano kompozitler üretmiştir. Üretilen nanokompozitlerin takviyesiz AZ91 alaşımına göre daha üstün mekanik ve tribolojik özelliklere sahip oldukları gösterilmiştir [26]. Mahathanabodee ve ark., yapmış oldukları çalışmada, 316L paslanmaz çeliğine hBN ve MoS_2 takviyeleri eklenerek kompozit numuneler üretmiştir. Üretilen numunelerin aşınma direncini artırırken sürtünmeyi azaltma potansiyeline sahip olduğu görülmüştür [27].

Bu çalışmada, hBN nanoparçacıkları ile takviye edilen AZ91 magnezyum alaşımlı matris kompozitlerin toz metalurijisi yöntemiyle üretimlerinin daha önce yapılmadığı görülmüştür. Çalışmada ilk olarak hBN nanoparçacıkları ile AZ91 magnezyum alaşımının homojen bir şekilde karışımları yapılmıştır. Numunelerin mikroyapısı, mikrosertliği ve 3 farklı yük altındaki aşınma deneyleri gerçekleştirilmiştir.

2. Malzemeler ve Yöntemler (Materials and Methods)

2.1. Malzemeler (Materials)

Çalışmada kullanılan %99,95 saflık ve 44 µm parçacık boyutuna sahip AZ91 alaşımı ve %99,85 saflık ve 65-75 nm parçacık boyutuna sahip hBN, Nanografi (Türkiye) firmasından temin edilmiştir. AZ91 alaşımının kimyasal analizi Tablo 1'de verilmiştir.

Tablo 1. AZ91 alaşımının kimyasal analizi (Chemical analysis of AZ91 alloy).

Element	İçerik (%)	Element	İçerik (%)
Al	11,34	**Fe**	0,0214
Ag	0,0004	**La**	<0,0010
Ca	0,0009	**Mn**	0,0043
Cu	<0,0002	**Nd**	<0,0020
Mg	87,24	**Ni**	<0,0001
Zr	0,0046	**Y**	<0,0050
Pb	0,0022	**Si**	0,848
Pr	<0,0005	**Sn**	0,0046
Zn	1,301	**Ti**	0,0017

2.1. Yöntemler (Methods)

2.2.1. Numunelerin üretilmesi (Production of samples)

AZ91 magnezyum alaşımının hava ile temasının kesilmesi ve numunelerin argon gazı atmosferinde hava ile teması olmayan bir ortamda karıştırılmıştır (glove box). hBN nanoparçacıkları bir beherde 30 ml metanole eklenmiş ve 30 dk süresince ultrasonik karıştırıcıda karıştırılmıştır. Diğer bir beherde, ağırlıkça yüzde (ağ. %) 90 olacak şekilde hazırlanan AZ91 tozları eklenmiş ve 30 dakika ultrasonik karıştırıcıda karıştırılmıştır. Karışım oranlarının belirlenmesinde literatüre göre en uygun ağırlıkça % oranlar baz alınmıştır [28,29]. hBN nanoparçacığı magnezyum karışımına eklenmiş ve 30 dakika daha ultrasonik karıştırıcıda karıştırılmıştır. Tanecik boyutları birbirine yakın seçilen tozların homojen bir şekilde karışımları tamamlanmıştır. Karıştırma işlemi tamamlanan nanoparçacıkların süzülme işlemi gerçekleştirilmiştir. Süzülen nanoparçacıklar havasız ortam içerisinde kurutulmuştur. Son işlem basamağı olarak kurutulma işlemi tamamlanan AZ91-hBN nanoparçacıkları tekrar bir karıştırma işleminden geçirilerek manyetik karıştırıcıda 500 rpm'de 4 saat süreyle karıştırıldı [30]. Üretilen numunelerdeki ağırlıkça kullanılan numune miktarları ve numunelerin adlandırılması Tablo 2'de gösterilmiştir.

Tablo 2. Numunelerin adlandırılması ve ağırlıkça katkı miktarları (Identification of the samples and additive amounts by weight).

	AZ91	hBN
AZ91	%100	-
AZ91-hBN	%90	%10

Üretimleri tamamlanan numunelerin presleme işlemleri gerçekleştirilmiştir. Presleme işleminde kalıba 400 MPa 'lık bir basınç uygulanarak numuneler oluşturulmuştur. Kalıba tozların yerleşimi esnasında numunelerin kalıptan daha rahat bir şekilde çıkartılabilmesi için kalıbın içerisi $Zn(C_{18}H_{35}O_2)_2$ (Çinko stearat) ile yağlanmıştır. TM'si üretim parametreleri Tablo 3'te verilmiştir.

Tablo 3. TM yöntemi ile üretilen hBN takviyeli ve takviyesiz AZ91 numunelerinin üretim parametreleri (Production parameters of hBN reinforced and non-reinforced AZ91 samples produced by powder metallurgy method).

	Presleme Basıncı	Sinterleme		
		Sıcaklığı (°C)	Ortamı	Süresi (sa)
AZ91	400 MPa	590	Argon	8
AZ91-hBN	400 MPa	590	Argon	8

Preslemeişlemleritamamlanannumunelerinsinterleme işlemi azot ortamında fırında gerçekleştirilmiştir. Sinterleme sonrasındaki numunelerin görüntüleri ise Şekil 1'de gösterilmiştir.

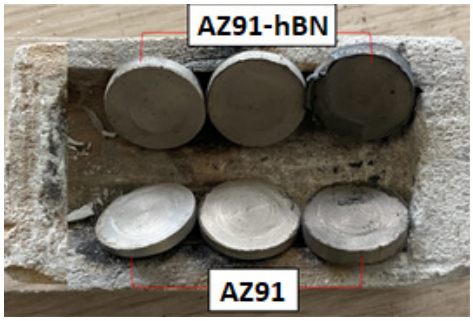

Şekil 1. Sinterleme işlemi tamamlanan numuneler (Samples with completed sinterings).

2.2.2. Numunelerin zımparalanması ve parlatılması (Sanding and polishing of specimens)

Üretimi, preslemesi ve sinterlenmesi tamamlanan numunelerin mikroyapılarının daha net bir şekilde incelenmesi için zımparalama işlemi sırasıyla 100, 240, 400, 600, 800, 1000 ve 1200 lük SiC zımpara kağıtları üzerinde ve daha sonra 3 µm'lik elmas pasta kullanılarak çuha ile parlatma işlemleri gerçekleştirilmiştir.

2.2.3. Numunelerin mikroyapılarının incelenmesi (Investigation of microstructures of samples)

Üretimi, preslemesi, sinterlenmesi, zımparalanması ve parlatılması tamamlanan numunelerin mikroyapılarının incelenmesi için Zeiss EVO MA10 markalı SEM cihazı kullanılarak SEM ve EDX analizleri yapılmıştır.

2.2.4. Numunelerin sertlik deneylerinin yapılması (Hardness tests of samples)

Sertlik deneylerinde Rockwell-B cinsinden sertlik değerleri incelendi. Numunelerin 5 farklı noktasından sertlik değerleri alındı ve bu sertlik değerlerinin ortalaması alınarak ortalama sertlik değerleri belirlenmşitir. Sertlik deneyinde 1/16 inç batıcı uç kullanılarak 100 kg yük uygulanarak 20 sn süreyle sertlik deneyleri yapılmıştır.

2.2.5. Numunelerin aşınma deneylerinin yapılması ve sürtünme katsayılarının belirlenmesi (Abrasion tests of samples and determination of friction coefficient)

Numunelerde aşınma testleri, pin-on-disk aşınma test cihazıyla 3 farklı yük altında (5N, 10N, 15N) 50 mm/sn kayma hızında ve 300 metre kayma mesafesinde gerçekleştirildi. Toplam 300 metre kayma mesafesinde 50 metrede bir kompozitlerin ağırlık kayıpları 10^{-5} hassasiyet değerine sahip terazide ölçüldü ve ölçülen değerler kayıt altına alınarak mesafeye göre her numune için ağırlık kaybı grafikleri oluşturulmuştur. Aşınma deneylerindeki diğer işlem olan sürtünme katsayılarının belirlenmesi için her bir numune 300

metre kayma mesafesi boyunca aşındırılmış ve aşınma test cihazında kompozitlerin sürtünme katsayısı değerleri kayıt altına alınmıştır. Kayıt altına alınan sürtünme katsayı değerleri bilgisayara aktarılarak sürtünme katsayısı grafikleri çıkarılmıştır.

3. Sonuçlar ve Tartışma (Results and Discussion)

3.1. Mikroyapı (Microstructure)

Numunelerin mikroyapılarında AZ91 matris yapı içerisinde dağılım sergileyen takviye elemanı parçacık tayini için SEM ve EDX analizleri yapılmıştır. SEM analizleri sonucunda alınan saf AZ91 ve hBN katkılı kompozitlerin SEM görüntüleri Şekil 2'de gösterilmiştir. SEM analizlerinde hBN katkı miktarının AZ91 magnezyum alaşımı üzerinde oluştuğu görülmüştür.

Kompozit numunelerin EDX analizleri sonucunda AZ91 magnezyum alaşımının kimyasal bileşimine benzer sonuçlar alınmıştır [31]. hBN takviyesiyle EDX analizinde B ve N'nin oluştuğu gözlemlenmiştir. EDX analiz sonuçları Şekil 3'te ve oluşan ağırlıkça katkı miktarları Tablo 4'te gösterilmiştir.

Tablo 4. EDX analiz sonuçlarında numunelerin ağırlıkça katkı miktarları (Additive amounts by weight of samples in EDX analysis results).

Numune	Mg	O	Al	Zn	C	N	B
AZ91	77,21	14,09	6,37	0,55	1,78	-	-
AZ91-hBN	69,27	12,65	6,01	0,46	2,56	2,39	6,66

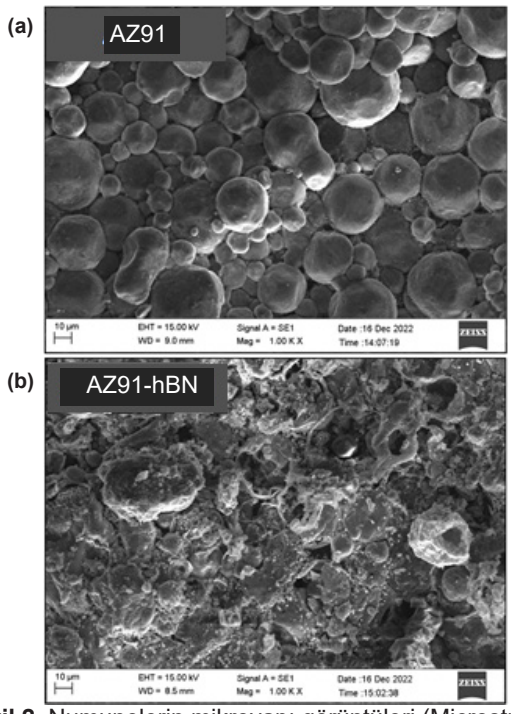

Şekil 2. Numunelerin mikroyapı görüntüleri (Microstructure images of samples).

3.2. Sertlik (Hardness)

Numunelerin sertlik değerleri Rockwell-B sertliğinde bulunmuştur ve bulunan değerler brinell (HB) cinsine çevrilmiştir. Yapılan sertlik deneylerinde saf AZ91 değerinin sertlik değeri literatür değerlerine benzer

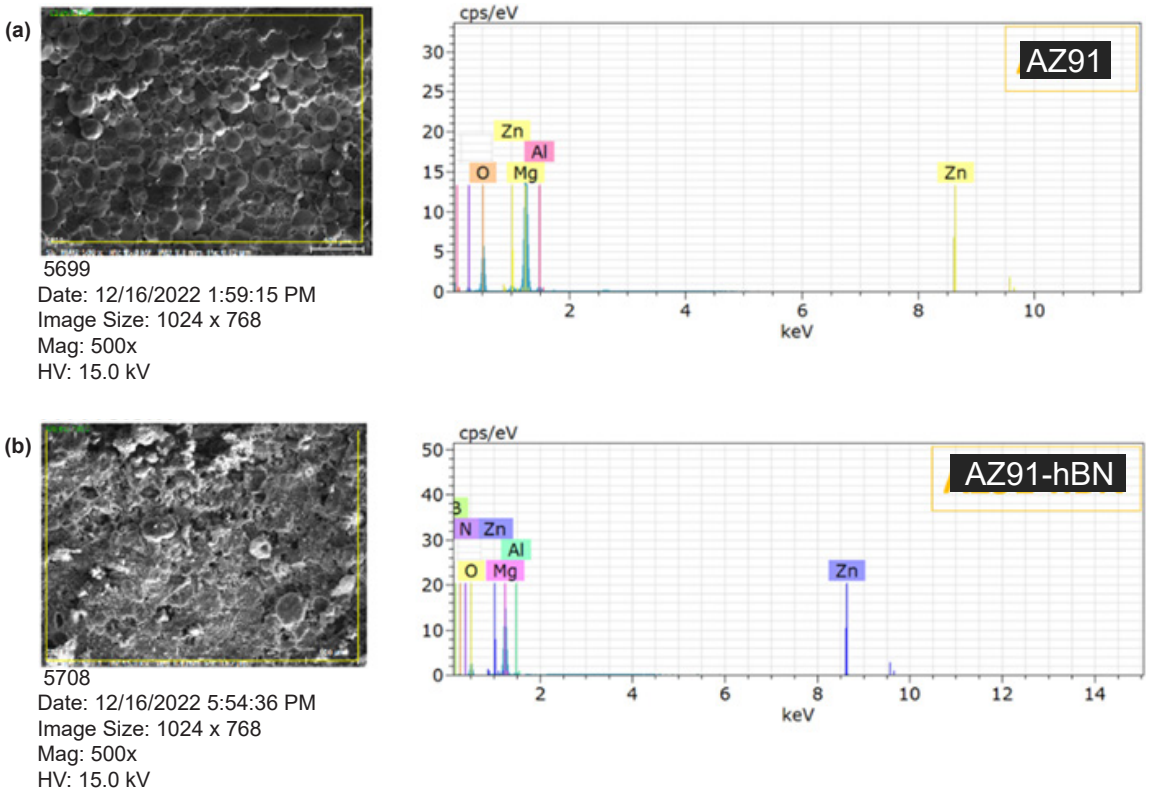

Şekil 3. Numunelerin EDX analiz sonuçları (EDX analysis results of samples).

değerler çıktığı görülmüştür [30]. Sertlik deneylerinde hBN katkı miktarının AZ91-hBN numunelerinin sertliğini daha da artırdığı görülmüştür [31-36]. Numunelerin 5 farklı noktasından alınan sertlik değerleri ve ortalama sertlik değerleri ve bakalite alınan, mikroyapıları ve sertlikleri incelenen kompozit numuneler Şekil 4'te gösterilmiştir.

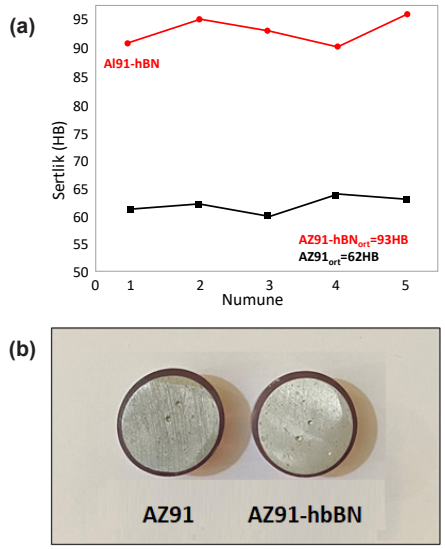

Şekil 4. a). 91 matrisli kompozitlerin sertlik değerleri, b). Mikroyapıları ve sertlikleri incelenen numuneler (a. Hardness values of AZ91 matrix composites, b). Samples whose microstructures and hardness were examined).

3.3. Triboloji (Tribology)

Aşınma deneylerinde 13 mm çapında ve 5 mm yüksekliğinde numuneler üzerinde gerçekleştirilmiştir. hBN katkılı numunelerin ağırlık kaybı miktarlarında saf AZ91'e göre daha iyi bir aşınma direnci gösterdiği görüldü. hBN takviyesiyle aşınma direncinde olumlu yönde etkilerin olduğu literatür çalışmalarında da görülmüştür (ağırlıkça %7,5 hBN [33] , ağırlıkça %5-10 hBN [34], ağırlıkça %4 hBN [35], ağırlıkça %10, 15, 20 hBN [36]). Bu durumun hBN nanoparçacıklarının iyi bir yağlayıcı özelliği olması ve sertlik değerlerinin yüksek olması aşınma özelliklerini ve aşınma direncini olumlu yönde etkilediği düşünülmektedir [35,36]. 5 N,10 N ve 15N yük altındaki aşınma ağırlık kayıpları ve aşınma deneyleri tamamlanan numunelerin son hali Şekil 5'te gösterilmiştir.

Kompozitlerde 3 farklı yük altında yeni numuneler için toplam 300 metre kayma mesafesinde meydana gelen sürtünme katsayısındaki değişimler Şekil 6'da gösterilmiştir. hBN katkısının sürtünme katsayısını düşürdüğü literatür çalışmalarında da görülmüştür [26,27,33-36]. Aşınma yüzeylerine uygulanan kuvvetin artmasıyla sürtünme katsayısında artış meydana gelmiştir.

Aşınma deneyleri tamamlanan kompozitlerin aşınma yüzeylerinin mikroyapılarının incelenmesi için SEM analizi uygulanmıştır. SEM analizleri

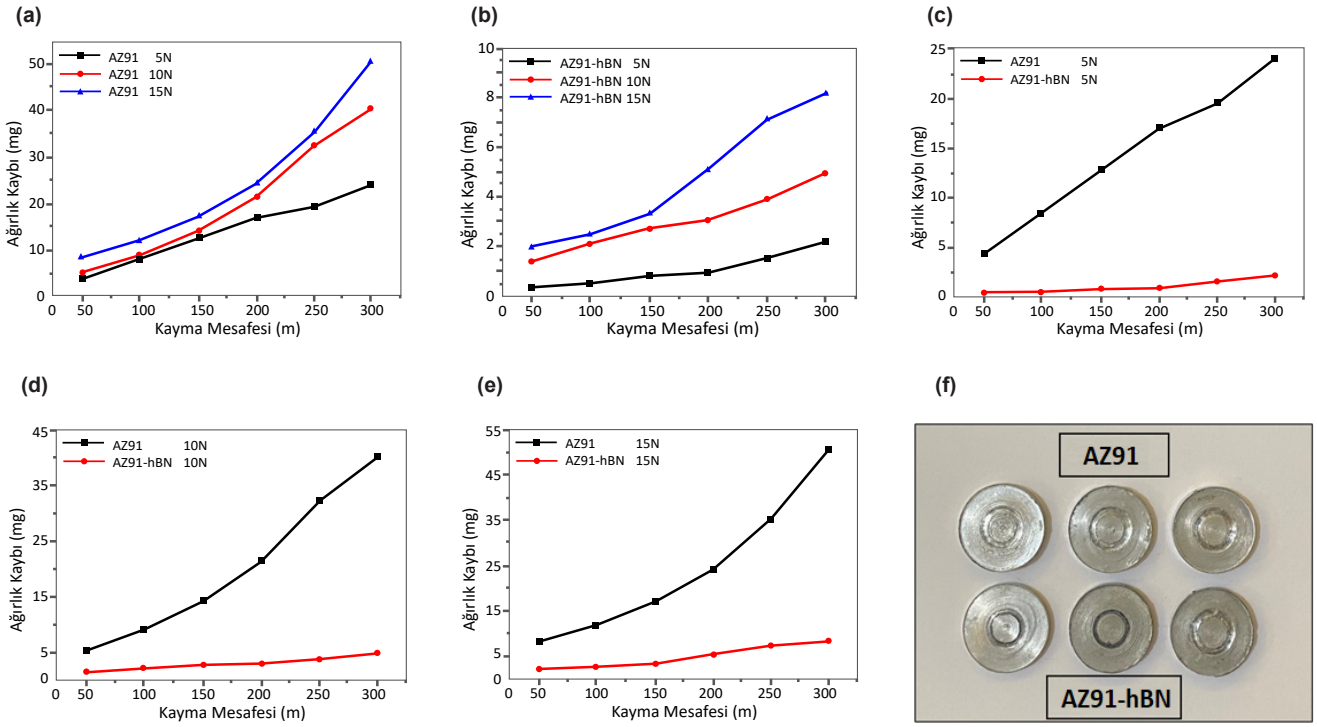

Şekil 5. a). AZ91, b). Z91-hBN kompozitinin 3 kuvvet altındaki aşınma ağırlık kaybı miktarları. Z91 ve AZ91-hBN kompozitinin 3 kuvvet altındaki c). 5N, d). 10N, e). 15N aşınma ağırlık kaybı miktarları. f). Mikroyapıları ve sertlikleri incelenen numuneler (Wear weight loss amounts of a). AZ91, b). AZ91-hBN composite under 3 forces. Wear weight loss amounts of AZ91 and AZ91-hBN composite under 3 forces c). 5N, d). 10N, e). 15N. f). Samples whose microstructures and hardness were examined).

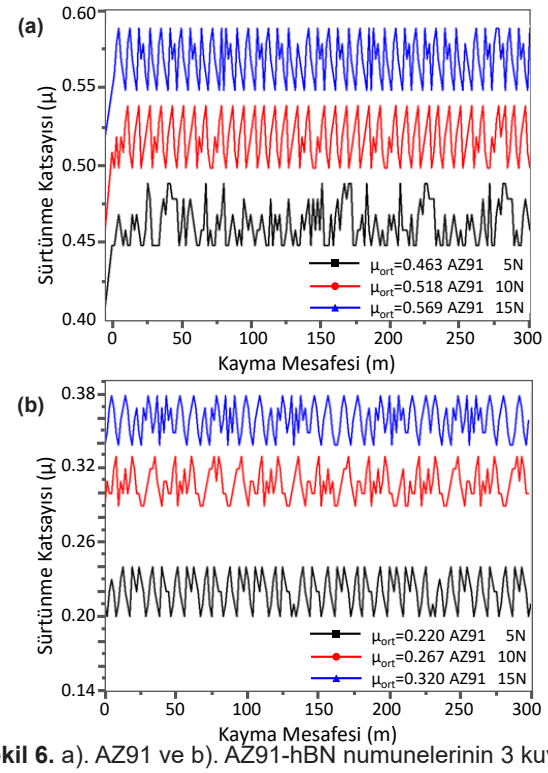

Şekil 6. a). AZ91 ve b). AZ91-hBN numunelerinin 3 kuvvet altındaki sürtünme katsayısı değerleri (a). AZ91 and b). AZ91-hBN samples friction coefficient values under 3 forces).

sonucunda saf AZ91 kompozesindeki meydana gelen aşınma durumları ile hBN katkılı kompozit numunelerde meydana gelen numuneler arasında belirgin bir aşınmaya karşı gösterilen direncin arttığı gözlemlenmiştir. Bu duruma hBN katkısının sebep olduğu düşünülmektedir [27-32]. AZ91 alaşımına hBN takviyesinin aşınma direncini ve aşınma izlerini belirgin şekilde etkilemiştir. Aşınma kuvvetinin artmasıyla kompozit numunelerdeki aşınma izlerinin daha net bir şekilde görülmüştür. 5 N, 10 N ve 15 N yük altındaki aşınma yüzeylerinin 3 farklı büyüklükteki SEM görüntüleri Şekil 7'de gösterilmiştir.

4. Sonuçlar (Conclusions)

Çalışmada AZ91 magnezyum ve alaşımı ve AZ91 alaşımına ağırlıkça %10 hBN nanoparçacıkları takviye edilerek homojen kompozit malzeme karışımları yapılmıştır. Soğuk presleme tekniği ile hazırlanan tozların preslenmesi ve argon atmosferinde sinterlemeleri gerçekleştirilmiştir. Hazırlanan numunelerin mikroyapı, sertlik, kuru ortam şartlarında aşınma ve sürtünme katsayısı özellikleri deneysel olarak incelenmiştir. Yapılan sentezlemeler ve üretimlerin sonucunda AZ91 magnezyum alaşımı ile birleşimi yapılan hBN nanoparçacıklarının AZ91 alaşımıyla birleştiği mikroyapı görüntüleri üzerinde görülmüştür. Yapılan aşınma deneylerinde hBN takviyesiyle aşınma sonucunda meydana gelen ağırlık kayıplarında azalmalar meydana geldiği görülmüştür. Bu durumun hBN nanoparçacıklarının iyi bir yağlayıcı özelliği taşıdığından ve hBN nanoparçacıklarının

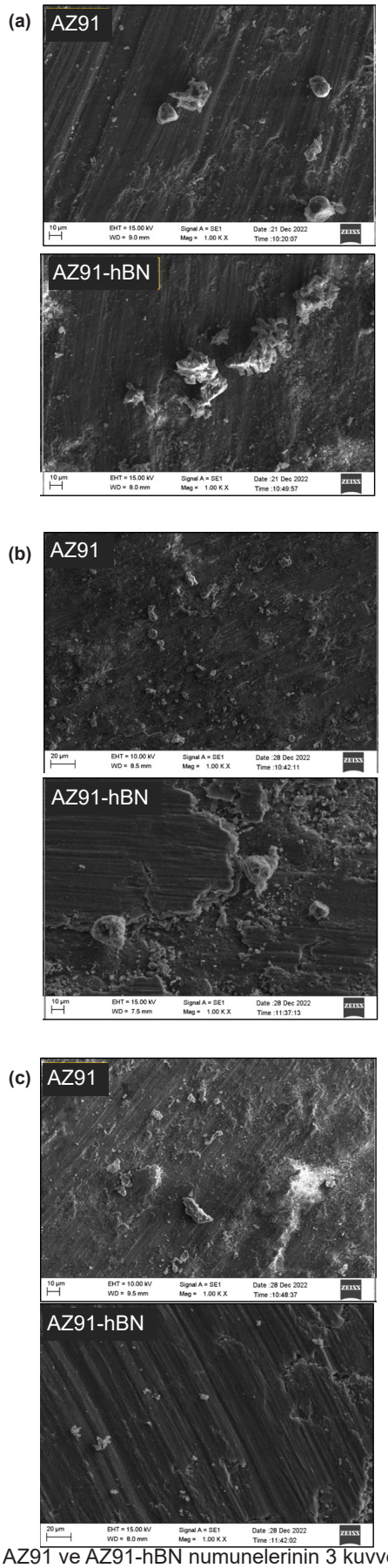

Şekil 7. AZ91 ve AZ91-hBN numunelerinin 3 kuvvet altındaki a) 5 N, b) 10 N ve c) 15 N aşınma yüzeyi SEM görüntüleri (SEM images of AZ91 and AZ91-hBN specimens under 3 forces a) 5 N, b) 10 N and c) 15 N wear surface).

sertlik değerlerinin yüksek olmasının aşınma özelliklerinde hBN katkısının aşınma direncini olumlu yönde etkilediği düşünülmektedir. Yapılan sertlik deneylerinde saf AZ91 değerinin sertlik değeri literatür değerlerine benzer değerler çıktığı görülmüştür. Sertlik deneylerinde hBN takviyesinin sertlik değerini belirgin şekilde arttığı görülmüştür.

Teşekkür (Acknowledgement)

Yazarlar, bu çalışmaya maddi katkıları ve destekleri için Fırat Üniversitesi Araştırma Fonu'na (FUBAP MF.21.74) teşekkür eder.

Kaynaklar (References)

[1] Easton, M., Song, W. Q., & Abbott, T. (2006). A comparison of the deformation of magnesium alloys with aluminium and steel in tension, bending and buckling. *Materials & Design*, *27*(10), 935-946. https://doi.org/10.1016/j.matdes.2005.03.005.

[2] Bagheri, B., Abbasi, M., Abdollahzadeh, A., & Kokabi, A. H. (2020). A comparative study between friction stir processing and friction stir vibration processing to develop magnesium surface nanocomposites. *International Journal of Minerals, Metallurgy and Materials*, *27*, 1133-1146. https://doi.org/10.1007/s12613-020-1993-4.

[3] Bagheri, B., & Abbasi, M. (2020). Development of AZ91/SiC surface composite by FSP: Effect of vibration and process parameters on microstructure and mechanical characteristics. *Advances in Manufacturing*, *8*(1), 82-96. https://doi.org/10.1007/s40436-019-00288-9.

[4] Tandon, R., & Madan, D. (2014). Emerging applications using magnesium alloy powders: A feasibility study. In: Alderman, M., Manuel, M.V., Hort, N., & Neelameggham, N.R. (eds). *Magnesium Technology 2014*. (pp. 21-25). Springer. https://doi.org/10.1007/978-3-319-48231-6_7. ISBN 9783319482316.

[5] Burke, P., Kipouros, Y. G., Judge, W. D., & Kipouros, G. J. (2019). Surprises and pitfalls in the development of magnesium powder metallurgy alloys. *Magnesium and Its Alloys*. (pp. 337-373). CRC Press. ISBN 9781351045476.

[6] Fenker, M., Balzer, M., & Kappl, H. (2014). Corrosion protection with hard coatings on steel: Past approaches and current research efforts. *Surface and Coatings Technology*, *257*, 182-205. https://doi.org/10.1016/j.surfcoat.2014.08.069.

[7] Gökçe, A., Fındık, F., & Kurt, A. O. (2011). Microstructural examination and properties of premixed Al–Cu–Mg powder metallurgy alloy. *Materials Characterization*, *62*(7), 730-735. https://doi.org/10.1016/j.matchar.2011.04.021.

[8] Jabbari Taleghani, M. A. (2014). *Processing and properties of high performance 7075 Al and AZ91 Mg powder metallurgy alloys* [Doctoral dissertation, Universidad Carlos III de Madrid]. http://hdl.handle.net/10016/20871.

[9] Aydoğmuş, T., Kelen, F., & Aydemir, E. (2020). Processing of AZ91 Magnesium Alloy via Hot Pressing Technique. *Bitlis Eren University Journal of Science*, *9*(1), 277-287. https://doi.org/10.17798/bitlisfen.555946

[10] Yuan, Q. H., Zeng, X. S., Liu, Y., Luo, L., Wu, J. B., Wang, Y. C., & Zhou, G. H. (2016). Microstructure and mechanical properties of AZ91 alloy reinforced by carbon nanotubes coated with MgO. *Carbon*, *96*, 843-855. https://doi.org/10.1016/j.carbon.2015.10.018.

[11] Nouri, M., & Li, D. Y. (2017). Maximizing the benefit of aluminizing to AZ31 alloy by surface nanocrystallization for elevated resistance to wear and corrosive wear. *Tribology International*, *111*, 211-219. https://doi.org/10.1016/j.triboint.2017.03.009.

[12] Dinaharan, I., Zhang, S., Chen, G., & Shi, Q. (2022). Assessment of Ti-6Al-4V particles as a reinforcement for AZ31 magnesium alloy-based composites to boost ductility incorporated through friction stir processing. *Journal of Magnesium and Alloys*, *10*(4), 979-992. https://doi.org/10.1016/j.jma.2020.09.026.

[13] Bagheri, B., Abbasi, M., Abdollahzadeh, A., & Mirsalehi, S. E. (2020). Effect of second-phase particle size and presence of vibration on AZ91/SiC surface composite layer produced by FSP. *Transactions of Nonferrous Metals Society of China*, *30*(4), 905-916. https://doi.org/10.1016/S1003-6326(20)65264-5.

[14] Yu, W., Wang, X., Zhao, H., Ding, C., Huang, Z., Zhai, H., … & Xiong, S. (2017). Microstructure, mechanical properties and fracture mechanism of Ti2AlC reinforced AZ91D composites fabricated by stir casting. *Journal of Alloys and Compounds*, *702*, 199-208. https://doi.org/10.1016/j.jallcom.2017.01.231.

[15] Aatthisugan, I., Razal Rose, A., & Selwyn Jebadurai, D. (2017). Mechanical and wear behaviour of AZ91D magnesium matrix hybrid composite reinforced with boron carbide and graphite. *Journal of Magnesium and Alloys*, *5*(1), 20-25. https://doi.org/10.1016/j.jma.2016.12.004.

[16] Meher, A., Mahapatra, M. M., Samal, P., & Vundavilli, P. R. (2020). Study on effect of TiB2 reinforcement on the microstructural and mechanical properties of magnesium RZ5 alloy based metal matrix composites. *Journal of Magnesium and Alloys*, *8*(3), 780-792. https://doi.org/10.1016/j.jma.2016.12.004.

[17] Liu, P., Jiang, H., Cai, Z., Kang, Q.,n & Zhang, Y. (2016). The effect of Y, Ce and Gd on texture, recrystallization and mechanical property of Mg–Zn alloys. *Journal of Magnesium and Alloys*, *4*(3), 188-196. https://doi.org/10.1016/j.jma.2016.07.001.

[18] Wang, C. J., Kang, J. W., Deng, K. K., Nie, K. B., Liang, W., Li, W. G. (2020). Microstructure and mechanical properties of Mg-4Zn-xGd (x=0, 0.5, 1, 2) alloys. *Journal of Magnesium and Alloys*, *8*(2), 441-451. https://doi.org/10.1016/j.jma.2019.06.005.

[19] Song, J., She, J., Chen, D., & Pan, F. (2020). Latest research advances on magnesium and magnesium alloys worldwide. *Journal of Magnesium and Alloys*, *8*(1), 1-41. https://doi.org/10.1016/j.jma.2020.02.003.

[20] Haubner, R., Herrmann, M., Lux, B., Petzow, G., Weissenbacher, R., & Wilhelm, M. (2003). *High performance non-oxide ceramics II* (Vol. 102). Springer. https://doi.org/10.1007/3-540-45623-6.

[21] Tyagi, R., Xiong, D., & Li, J. (2011). Effect of load and sliding speed on friction and wear behavior of silver/h-BN containing Ni-base P/M composites. *Wear*, *270*(7-8),

423-430. https://doi.org/10.1016/j.wear.2010.08.013.

[22] Chen, B., Bi, Q., Yang, J., Xia, Y., & Hao, J. (2008). Tribological properties of solid lubricants (graphite, h-BN) for Cu-based P/M friction composites. *Tribology International*, *41*(12), 1145-1152. https://doi.org/10.1016/j.triboint.2008.02.014.

[23] Tyagi, R., Xiong, D. S., Li, J. L., & Dai, J. (2010). High-temperature friction and wear of Ag/h-BN-containing Ni-based composites against steel. *Tribology Letters*, *40*, 181-186. https://doi.org/10.1007/s11249-010-9655-8.

[24] Yan, Y., Cao, H., Kang, Y., Yu, K., Xiao, T., Luo, J., & Dai, Y. (2017). Effects of Zn concentration and heat treatment on the microstructure, mechanical properties and corrosion behavior of as-extruded Mg-Zn alloys produced by powder metallurgy. *Journal of Alloys and Compounds*, *693*, 1277-1289. https://doi.org/10.1016/j.jallcom.2016.10.017.

[25] Rashad, M., Pan, F., Asif, M., & Tang, A. (2014). Powder metallurgy of Mg-1% Al-1% Sn alloy reinforced with low content of graphene nanoplatelets (GNPs). *Journal of Industrial and Engineering Chemistry*, *20*(6), 4250-4255. https://doi.org/10.1016/j.jiec.2014.01.028.

[26] Lingaraju, S. V., Mallikarjuna, C., Annappa, A. R., & Venkatesha, B. K. (2022). Processing, and characterization of AZ91D magnesium alloy reinforced nano TiC, B4C, and HBN composites. *Materials Today: Proceedings*, *54*, 479-485. https://doi.org/10.1016/j.matpr.2021.11.118.

[27] Mahathanabodee, S., Palathai, T., Raadnui, S., Tongsri, R., & Sombatsompop, N. (2014). Dry sliding wear behavior of SS316L composites containing h-BN and MoS2 solid lubricants. *Wear*, *316*(1-2), 37-48. https://doi.org/10.1016/j.wear.2014.04.015.

[28] Baradeswaran, A., & Elaya Perumal, A.(2013). Influence of B4C on the tribological and mechanical properties of Al 7075-B4C composites. *Composites Part B: Engineering*, *54*, 146-152. https://doi.org/10.1016/j.compositesb.2013.05.012.

[29] Sharma, P., Sharma, S., & Khanduja, D. (2015). Production and some properties of Si3N4 reinforced aluminium alloy composites. *Journal of Asian Ceramic Societies*, *3*(3), 352-359. https://doi.org/10.1016/j.jascer.2015.07.002.

[30] Yuan, Q. H., Zeng, X. S., Liu, Y., Luo, L., Wu, J. B., Wang, Y. C., & Zhou, G. H. (2016). Microstructure and mechanical properties of AZ91 alloy reinforced by carbon nanotubes coated with MgO. *Carbon*, *96*, 843-855. https://doi.org/10.1016/j.carbon.2015.10.018.

[31] Yıldırım, M., & Özyürek, D. An investigation of wear behaviours of Mg matrix composites reinforced carbon nanotube produced by powder metallurgy method. *International Journal of Engineering Research and Development*, *13*(3), 1-8. https://doi.org/10.29137/umagd.1038336.

[32] Turan, M. E., Zengin, H., & Sun, Y. (2020). Dry sliding wear behavior of (MWCNT+GNPs) reinforced AZ91 magnesium matrix hybrid composites. *Metals and Materials International*, *26*, 541-550. https://doi.org/10.1007/s12540-019-00338-8.

[33] Loganathan, P., Gnanavelbabu, A., & Rajkumar, K. (2021). Investigation on mechanical and wear behaviour of AA2024/hBN composites synthesized via powder metallurgy routine. *Materials Today: Proceedings*, *45*, 7865-7870. https://doi.org/10.1016/j.matpr.2020.12.503.

[34] Ayyanar, S., Gnanavelbabu, A., Rajkumar, K., & Loganathan, P. (2021). Studies on high temperature wear and friction behaviour of AA6061/B 4 C/hBN hybrid composites. *Metals and Materials International*, *27*, 3040-3057. https://doi.org/10.1007/s12540-020-00710-z.

[35] Tyagi, R., Xiong, D., & Li, J. (2011). Effect of load and sliding speed on friction and wear behavior of silver/h-BN containing Ni-base P/M composites. *Wear*, *270*(7-8), 423-430. https://doi.org/10.1016/j.wear.2010.08.013.

[36] Mahathanabodee, S., Palathai, T., Raadnui, S., Tongsri, R., & Sombatsompop, N. (2013). Effects of hexagonal boron nitride and sintering temperature on mechanical and tribological properties of SS316L/h-BN composites. *Materials & Design*, *46*, 588-597. https://doi.org/10.1016/j.matdes.2012.11.038.

YAZAR KILAVUZU

Genel Bilgiler
- Makale başvurusu için Makale Kontrol Listesi, Kapak Sayfası, Makale Metni Dosyası, Telif Hakkı Devir Dosyası ve Benzerlik Oran Dosyası olmak üzere 5 ayrı formun doldurulması ve sisteme yüklenmesi gerekmektedir.
- Başvurularda iletişimde bulunulacak yazar ve diğer yazarların iletişim bilgileri bulunmalıdır.
- Her makale, konusu ile ilgili en az iki hakeme gönderilerek şekil, içerik, özgün değer, uluslararası literatüre katkısı bakımından incelettirilir. Hakem görüşlerinde belirtilen eksikler tamamlandıktan sonra, son baskı formatına getirilir ve yazarlardan makalenin son halinin onayı alınır. Dergide basıldığı haliyle makale içinde bulunabilecek hataların sorumluluğu yazarlara aittir.

Makale Kontrol Listesi
- Makale kontrol listesi, makalenin dergi yazım kurallarına uygunluğunun kabul edildiğini gösteren formdur.
- Derginin formatına uygun olmayan veya kontrol listesi doldurulmamış olan başvurulan değerlendirilmeye alınmayacaktır.

Kapak Sayfası
- Yazarlara ait afiliasyon, elektronik posta adresi ve ait ORCID bilgileri kapak sayfasında yer almalıdır.
- Makaleye ait başlık, özet ve anahtar kelimeler kapak sayfasında yer almalıdır.

Makale Metni Dosyası
- Makale metninin yazımında Yazım Kuralları'na uyulması gerekmektedir.
- Makale metninde kapsayıcı ve bilimsel bir dil kullanılmalıdır.
- Makale metni referanslar dahil araştırma makaleleri için 14.000 kelimeyi tarama makaleleri için ise 22.000 kelimeyi geçmemelidir.
- Makalenin metni, Times New Roman 12 punto ile Makale Metni Dosyası'nın sayfa düzeni değiştirilmeden yazılmalıdır.
- Makale metninin Microsoft Office Word 2010 ve üzeri bir kelime işlemci ile hazırlanması ve yazım hatalarının kontrol edilmesi ve düzeltilmesi gerekmektedir.
- Eğer makale Türkçe ise, Türkçe başlıklarla bire bir uyumlu olacak şekilde oluşturulmuş İngilizce başlıklar parantez içerisinde yazılmalıdır.
- Makale içerisinde kullanılan kısaltma ve sembollerin anlamları ilk kullanıldıklarında açıklanmalıdır.
- Makale metni içerisindeki alt başlıklar numaralandırılmalıdır. Numaralandırma işlemleri ana bölümler için 1.'den başlamalı ve tüm ana başlıklar (Özet, Teşekkür ve Kaynaklar ve Ekler bölümleri hariç) için devam etmelidir. İkincil başlıklar ana bölüm numaralandırmasına uygun olarak 1.1., 1.2., 1.3., ... şeklinde devam etmelidir. Üçüncü başlıklar ikinci başlıklara uygun olarak 1.1.1., 1.1.2., 1.1.3., ... şeklinde devam etmelidir.

Telif Hakkı Devir Dosyası
- İmzalı Telif Hakkı Devir Dosyası taranarak sisteme yüklenmelidir.
- İmzalı Telif Hakkı Devir Dosyası'nı göndermeyen yazarların başvuruları değerlendirmeye alınmaz.

Benzerlik Oran Dosyası
- Makalenin referanslar bölümü hariç metni "iThenticate" veya "Turnitin" programları ile taranmalıdır.
- Benzerlik oranı raporunun PDF formatında sisteme yüklenmelidir.
- Benzerlik oranı %15'in üzerinde olmamalıdır.

Revizyonlar
- Yazarlar, hakemlere cevap dosyası hazırlamalı ve sisteme ayrı bir doküman olarak yüklemelidir.
- Hakemlere cevap dosyası, hakem yorumlarını ve bu yorumlara verilen cevapları içermelidir.
- Makale metninin revizyon sonrası güncel hali sisteme yüklenmelidir. Makale metninde yapılan değişiklikler farklı kırmızı renkte yazı ile belirtilmelidir.

Gizlilik Politikası

Journal of Boron gizliliğe saygı duymaktadır. Kişisel bilgiler, sadece derginin belirtilen amaçları doğrultusunda kullanılacak ve üçüncü kişilerle paylaşılmayacaktır.

YAZIM KURALLARI

Makale Başlığı
- Makale başlığı, Kapak Sayfası ve Makale Metni içerisinde yer almalıdır.
- Makale başlığı standart kısaltmalarla birlikte en çok 15 kelimeden oluşmalıdır.
- Eğer makale Türkçe ise, İngilizce başlıkla bire bir uyumlu olacak şekilde Türkçe makale başlığı da oluşturulmalıdır.

Özet
- Özet, Kapak Sayfası içerisinde yer almalıdır.
- Özet, 250 kelimeyi geçmemelidir.
- Standart olmayan kısaltmalar ilk kullanıldığında tam açıklamalarından sonra parantez içerisinde yazılmalıdır.
- Eğer makale Türkçe ise, İngilizce özetle bire bir uyumlu olacak şekilde Türkçe özet de oluşturulmalıdır.

Anahtar Kelimeler
- Anahtar kelimeler Kapak Sayfası içerisinde yer almalıdır.
- En fazla 5 anahtar kelime, alfabetik sıraya göre yazılmalıdır.
- Kısaltmalar anahtar kelime olarak kullanılmamalıdır.
- Eğer makale Türkçe ise, İngilizce anahtar kelimelerle bire bir uyumlu olacak şekilde Türkçe anahtar kelimelere de oluşturulmalıdır.

Giriş
- Giriş bölümü, Makale Metni içerisinde yer almalıdır.
- İlgili literatürün özeti, çalışmanın amacı ve özgün değeri ve kurulmuş olan hipotezi içermelidir.
- Kaynaklar, toplu olarak ve aralıklı verilmemeli (örnek [1-5] veya [1, 2, 3, 5, 8]), her kaynağın çalışmaya katkısı irdelenmeli ve metin içerisinde belirtilmelidir.

Malzemeler ve Yöntemler
- Malzemeler ve yöntemler bölümü, Makale Metni içerisinde yer almalıdır.
- Yürütülmüş olan çalışma deneysel bir çalışma ise deney prosedürü/metodu anlaşılır bir şekilde açıklanmalıdır.
- Teorik bir çalışma yürütülmüşse teorik metodu detaylı bir şekilde verilmelidir.
- Yapılan çalışmada kullanılan metot daha önce yayınlanmış bir metot ise diğer çalışmaya atıf yapılarak bu çalışmanın diğer çalışmadan farklı belirtilmelidir.

Sonuçlar ve Tartışma
- Sonuçlar ve tartışma bölümü, Makale Metni içerisinde yer almalıdır.
- Elde edilen sonuçlar açık ve öz bir şekilde verilmelidir.
- Elde edilen tüm sonuçlar atıf yapılarak literatür ile karşılaştırılmalıdır.
- Tablolar numaralandırılmalıdır ve düzenlenebilir formatta olmalıdır. Eğer makale Türkçe ise, tablo üst yazılarının bire bir İngilizce çevirileri parantez içerisinde verilmelidir.
- Makale içerisindeki şekiller numaralandırılmalıdır ve en az 300 dpi çözünürlükte olmalıdır. Şekillerin üzerindeki yazılar okunabilir büyüklükte ve yazı tipinde olmalıdır. Kabul edilen şekil formatları TIFF, JPG ve JPEG'dir. Eğer makale Türkçe ise, şekil alt yazılarının bire bir İngilizce çevirileri parantez içerisinde verilmelidir..

Sonuçlar
- Sonuçlar bölümü, Makale Metni içerisinde yer almalıdır.
- Çalışmadan elde edilen ana sonuçlar ve çıkarımlar kısa ve öz bir şekilde verilmelidir.
- Çalışmaya ait gelecek perspektifleri bu bölümde verilir.

Teşekkürler
- Teşekkürler bölümü, Makale Metni içerisinde yer almalıdır.
- Çalışmanın gerçekleşmesi için sağlanan maddi kaynaklar ve kullanılan altyapı bu bölümde belirtilir.

Yazar Katkı Beyanı
- Yazar Katkı Beyanı, Makale Metni içerisinde yer almalıdır.
- Her yazarın katkıları belirtilmelidir.
- Katkı rolleri şu şekildedir: kavramsallaştırma, veri analizi, veri iyileştirme, finansman sağlama, metodoloji, proje yönetimi, kaynak sağlama, yazılım analizi, denetim, doğrulama, görselleştirme, orijinal taslak yazma, inceleme yazma ve düzenleme.

Kaynaklar
- Kaynaklar, Makale Metni içerisinde yer almalıdır.
- Basılmış kaynakların DOI ve ISBN numarası belirtilmelidir.
- İnternet sitesi adresleri (URL) kaynak olarak verilmemelidir. Ancak metin içerisinde istatistiksel bir verinin geçtiği yerde veriden sonra belirtilebilir.
- Kaynaklar listesi metin içerisinden kullanılma sırasına uygun olarak numaralandırılmalıdır.
- Kaynaklar, "APA Publication Manual, Seventh Edition" kurallarına uygun olarak hazırlanmalıdır.
- Kaynaklar İngilizce olarak hazırlanmalıdır. Türkçe kaynakların İngilizce karşılıkları köşeli parantez içerisinde belirtilmelidir.
- APA formatı ve örneklere aşağıdaki bağlantıdan ulaşılabilir.

https://apastyle.apa.org/style-grammar-guidelines/references/examples

Ekler
- Makaledeki ekler EK A (Appendix A), EK B (Appendix B) ve EK C (Appendix C) vb. olarak adlandırılmalıdır.
- Ekler içerisindeki denklemler A1, A2, A3 vb. olarak adlandırılmalıdır, tablo ve şekiller Tablo A1, Tablo A2, Şekil A1, Şekil A2 vb. olarak adlandırılmalıdır.

AUTHOR GUIDELINE

General Information

- For article application, 5 individual files which are Article Checklist, Cover Page, Manuscript File, Copyright Transfer File and Similarity Ratio File, must be filled in and uploaded to the system.
- Applications should include the contact information of the author and other authors to be contacted.
- The article checklist and cover page in the Manuscript File should be filled in completely.
- Each article is sent to at least two referees related to its subject and examined in terms of format, content, novelty, contribution to literature.
- After the deficiencies stated in the referee's comments are completed, it is brought to the final print format and the approval of the final version of the article is obtained from the authors. The responsibility of errors that may be found in the article as it is published in the journal belongs to the authors.

Article Checklist

- Article checklist is the form that shows that the article's compliance with the journal writing rules is accepted.
- Applications that do not comply with the journal's format or whose checklist is not filled will not be considered.

Cover Page

- Affiliation, e-mail address and ORCID informations belonging to the authors must be included in the cover page.
- •The title, abstract and keywords of the article should be included in the cover page.

Manuscript

- Writing Rules must be followed, during writing of the manuscript.
- Inclusive and Scientific language must be used in the manuscript.
- Manuscript should not exceed 14,000 words for research articles and 22,000 words for review articles, including references.
- The manuscript should be written in Times New Roman 12 points without changing the page layout of the Manuscript File.
- The manuscript should be prepared with a word processor of Microsoft Office Word 2010 and above, and spelling errors should be checked and corrected.
- Abbreviations and symbols used in the manuscript must be explained when used fort he first time.
- Subheadings in the article should be numbered. Numbering should start at 1 for the main section and continue for all main headings (except the Summary, Acknowledgments and References and Appendices sections). Secondary titles continue as 1.1., 1.2., 1.3., ... in accordance with the main chapter numbering. The third headings continue as 1.1.1., 1.1.2., 1.1.3., ... in accordance with the second headings.

Copyright Transfer File

- Signed Copyright Transfer File should be scanned and uploaded to the system.
- Applications of the authors who do not send the signed Copyright Transfer File will not be evaluated.

Similarity Ratio File

- The manuscript should be scanned with "iThenticate" or "Turnitin" programs, except for the references section.
- The similarity ratio report should be uploaded to the system in PDF format.
- The similarity ratio should not exceed 15%.

Revisions

- Authors must prepare an answers to the reviewers file and upload it to the system as a separate document.
- Answers to the reviewers file must include reviewers's comments and their corresponding answers.
- The updated version of the manuscript after the revision must be uploaded to the system. Changes that were made in the manuscript must be indicated with red text.

Privacy Policy

Journal of Boron respects privacy. Any personal information will only be used in line with the stated purposes of the journal and will not be shared with third parties.

WRITING RULES

Title
- Title of the manuscript must be included in Cover Page and Manuscript.
- The title of the manuscript should consist of a maximum of 15 words with standard abbreviations.

Abstract
- Abstract must be included in Cover Page.
- The abstract must not exceed 250 words.
- Non-standard abbreviations should be written in parentheses after their full explanation, when they are used for the first time.

Keywords
- Keywords must be included in Cover Page.
- A maximum of 5 keywords should be written in alphabetical order.
- Abbreviations should not be used as keywords.

Introduction
- Introduction must be included in Manuscript.
- The summary of the relevant literature, aim and novelty of the study, and the established hypothesis should be included.
- References should not be given in bulk and in intervals (example [1-5] or [1, 2, 3, 5, 8]), the contribution of each source to the study should be examined and stated in the text.

Materials and Methods
- Materials and methods must be included in Manuscript.
- If the study carried out is an experimental study, the test procedure/method should be clearly explained.
- If a theoretical study has been carried out, the theoretical method should be given in detail.
- If the method used in the study is a previously published method, the other study should be mentioned by citing.

Results and Discussion
- Results and discussion must be included in Manuscript.
- Obtained results should be given in a clear and concise manner.
- All of the results should be compared with the literature by citing.
- Tables should be numbered and in editable format.
- Figures in the manuscript should be numbered and have at least 300 dpi resolution. The texts on the figures should be in legible size and font. Accepted figure formats are TIFF, JPG, and JPEG.

Conclusions
- Conclusions must be included in Manuscript.
- Main conclusions and inferences obtained from the study should be given concisely.
- Future perspectives of the study are given in this section.

Acknowledgements
- Acknowledgements must be included in Manuscript.
- The financial resources provided and the infrastructure used during the study are specified in this section..

Author Contributions
- Author contributions must be included in Manuscript.
- Contributions of each author must be stated.
- Contribution roles are as follows: conceptualization, data analysis, data curation, funding acquisition, methodology, project administration, sourcing, software analysis, supervision, validation, visualization, writing original draft, writing review and editing.

References
- References must be included in Manuscript.
- DOI and ISBN numbers of printed sources should be specified.
- Website addresses (URLs) should not be given as a source. However, it can be specified after the data where statistical data is mentioned in the text.
- The list of references should be numbered according to the order in which they are used in the text.
- References should be prepared in accordance with the rules of “APA Publication Manual, Seventh Edition”.
- References should be prepared in English. English equivalents of sources should be indicated in square brackets.
- APA format and examples can be found at the link below.

https://apastyle.apa.org/style-grammar-guidelines/references/examples

Appendices
- Appendices must be included in Manuscript.
- Appendices in the manuscript must be named as Appendix A (Appendix A), Appendix B (Appendix B) and Appendix C (Appendix C) etc.
- Equations in the appendices must be named as A1, A2, A3, etc., and table and figures numberings must be named as Table A1, Table A2, Figure A1, Figure A2 etc..

BOR DERGİSİ
JOURNAL OF BORON
https://dergipark.org.tr/boron

İÇİNDEKİLER/CONTENTS

TENMAK Bor Araştırma Enstitüsü

Dumlupınar Bulvarı (Eskişehir Yolu 7. km), No:166, D Blok, 06530, Ankara
Tel: (0312) 201 36 00
Faks: (0312) 219 80 55
e-mail: boren.journal@tenmak.gov.tr
web:https://dergipark.org.tr/boron